

METAL AND INHIBITOR BINDING STUDIES ON METALLO-BETA-LACTAMASES

Dissertation

zur Erlangung des Grades
des Doktors der Naturwissenschaften
der Naturwissenschaftlich-Technischen Fakultät III-
Chemie, Pharmazie, Bio- und Werkstoffwissenschaften
der Universität des Saarlandes

von

Nathalie Selevsek

Saarbrücken

2007

Tag des Kolloquiums: 28.04.2008

Dekan: Univ.-Prof. Dr. rer.nat. Uli Müller

Berichterstatter: Prof. Dipl. Ing. Dr. tech. Elmar Heinzle

Priv. Doz. Dr. Hans-Werner Adolph

Prof. Dr. Wolfgang E. Trommer

Acknowledgement

This dissertation is the result of three and a half years of work during which many people have supported me. I would like to thank all of them in the next lines:

First of all, special thanks go to my supervisor Priv. Doz. Dr. Hans-Werner Adolph for its helpful and stimulating discussions during this work and for the reviewing of the thesis.

I would also like to sincerely thank Prof. Dipl. Ing. Dr. tech. Elmar Heinzle, who gave me the opportunity to graduate in his research group at the Institute of Biochemical Engineering in Saarbrücken and for reviewing this PhD thesis.

I also want to greatly thank other colleagues of the Biochemical Engineering Group, in Saarbrücken: many thanks to Priv. Doz. Dr. Andreas Tholey for his advises in the mass spectrometry field and the supervision of my project; Dr. Masoud Zabet-Moghaddam, Dr. Ditte Bungert, Dr. Tae Hoon Yang, Maria Lasaos and Rahul Deshpande for their stimulating remarks during this work; and also Michel Fritz for the technical assistance.

Many and best thanks go to my EU partners in Oxford: Prof. Christopher J. Schofield, who allowed me to work four months in his Chemistry Research group and for the great scientifically support during this time, my colleague and friend Dr. Benoît M. Liénard for the reading and meticulous revision of my dissertation and also for his kindly support during my stay in Oxford. I also would like to thank Dr. Neil J. Oldham for the helpful remarks.

Sincere thanks go to my supervisor in Liege, Prof. Jean-Marie Frère, who was a grand support during my stay in his working group at the Center of Protein Engineering.

Best thanks go also to Dr. Sandra Jost, Uwe Heinz, Dr. Nathanaël Delmotte and Dr. Hansjöerg Toll.

Finally, I would like to affectionately acknowledge my family and my friends for their patience, tolerance and moral support.

Most parts of the work have been published in the following articles:

Selevsek N, Tholey A, Heinzle E, Liénard BM, Oldham NJ, Schofield CJ, Heinz U, Adolph HW, Frère JM. (2006) Studies on ternary metallo-beta-lactamase-inhibitor complexes using electrospray ionization mass spectrometry. *J Am Soc Mass Spectrom.* 17(7): 1000-1004

Liénard BM, Selevsek N, Oldham NJ, Schofield CJ. (2007) Combined mass spectrometry and dynamic chemistry approach to identify metalloenzyme inhibitors. *ChemMedChem.* 2(2): 175-179

Selevsek N, Tholey A, Heinzle E, Adolph HW. Metal ion-specific modifications of structure and flexibility of metallo-beta-lactamase BcII: An amide hydrogen exchange study. (*Submitted*)

TABLE OF CONTENTS	
ABBREVIATIONS	8
ABSTRACT/ZUSAMMENFASSUNG	11
INTRODUCTION	13
1 THEORETICAL BACKGROUND	16
1.1 β -Lactam resistance.....	16
1.2 β -Lactamases	16
1.3 Metallo- β -Lactamases.....	17
1.3.1 Emergence of MBLs.....	17
1.3.2 Characteristic of MBLs subclasses	17
1.3.3 The MBL fold.....	18
1.3.4 Catalytic mechanism of MBLs.....	19
1.3.5 Flexibility/Dynamics at the active site of MBLs.....	20
1.3.6 MBL inhibition.....	21
1.4 Non-covalent interactions.....	22
1.4.1 Techniques for the study of non-covalent complexes	22
1.4.2 Study of metalloproteins using “native” ESI-MS.....	24
1.5 ESI-MS.....	26
1.5.1 Principle	26
1.5.2 ESI ion source design	28
1.5.3 Atmospheric-Vacuum Interface.....	29
1.5.4 Analysers	30
1.6 Hydrogen-Deuterium Exchange Mass Spectrometry (HDX-MS).....	32
1.6.1 Development of HDX-MS.....	32
1.6.2 Theory of the H/D exchange	33
1.6.3 Measurement of H/D rates by mass spectrometry	36
1.6.4 General procedure for HDX-MS experiments.....	37
1.6.5 Pepsin digestion.....	38
1.6.6 Loss of deuterium during sample preparation for MS analysis.....	38
1.6.7 Determination of hydrogen exchange rate constants.....	39
1.6.8 HDX with MALDI-MS.....	39
2 EXPERIMENTAL PROCEDURES	42
2.1 Materials.....	42
2.1.1 Substrates and Inhibitors	42

2.1.2	Reagents and Chemicals	42
2.1.3	Membranes and columns	43
2.2	Methods	43
2.2.1	Production and characterization of Enzymes and Apo-Enzymes	43
2.2.2	Quantitation of sulfhydryl groups using Ellman's reagent	44
2.2.3	Determination of Metal ion Affinities	44
2.2.4	Determination of inhibition constants	46
2.2.5	Preparation of samples for "native"- ESI-MS	47
2.2.6	"Native"-ESI-MS analysis	47
2.2.7	Preparation of samples for HDX-MS	48
2.2.8	Pepsin digestion	48
2.2.9	Assignment of peptic -peptides	49
2.2.10	Hydrogen deuterium exchange (HDX) experiments	49
2.2.11	Determination of deuterium content	50
2.2.12	Evaluation of HDX kinetics	50
2.2.13	MALDI-MS analysis	51
2.2.14	Circular Dichroism Spectroscopy	51
3	METAL AND INHIBITOR BINDING STUDIES USING „NATIVE“-ESI-MS AND UV SPECTROSCOPY: RESULTS	53
3.1	Importance of the buffer system for the measurement of metal-protein complexes by ESI-MS	53
3.2	Metal binding studies monitored using ESI-MS	54
3.2.1	Specificity of the metal - protein complex by ESI-MS	54
3.2.2	Determination of the metal binding mode with ESI-MS	58
3.3	Inhibitor binding studies performed by ESI-MS	60
3.3.1	Development/validation of the native ESI-MS technique for the screening of MBL inhibitors	60
3.3.2	Screening of new inhibitors using a Dynamic chemistry approach combined with "native" ESI-MS	66
3.4	Effect of inhibitors on the metal stoichiometry of MBLs determined by ESI-MS	67
3.4.1	Binding of inhibitors to cadmium and zinc BclII enzyme	69
3.4.2	Binding mode of (R,S)-thiomandelate to the CphA MBL	72
3.5	Effect of inhibitors on the metal binding mode of MBLs using UV	

spectroscopy	73
3.6 DISCUSSION	76
3.6.1 Validity of the ESI-MS method for the study of MBLs.....	76
3.6.2 Metal binding to MBLs.....	79
3.6.3 Inhibition of native and cadmium-bound MBLs.....	81
4 METAL AND INHIBITOR DEPENDENT PROTEIN FLEXIBILITY.....	87
RESULTS.....	87
4.1 Circular Dichroism (CD) spectroscopy	87
4.2 Hydrogen/Deuterium Exchange-Mass Spectrometry	88
4.2.1 Assignment of the peptic-peptides to BcII protein	88
4.2.2 Determination of the deuterium uptake for one in-exchange time	90
4.2.3 Quantification and structural interpretation of the Hydrogen/Deuterium Exchange kinetics	92
4.2.4 Hydrogen/Deuterium Exchange in the N-terminal domain of BcII	93
4.2.5 Hydrogen/Deuterium Exchange in the C-terminal domain of BcII	94
4.2.6 Effect of the inhibitor thiomandelate on HDX-MS for the different BcII protein species	97
4.3 DISCUSSION	100
4.3.1 Metal dependent protein structure and flexibility in BcII	100
4.3.1.1 Comparison of the apo-BcII and Me ₂ -enzyme	100
4.3.1.2 Comparing Cd ₂ -and Zn ₂ -BcII enzymes	102
4.3.1.3 Me ₁ -BcII enzymes	102
4.3.2 The influence of the inhibitor thiomandelate on the protein flexibility	
of BcII.....	104
4.3.2.1 Me ₂ -species.....	104
4.3.2.2 Me ₁ -species.....	104
5 CONCLUSION AND OUTLOOK	105
6 REFERENCES.....	107
APPENDICES	

ABBREVIATIONS

AAS	atomic absorption spectroscopy
AES	atomic emission spectroscopy
ATP	adenosine triphosphate
BclI	metallo- β -lactamase from <i>Bacillus cereus</i> 569/H/9
BlaB	metallo- β -lactamase from <i>Chryseobacterium meningosepticum</i>
cAMP	cyclic adenosine monophosphate
CCA	α -cyano-4-hydroxycinnamic acid
CcrA	metallo- β -lactamase from <i>Bacteroides fragilis</i>
CD	circular dichroism
CID	collision induced dissociation
CMP	cytosine monophosphate
CphA	metallo- β -lactamase from <i>Aeromonas hydrophilia</i>
Da	dalton
DCC	dynamic combinatorial chemistry
DMSO	dimethyl sulfoxide
DNA	deoxyribonucleic acid
DTNB	5,5'-dithiobis-(2-nitrobenzoic acid)
EDTA	diaminoethane tetraacetic acid
ESI	electrospray ionization
EXAFS	extended X-ray absorption fine structure
FA	formic acid
FAB	fast atom bombardment
Fez-1	metallo- β -lactamase from <i>Legionella (Fluoribacter) gormanii</i>
FTICR	fourier transform ion cyclotron resonance
FWHM	full width of half-maximum
H/D	hydrogen/deuterium
HDX	hydrogen/deuterium exchange
HEPES	4-(2-hydroxyethyl)-1-piperazine ethanesulfonic acid
HSQC	heteronuclear single quantum coherence
LC	liquid chromatography
ICP	inductively coupled plasma
ID	inner diameter

IMP-1	metallo- β -lactamase from <i>Pseudomonas aeruginosa</i>
IR	infrared
ITC	isothermal titration calorimetry
L1	metallo- β -lactamase from <i>Stenotrophomonas maltophilia</i>
LB	Luria-Bertani
MALDI	matrix assisted laser desorption/ionization
MBL	metallo- β -lactamase
mc	main chain
MCP	micro-channel plate
MF	mag-fura 2
MM	minimal medium
MS	mass spectrometry
m/z	mass to charge ratio
NMR	nuclear magnetic resonance
OD	outer diameter
PAC	perturbed angular correlation of γ -rays
PDB	protein data bank
PMF	peptide mass fingerprint
PSD	post source decay
Q-ToF	quadrupole-time of flight
RF	radio frequency
RNA	ribonucleic acid
SAR	structure activity relationship
sc	side chain
SDS	sodium dodecyl sulphate
SPR	surface plasmon resonance
TFA	trifluoroacetic acid
TM	thiomandelate
TRIS	2-amino-2-hydroxymethyl-1,3-propanediol
ToF	time of flight
VC	sample cone voltage
UV	ultraviolet

TABLE OF STANDARD AMINO ACID ABBREVIATIONS

1-letter code	3-letter code	Name	1-letter code	3-letter code	Name
A	Ala	alanine	M	Met	methionine
C	Cys	cysteine	N	Asn	asparagine
D	Asp	aspartic acid	P	Pro	proline
E	Glu	glutamic acid	Q	Gln	glutamine
F	Phe	phenylalanine	R	Arg	arginine
G	Gly	glycine	S	Ser	serine
H	His	histidine	T	Thr	threonine
I	Ile	isoleucine	V	Val	valine
K	Lys	lysine	W	Trp	tryptophan
L	Leu	leucine	Y	Tyr	tyrosine

ABSTRACT

The heterogeneity of the metal content observed in Metallo- β -Lactamases (MBLs) hampers the design of potential inhibitors. In the first part of the work, three representative members of the MBLs, namely BcII, CphA and L1 were investigated using mass spectrometric and spectroscopic methods. Experimental parameters for the detection of the metal-protein and ternary metalloprotein-inhibitor complexes using ESI-MS¹ were evaluated and optimized. SAR¹ determined in the gas phase were in agreement with kinetic assays performed in solution. This demonstrates the suitability of this technique for the screening for new inhibitors of MBLs and for the detection of metal:enzyme:inhibitor ratios. Competition-titrations in combination with ESI-MS, revealed that for different subclasses of the MBL, the inhibition by (*R,S*)-thiomandelate and *D*-captopril is strongly influenced by the nature of the metal ion and the metal content of the protein.

In the second part of the work, the metal ion dependent flexibility of different parts of the BcII protein was investigated using HDX-MS¹. It was shown that the metal-free enzyme was the least ordered structure and that the high flexibility at the metal binding site and the domain interface region in the Cd₁-enzyme might facilitate the transfer of the metal between the two binding sites. These findings deliver important parameters for future development of efficient inhibitors for these enzymes.

¹Abbreviations used are: ESI-MS, electrospray ionization mass spectrometry; SAR, structure activity relationship; HDX-MS, hydrogen deuterium exchange mass spectrometry

ZUSAMMENFASSUNG

Die heterogene Metallbesetzung in Metallo- β -Lactamasen (MBLs) ist einer der Hauptgründe für den bislang geringen Erfolg bei der Entwicklung effizienter Inhibitoren für diese Enzymklasse. Im ersten Teil der Arbeit wurden drei repräsentative Vertreter der MBLs (BcII, CphA und L1) mit massenspektrometrischen und spektroskopischen Methoden untersucht. Es wurden Methoden der „nicht denaturierenden“ ESI-MS¹ für den Nachweis von Metall-Protein- sowie ternärer Metallprotein-Inhibitor-Interaktionen entwickelt. Die mittels ESI-MS in der Gasphase ermittelten SAR¹ stimmten sehr gut mit den zuvor in Lösung ermittelten überein. Somit konnte gezeigt werden, dass ESI-MS eine geeignete Methode für die Bestimmung von Metall-Enzym-Inhibitor-Stöchiometrien und damit für die Identifizierung neuer effizienter Inhibitoren darstellt. Durch die Kombination von ESI-MS Experimenten mit Konkurrenztitrationen zeigte sich, dass die Hemmung verschiedener MBL-Subklassen mittels (*R,S*)-Thiomandelsäure und *D*-Captopril stark von der Art des gebundenen Metalls sowie von der Metall-Protein-Stöchiometrie beeinflusst wird.

Im zweiten Teil der Arbeit konnte mittels HDX-MS¹ gezeigt werden, dass beim metallfreien Enzym die Sekundärstruktur am wenigsten ausgeprägt ist und dass das Cd₁-BcII Enzym der metal-freien BcII Spezies sehr zu ähneln scheint, wenn nur das aktive Zentrum und die Interdomainen-Region betrachtet werden. Dies liefert ein tiefgehendes Verständnis der MBL sowie Grundlagen zur Entwicklung neuer Inhibitoren.

¹Abkürzungen: ESI-MS, Massenspektrometrie der Electrospray Ionisierung; SAR, Struktur Aktivitäts Beziehungen; HDX-MS, Wasserstoff Deuterium Austausch Massenspektrometrie

INTRODUCTION

One of the major bacterial resistance mechanisms against β -lactams is the production of metallo- β -lactamases (MBLs); they can inactivate β -lactams by hydrolysing their β -lactam ring using zinc ions as cofactors. The emergence of MBLs in pathogenic bacterial strains and their low sensitivity against carbapenems, compounds usually administered for the inhibition of the serine- β -lactamases, make them clinically relevant. To date, not a single MBL inhibitor has been found to be used in clinical therapy settings. In fact, the design of potent drugs is hindered by the little understanding of the real metal state of MBLs *in vivo* (1). The importance of the metal requirement for catalytic activity of the three subclasses B1-B3 MBLs is still matter of debate.

Although most crystal structures of subclass B1 enzymes show that both metal sites are occupied (1), the enzymes BcII from *Bacillus cereus* 569/H/9, CcrA from *Bacteroides fragilis*, BlaB from *Chryseobacterium meningosepticum*, and IMP-1 from *Pseudomonas aeruginosa* are active as mono- as well as di-zinc enzymes (2-5). Moreover, the B2 enzymes CphA from *Aeromonas hydrophilia* and ImiS from *Aeromonas veronii* *bv. sobria* are most active in their monozinc form (6, 7). For enzymes belonging to the subclass B3, which are generally considered as dizinc enzymes, it has been shown that for instance L1 from *Stenotrophomonas maltophilia* is also active as a monozinc enzyme (4). More recently, GOB from *Elizabethkingia meningoseptica* has been reported as a mono-zinc subclass B3 enzyme with a novel active site geometry (8).

In presence of substrates or inhibitors, the MBLs can adopt different metal stoichiometries. Wommer *et al.*, 2002 showed that the substrate imipenem induced negative cooperativity in metal ion binding for representative enzymes of subclasses B1-B3 (4). The authors proposed that the monozinc-MBLs are physiologically relevant species due to the fact that the free zinc concentration in the bacterial cytosol is only femtomolar. Binuclear zinc MBLs might be an artefact due to the high concentrations of zinc usually required for its production *in vitro*.

Known inhibitors of MBLs have also been shown to influence the MBL metal content. Most of the reported data were acquired on cadmium-substituted MBLs, also representing catalytically active species. For the cadmium-substituted BcII enzyme

positive cooperativity in metal binding was observed in presence of thiomandelate, a known MBL broad-spectrum thiol inhibitor (9), whereas the presence of *D*-captopril (another potent *in-vitro* MBL thiol inhibitor) decreased the affinity for a second cadmium ion binding (10). Furthermore, structural data in solution and in the crystal state have revealed that *D*-captopril adopts different binding modes when bound to a sub-class B1, B2 or B3 MBL (1).

Another particular feature of the MBLs is the important variation in position, number and type of solvent molecules required for metal coordination. The positions of the amino acids interacting with the metal ions can be different even within the same subclass. Perturbed angular correlation spectroscopy (PAC) or Nuclear magnetic resonance spectroscopy (NMR) have been used to provide some valuable information on the metal coordination geometry. The combination of PAC and NMR have revealed a dynamic process at the metal binding sites, demonstrating an intramolecular exchange of the cadmium between the two available binding sites (11).

AIMS OF THE WORK

In the first part of this work and in collaboration with partners from the European network MEBEL, it has been set to develop and apply a “non-denaturing”-Electrospray Ionization Mass Spectrometry (ESI-MS) method in order to detect potential metalloprotein-ligand complexes with the aim to identify new MBL inhibitors. Additionally, the influence of the inhibitors on the metal stoichiometry in MBLs has been investigated using the ESI-MS approach together with competition titrations performed in solution.

The second part of the work is focused on the overall protein flexibility and the modification of MBL active site dynamics upon metal and ligand binding using a hydrogen-deuterium exchange mass spectrometry (HDX-MS) method.

CHAPTER I

THEORETICAL BACKGROUND

1 THEORETICAL BACKGROUND

1.1 β -Lactam resistance

β -lactam antibiotics are potent antimicrobial agents that inactivate the transpeptidases (eg. Penicillins-Binding Proteins or PBPs) involved in the bacterial cell wall synthesis (12). They have been administered for over five decades for the treatment of community-acquired infections. However, the emergence of several pathogenic strains resistant to β -lactams led to the revision of the current therapies. In fact, bacteria have developed different escape strategies against the antimicrobial drugs. The most common mechanism of resistance is the production of β -lactamases which can inactivate the antibiotic by hydrolysing the amide bond of its β -lactam ring (Figure 1.1).

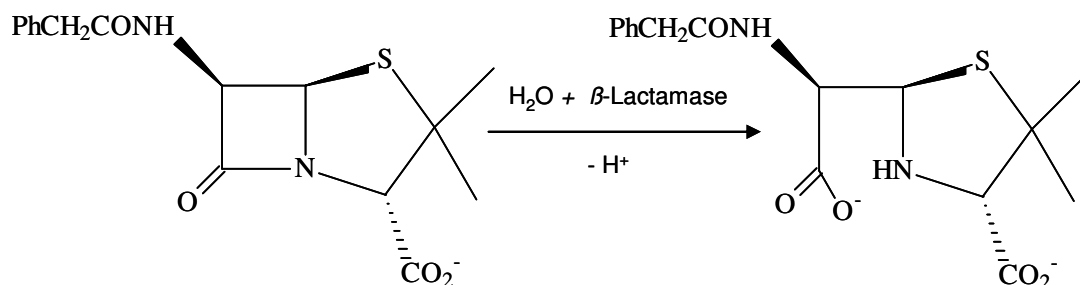


Figure 1.1: Scheme of the hydrolysis of a β -lactam antibiotic (benzylpenicillin) by a β -lactamase.

1.2 β -Lactamases

β -lactamases have been divided into four classes (A-D) based on either their molecular structure or function (13). Classes A, C and D are serine- β -lactamases which require an active site serine residue to catalyse the ring opening of the β -lactams and are mostly penicillininases or cephalosporinases. Class B enzymes, called metallo- β -lactamases (MBLs), use one or two zinc ions in their active site for their activity and show a broader substrate profile as the serine- β -enzymes. MBLs also hydrolyse carbapenems (e.g. imipenem) and penems and are not inhibited by the clavams commonly used to inhibit the serine- β -lactamases (14). MBLs have now

become clinically extremely relevant and a lot of efforts have been put into the characterization of the MBLs in order to develop efficient inhibitors.

1.3 Metallo- β -Lactamases

1.3.1 Emergence of MBLs

The first MBL was isolated from *Bacillus cereus* 569/H/9 in 1966, where EDTA was shown to inhibit the cephalosporinase activity (15). As *Bacillus cereus* is a non-pathogen organism and the isolate was the only example of these zinc-dependent enzymes, the discovery was only considered as a curiosity. In the early 80's, an increased number of MBLs was isolated from many organisms even from pathogens such as *Stenotrophomonas maltophilia* or *Pseudomonas aeruginosa* (16). More frightening was the identification of a gene coding for a MBL in *Bacillus anthracis* (17). Their fast dissemination could be explained by the location of their encoding genes on mobile DNA plasmids, which allow horizontal gene transfer (18).

1.3.2 Characteristic of MBLs subclasses

Combination of X-ray structure data and sequence alignments enabled the division of the MBLs into three subclasses (B1-B3) (19). The classification is based on both, the metal-ligands composition of the two binding sites, and their substrate profile. In the subclass B1, three His constitute the metal binding site 1 and one His, one Cys and one Asp form the metal binding site 2 as shown for the BcII enzyme from *Bacillus cereus* (Figure 1.2A). In subclass B2, only one His is replaced by one Asn in the site 1, the rest of the active site residues being identical with those from subclass B1. Zinc- β -lactamase CphA from *Aeromonas hydrophilia* is one of the representative MBLs of subclass B2 (Figure 1.2B). The same metal-binding residues are present in site 1 for subclass B3 compared to subclass B1, but the Cys from metal binding site 2 is replaced by a His as illustrated in the case of the L1 enzyme from *Stenotrophomonas maltophilia* (Figure 1.2C). B1 and B3 enzymes generally exhibit a broad substrate profile, whereas the subclass B2 enzymes are carbapenem specific.

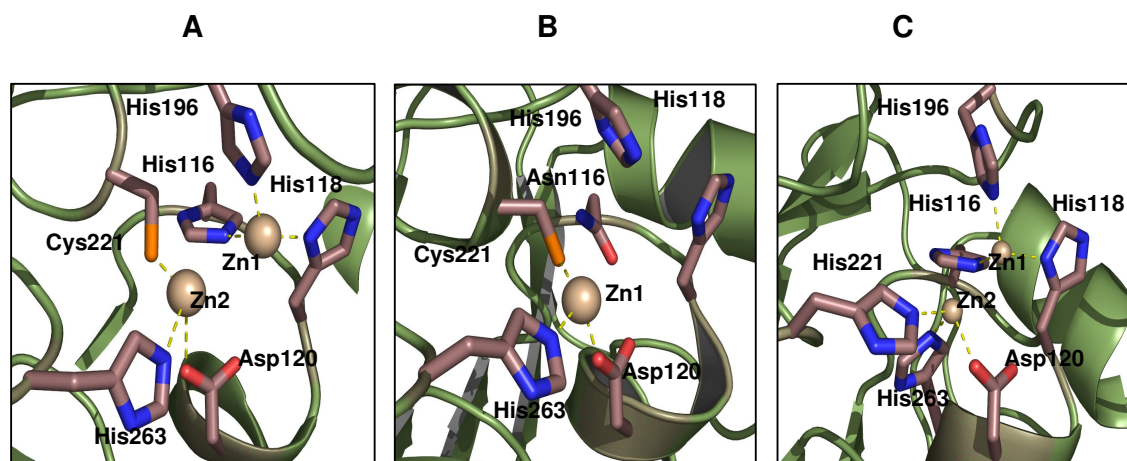


Figure 1.2: Active site views of Metallo- β -lactamases BclI from *Bacillus cereus* (A), CphA from *Aeromonas hydrophilia* (B) and L1 from *Stenotrophomonas maltophilia* (C) created with the PyMOL program. The metal ligands are represented as stick models and the metals as spheres. The atom coloring scheme is blue for nitrogen, red for oxygen, orange for sulfur, fawn for zinc, and gray for carbon. The residue-numbering scheme is the standardized version from reference (20).

1.3.3 The MBL fold

Despite the low similarity of their amino acid sequences, all known MBLs revealed a $\alpha\beta\beta\alpha$ fold composed by two central β -sheets and five solvent-exposed α -helices (Figure 1.3). The N- and C- terminal domains, containing one β -sheet and two α -helices each, can be superimposed by a 180° turn around a central axis, suggesting that the structure is the result of gene duplication (21). The active site is located in a long channel between both domains. Residues from each binding site are distributed between the N- and C- terminal domains. The MBL fold together with the highly conserved metal binding site are the characteristics of the MBL superfamily (22, 23), which contains a wide range of proteins with diverse functions like glyoxylase II, aryl sulfatase, cAMP phosphodiesterases or CMP-N-acetyl neuraminic acid hydrolases (23, 24). Interestingly, an independent group within the MBL superfamily, involved in DNA repair (e.g. Artemis) (25, 26), also contains the MBL fold, but its function remains unclear.

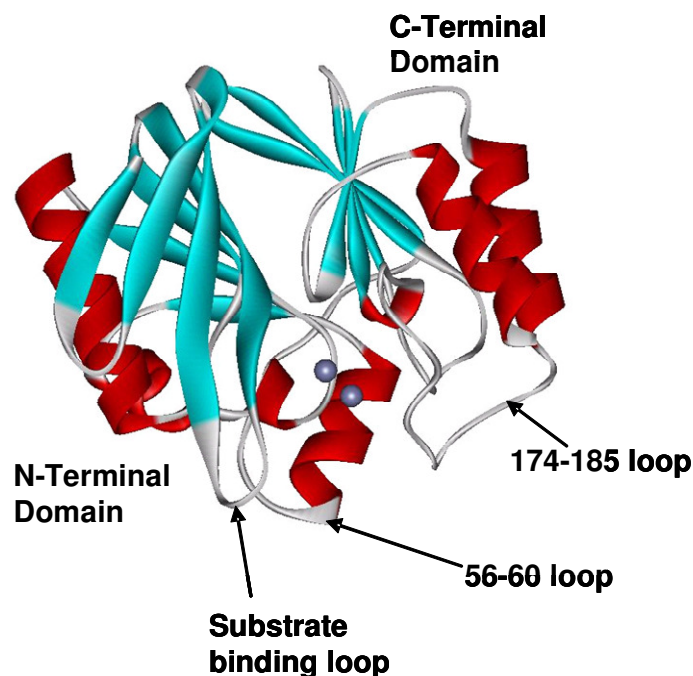


Figure 1.3: Ribbon representation of the BcII enzyme from *Bacillus cereus* 569/H/9 (Protein Data Bank, accession number 1BVT) created with the PyMOL program. BcII is a $\alpha\beta$ -sandwich structure with α -helices on the external faces. The N-terminal domain includes a β -sheet made of seven β -strands (in blue), three α -helices (in red) and two characteristic loops (i.e. substrate binding loop and 56-60 loop) (in grey). The C-terminal domain includes a β -sheet made of five β -strands (in blue), two α -helices (in red) and one characteristic loop (i.e. 174-185 loop) (in grey). The metal ions are represented as spheres (in violet).

1.3.4 Catalytic mechanism of MBLs

Although the active site of subclass B1 MBL is constituted of two metal binding sites (1), crystal structures of these enzymes were solved in complex with one and two Zn(II) ions (21, 27, 28). Furthermore the catalytic activity was shown to be dependent on the $[\text{Metal(II)}]/[\text{E}]$ ratio. Indeed, BcII a well know representative of subclass B1 MBL, is active with both one and two zinc ions in its active site which implies two different catalytic mechanisms (2). Similar conclusions were made for the CcrA enzyme of *Bacteroides fragilis* (3), which were later contradicted by another study demonstrating the positive cooperativity in metal binding, leading to the conclusion that only the di-Zn form of CcrA is relevant for the catalysis (29). Based on structural and kinetic data, two different catalytic mechanisms were proposed for the zinc-enzyme BcII. In the monozinc-form, Cys168 is proposed to act as a proton acceptor

for the Zn(II)-bound water; thus allowing the nucleophilic attack at the β -lactam carbonyl by the hydroxide ion which eventually leads to the amide bond fission. This fission might be facilitated through deprotonation of the tetrahedral intermediate by Asp90, which by generating a dianionic tetrahedral intermediate, donates the proton to the amine nitrogen (Figure 1.4) (30). In the di-zinc-form of BcII, Cys168 is not required to catalyse the reaction. Instead, the bridging hydroxide ion between the two metals directly attacks the β -lactam-ring (3, 31).

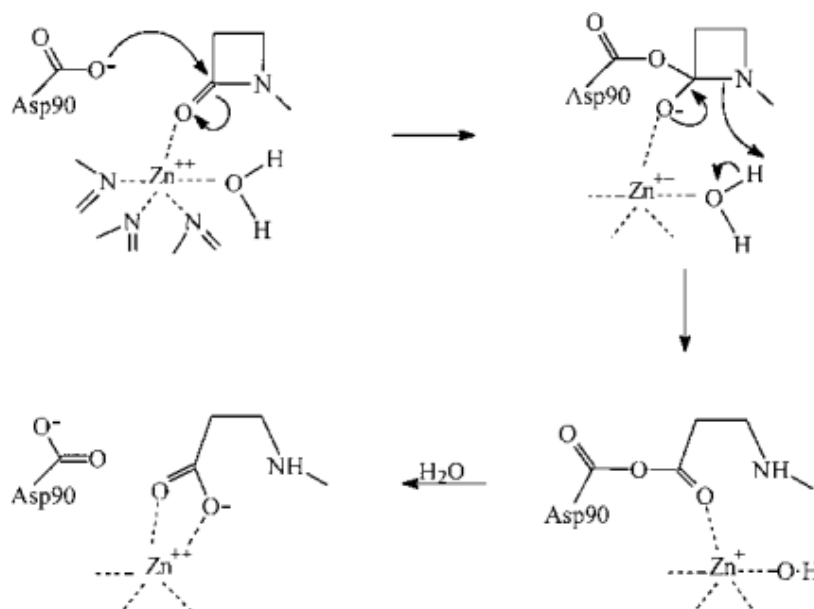


Figure 1.4: Catalytic mechanism of the β -lactam hydrolysis by the mono-Zn enzyme BcII from *Bacillus cereus* 569/H/9 (30). Possible reversible formation of the tetrahedral intermediate and its deprotonation by Asp90.

1.3.5 Flexibility/Dynamics at the active site of MBLs

Although the metal binding amino acids are identical among the available crystal structures of subclass B1, great variability in the position and type of solvent ligands have been detected, even for the position of the residues interacting with the metals (27, 28, 32-38). Consequently, several studies were carried out to investigate the degree of flexibility around the metal binding sites, especially focusing on the BcII enzyme. To provide some information on the metal coordination nature, spectroscopic techniques such as perturbed angular correlation (PAC) or nuclear magnetic resonance (NMR) can be used. In both techniques Zn(II) could not be

used as a spectroscopic probe and was always replaced by catalytically active Cd(II) (33). Previous studies using PAC spectroscopy performed on BcII indicated that at low [Cd(II)]/[E] ratios the single metal ion was distributed between both binding sites (33). Combination of PAC and NMR data revealed a dynamic process at the metal binding sites, due to the supposed intramolecular exchange of the cadmium ion between the two available binding sites (11). Later, this intramolecular exchange was also suggested for the zinc-enzyme (39).

1.3.6 MBL inhibition

To date, a considerable number of small organic molecules have been tested for inhibition of the MBLs. A recent review by Heinz *et al.*, 2004 has reviewed the different classes of reported MBL inhibitors (1): tricyclic natural products, trifluoromethyl alcohols and ketones, hydroxamic acids, mercaptocarboxylates, biphenyl tetrazoles, carbapenem and penicillin derivatives, cephamycins and moxalactam, thiols, cysteinyl peptides, inhibitors derived from single-domain antibody fragment elicited in the Camelidae, thioesters derivatives, phenazines from a *Streptomyces*, succinic acid derivatives, sulphonyl hydrazones, disulfides, thiol-substituted penicillin inhibitor, degradation products of cephalosporins, captopril, thiomandelic acid. Recently benzohydroxamic acids (40) and pyridine carboxylates (41) were also identified as potential inhibitors of MBLs.

Potent in-vitro MBL inhibitors such as succinic acid (42) and mercaptocarboxylic acid derivatives (38, 43) have also been reported, displaying some inhibition constants in the low nanomolar range. Most of the inhibition studies were performed using the di-Zn forms of the MBLs, at the exception of CphA which was considered as a monozinc-enzyme (6). In most cases, crystal structures revealed that the MBL bound inhibitor replaces the zinc bound-water molecules and acts as new metal ligand (1). For instance, it was shown that the sulphur group of thiol-containing inhibitors is chelated by both metal ions in binuclear enzymes (38, 44). Moreover, the same inhibitor can have different binding modes among the three MBL subclasses as it was shown for the inhibitor *D*-Captopril (10, 44, 45). Inhibitors can also change the affinity of the enzymes for the metal ions; mononuclear enzymes can be dinuclear in presence of an inhibitor (9) or the single metal ion can be stabilized in one binding site of the enzyme (10).

1.4 Non-covalent interactions

Weak reversible interactions between proteins, proteins and ligands or proteins and metal ions are involved in most of the biological processes such as in signal transduction pathways (e.g. binding of extra cellular signalling molecules to receptors), in DNA replication, in RNA and protein synthesis and in all metabolic pathways (e.g. substrate recognition by the enzymes). The reversibility of the interactions is a prerequisite for the correct regulation of many of these processes. These weak binding features are also required for the proper folding of proteins. There are four main types of non-covalent interactions: electrostatic, hydrophobic, hydrogen bonding and van-der-Waals interactions. The nature of binding differs by their strength, geometry and specificity (46). Table 1.1 summarises the different non-covalent interactions together with typical values of binding energies.

Table 1.1: Binding energies of the non-covalent interactions compared with those of the covalent interactions.

Non-covalent Forces	Binding energy (kJ/mol)
electrostatic	42
hydrogen bonding	8-21
hydrophobic	4-8
van der Waals	4
Covalent bonds (C-C)	300

1.4.1 Techniques for the study of non-covalent complexes

Conventional methods

There are several established methods that are used for the study of non-covalent macromolecular interactions: native gel electrophoresis, co-immunoprecipitation and two hybrid-screening techniques allow the identification of binding partners of weak complexes; gel permeation chromatography and analytical ultracentrifugation are used to determine the binding stoichiometry between the two associates in solution

whereas nuclear magnetic resonance (NMR) and X-ray crystallography deliver structural informations about the molecular interactions. Binding affinities can even be determined using surface plasmon resonance (SPR), circular dichroism (CD) spectroscopy, light scattering, UV and fluorescence spectroscopy, isothermal titration calorimetry (ITC) or radioactive and fluorescence labelling techniques. Most of these techniques are often time consuming, require high amounts of proteins and/or do not offer sufficient resolution to detect interactions between proteins and small compounds.

Mass spectrometry as a tool for the detection of non-covalent complexes

Since the development of Matrix Assisted Laser Desorption Ionization (MALDI) (47, 48) and Electrospray Ionization (ESI) (49), two soft ionisation methods, mass spectrometry (MS) has become an indispensable tool for protein analysis. In fact, the mass of a large number of macromolecules, such as peptides (50), oligonucleotides (51), small compounds (52) and also proteins with high molecular weight (53) can be determined. The speed, specificity and sensitivity (atomole amounts) of MS analysis are great advantages compared to conventional methods. Mass spectrometry techniques have first been applied for peptide sequencing (54, 55); after protein digestion, peptides are fragmented by collision induced dissociation (CID) and the experimental mass values are then compared with calculated fragment ion mass values which are stored in a database to enable protein identification. Later, the method was used for the study of protein-protein complexes in native (56) or denaturing gel electrophoresis by analysis of their protein digestion pattern. In denaturing gels, the molecules are crosslinked before they are loaded on the gel (57). Furthermore, to identify and determine binding constants of small compounds interacting with proteins, bioaffinity based liquid-chromatography-mass spectrometry (LC-MS) screening methods have been used (58). The binding partners are eluted from the chromatographic columns containing the target proteins and submitted to LC-MS for identification and quantification.

When “non-denaturing” (or “native”) conditions are used, mass spectrometry can be used for direct detection of non-covalent complexes. The groups of Ganem (59), Katta and Chait (60) were the pioneers of “native” mass spectrometry, demonstrating that weak interactions between proteins and ligands can survive the ionization process. Since then, many non-covalent complexes have been characterized using

“native” mass spectrometry including protein-protein- (61), protein-ligand- (62), protein-metal- (63) or protein-DNA- interactions (64). Most of these studies were performed using the electrospray as ionization technique. In contrast to MALDI, in ESI ions are generated directly from aqueous solutions under near physiological conditions, facilitating the detection of weak complexes. Further, the detection of unspecific cluster ions in mass spectra, normally hindering the correct evaluation of binding stoichiometries, is a major problem in MALDI-MS. These non-specific interactions might be formed in the gas-phase after the desorption process (65).

1.4.2 Study of metalloproteins using “native” ESI-MS

Metal-protein interactions

Together with “native” ESI-MS, many other techniques can be used to study metal-protein interactions. Atomic absorption spectroscopy (AAS) or inductively coupled plasma (ICP) with atomic emission spectroscopy (AES) or mass spectrometry (MS) detection allowed the determination of the metal content of metalloproteins. However they are unable to distinguish between the different metal-substituted species coexisting in solution. By combination of high pressure liquid chromatography (HPLC) using neutral pH elution conditions with ICP-MS and ESI-MS, metalloprotein isoforms such as metallothioneins can be separated and their metal stoichiometries can be determined (66). However, such techniques are mainly used for the study of metalloprotein isoforms already present in biological samples rather than for reconstituted metal-loaded species of purified proteins. The simultaneous detection of different metal-binding protein species can be easily performed by “native” ESI-MS. Generally, the binding of metal ions to the corresponding protein is observed by monitoring the m/z shifts of the ion peaks in the ESI mass spectra of the apoprotein. When titrating the apoprotein (P) with increasing amounts of metal ions (L), the ion intensities of metal-loaded species (PL_n) can be determined for each metal concentration. In 1990, Fenselau and coworkers were the first to apply “native” ESI-MS to metalloproteins by investigating the metal binding mode of Zn(II) and Cd(II) ions to metallothioneins (67). Later, Ca(II)-calmodulin (68) and Zn(II)-peptides stoichiometries (69) were determined using the same approach.

Metalloprotein-inhibitor interactions

“Native” ESI-MS is also a very useful tool for the direct detection of metalloprotein-inhibitor complexes. The relative intensities between the free and the ligand-bound metalloprotein ions observed in the ESI spectra can be compared to determine the ligand binding affinity. Competitive binding experiments can be performed by adding equimolar amounts of several inhibitors to the target protein in solution. The relative abundance of a ligand-bound species measured by ESI-MS depends on the relative affinity between this species and all the other complexes present in solution. As illustrated in Figure 1.5, the relative abundance observed for inhibitor B is higher than the one observed for inhibitor A. It can therefore be concluded that inhibitor B has a higher affinity for the target protein compared to inhibitor A.

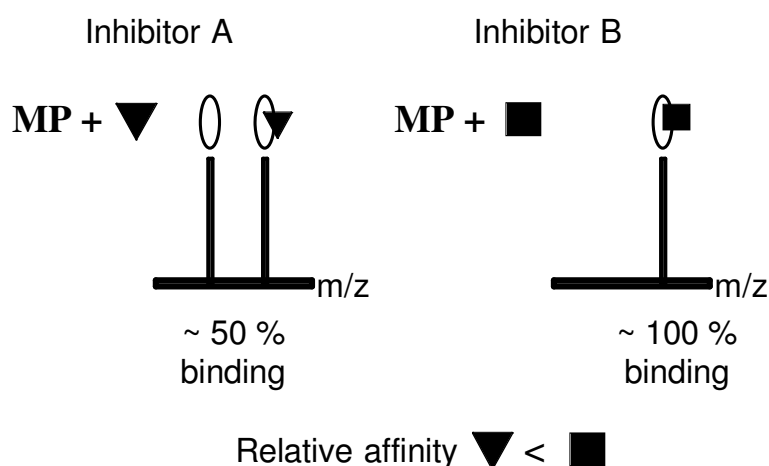


Figure 1.5: General procedure for the determination of relative binding affinities of ligands (inhibitors A and B) observed by “native” ESI-MS. MP represented a metalloprotein.

Cheng and coworkers applied this method for the screening of two small libraries (7 and 18 inhibitors derived from para-substituted benzenesulfonamides) for the bovine carbonic anhydrase II (70) and later with larger peptide libraries (289 and 256 compounds derived from 4-carboxybenzenesulfonamides) (71). Due to the complexity of the ESI mass spectrum, a high resolution ESI-mass spectrometer and tandem mass spectrometry (MS^n) experiments were required for the correct identification of the inhibitors. Additionally, the relative ion intensities of the free

ligands themselves in the low m/z range allowed to determine their relative binding affinities in solution. In complex compound mixtures, a mass analyser with high mass resolution, such as Fourier Transform Ion Cyclotron Resonance (FTICR), or the simplification of the mixture by a pre-separation step, is essential for the correct identification of the different inhibitors. To provide the absolute binding constant values, competitive binding experiments can be performed in presence of a ligand of known binding affinity to the target protein (72). Direct quantification of binding constants is also possible by scatchard plot analysis; here, the ion abundance of the bound and unbound species is monitored for increasing amounts of the selected inhibitor (73).

1.5 ESI-MS

Electrospray ionisation (ESI) mass spectrometry (MS) is one of the most prevalent techniques used for the study of non-covalent complexes (61). Together with the technical improvement of ESI sources and analysers, the number of published "native" ESI-MS studies has increased considerably during the last 15 years.

1.5.1 Principle

The generation of ions by the electrospray (ES) technique was first accomplished by Dole in the 1970's. In this report, a solution of high-molecular weight polystyrene was sprayed at atmospheric pressure. Unfortunately, the mass of the produced ions could not be directly determined (74, 75). Later, the Fenn group was able to observe the ions generated from smaller molecules with a quadrupole analyser, which provided a better understanding of the processes occurring during electrospray formation. In 1984, a mass spectrometer incorporating a highly sensitive electrospray ionisation source was designed (76, 77).

The ionisation by ES starts with spraying of a dilute sample solution through a strong electric field, which finally leads to an effective ionisation of the dissolved analytes. The electric field is formed by a high voltage difference between a capillary needle (metal), where the solution is infused, and a counter electrode. Due to the induced electric forces, the solution starts to nebulise and, because of the polarity of the capillary, the molecules are ionized with the excess of positive or negative charges.

Later, the ions are beamed through the orifice of the counter electrode and led into the mass spectrometer, where they can be separated according to their respective m/z ratios. Frequently the spray is pneumatically assisted with a concentric flow of an inert gas such as nitrogen to provide a better nebulisation. When the repulsion of similarly charged ions and the attraction of the counter electrode exceed the surface tension of the solution, the destabilised liquid forms a cone ("Taylor cone") as schematised in Figure 1.6.

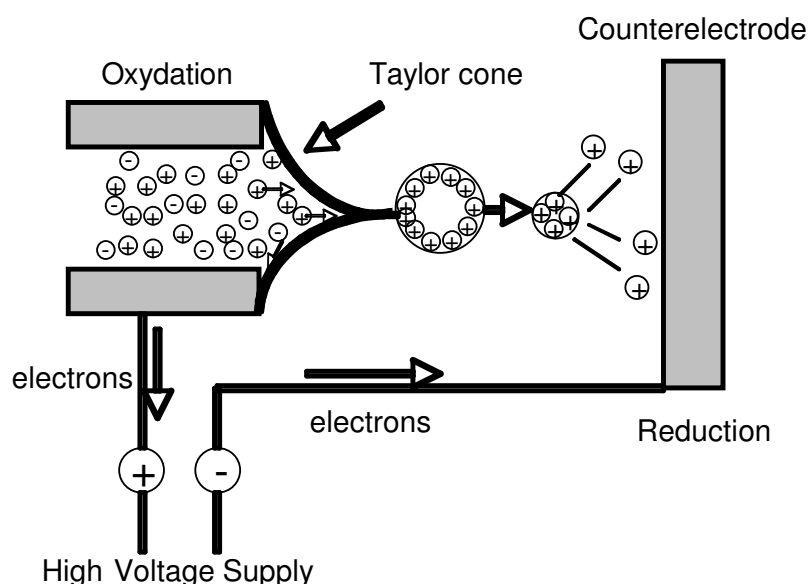


Figure 1.6: Schematic representation of the electrospray ionisation process, resulting in the formation of the "Taylor cone" and small offspring charged droplets.

At the end of the Taylor cone, the charged droplets are then emitted (liquid filament). The continuous evaporation of the solvent in the droplets progressively induces a diminution of its size. Thus, the charge density increases by a constant charge state of the droplet. When the radius of the droplet reaches a certain limit (Rayleigh stability limit), the repulsive Coulomb-forces exceed the surface tension forces of the liquid, which induces the explosion of the droplet into smaller offspring droplets. Two models have been proposed for the theory of the ion emission into the gas phase. The first one stipulates that successive explosions conduct to the formation of droplets, where only one ion is contained. The ion is then transferred into the gas phase by the evaporation of the solvent (74). The second theory postulates that when

the size of the droplets is relatively small, the field strength at the surface of the droplet is sufficiently strong to directly extract the ions from the droplet into the gas phase (78, 79).

1.5.2 ESI ion source design

Nano-electrospray

In many applications, nanoliter flow rates (20-50 nl/min) are required, which can be obtained with a nano-electrospray (nanoESI) device. Wilm and Mann demonstrated that the thinner the spray capillary, the smaller are the droplets and the lower are the flow rates (80). In nanoESI, the generated spray is not assisted by pneumatic nebulisation. The droplet size obtained from nanoESI is less than 200 nm, i.e their volume is about 100 to 1000 times smaller than the droplets generated using conventional ESI. Consequently, the nanoESI sources enable the analysis of samples in high polarity solvents such as pure water; the effect of corona discharge is there minimized. Lower sample consumption and higher salt concentration tolerance can also be achieved as with conventional ESI. In fact, the smaller size of the droplets in nanoESI reduces the competition between salt and analytes on the surface of the droplet (81).

Nano-electrospray from a chip

For high sample throughput in nanoESI experiments, a silicon chip with 10 X 10 array of nanoESI spray nozzles (10 um ID X 30 um OD X 75 um length) was developed (82). Sample solutions are supplied from a pipette tip making contact with the back of the chip. High voltage is applied on the electrically conducting coating of the tip. A robotic device called NanoMate® provides the automated infusion of samples at low flow rates. It also includes the ESI Chip and a software for automatic chip handling (Figure 1.7).

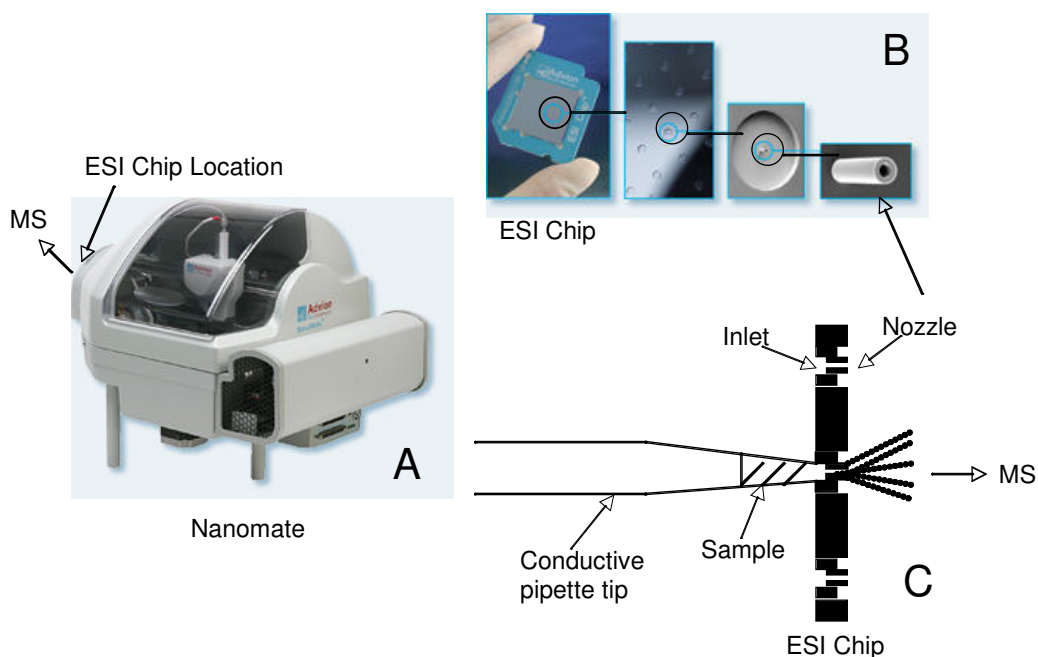


Figure 1.7: Nanomate® system developed by Advion Biosciences for the automatic infusion of MS samples (A). The 100 nozzles containing ESI chip with a close-up on a single spray nozzle are represented. Picture was downloaded from <http://www.advion.com/images/img-newesichip.gif> (B). Schematic representation of a conductive pipette tip making contact with the back of the Advion chip. Reproduced from the nanomate User's manual (C)

1.5.3 Atmospheric-Vacuum Interface

Following the ionisation process at atmospheric pressure, the ions are guided through an atmospheric-vacuum interface before they reach the analyzer. The interface consists of i) an orifice through which the ions are introduced, ii) pumping stages to reduce the pressure and iii) ion optics to improve the ion transmission to the analyser. The vacuum interface also helps to complete the desolvation of the ions. In this region, under a pressure of 1-3 mbar, the accelerated ions collide with the residual gas molecules leading to the break-up of solvent clusters. The ion acceleration is produced by applying a voltage (cone voltage) between the sampling cone and the next extraction lens (extraction cone). Increase of the accelerating voltage (VC), higher internal energy is communicated to the ions through collision with gas molecules, which induces the dissociation of the weakest binding interactions. This process is also called collision induced dissociation (CID) (83). The

effect of the accelerating voltage can be used for the study of the stability of non-covalent complexes (84).

1.5.4 Analysers

Time of Flight analyser

The principle of a time of flight (ToF) analyser is to measure the time of the ions to traverse a field-free tube (Figure 1.8). Since all ions of the same charge receive the same kinetic energy prior to their entrance into the flight tube, the lighter ions arrive earlier than heavier ones at the detector. The time of flight of an ion varies with the square root of its mass-to-charge ratio (m/z).

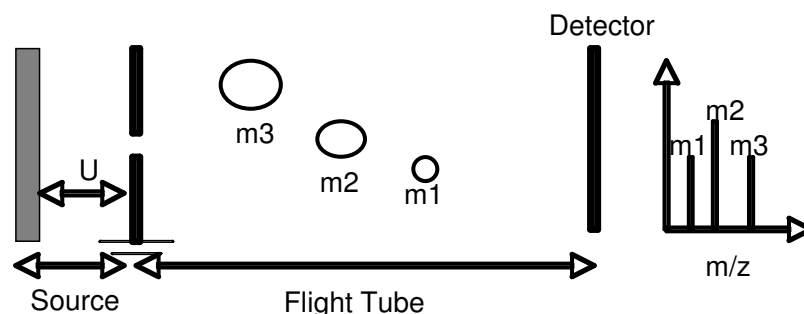


Figure 1.8: Schematic representation illustrating the principle of the time of flight (ToF) mass spectrometer. After acceleration through the electric field, the ions are separated in the flight tube according to their m/z ratios.

Resolution of a ToF mass analyser

The resolution of a ToF mass analyser is defined by the full width at half maximum (FWHM) of the peaks, $m/\Delta m_{\text{FWHM}}$. Δm_{FWHM} is the width of a single peak at 50 % height. Thus, the increase of the tube length will increase the mass precision. Furthermore, the resolution of the ToF analyser can also be improved with a reflectron installed at the end of the tube. The reflectron is composed of series of metal rings, where increased voltages are applied. The kinetic energy distribution of ions with same m/z ratios can then be corrected. In fact, ions with high kinetic energy can penetrate deeper into the potential gradient and take longer to turn around compared to ions with lower kinetic energy.

Hybride Q-ToF mass analyzer

Hybride mass analyses, which combines two mass analysers, are frequently used to perform tandem mass spectrometry. In the study of non-covalent complexes, a quadrupole analyser coupled with an orthogonal ToF analyser can be used (Figure 1.9). A continuous ion beam from the quadrupole hits the entrance of the ToF analyser. Packets of ions are reaccelerated into the ToF in a direction orthogonal to the axis of introduction. The reacceleration of ions is possible by pulsed injection via the pusher.

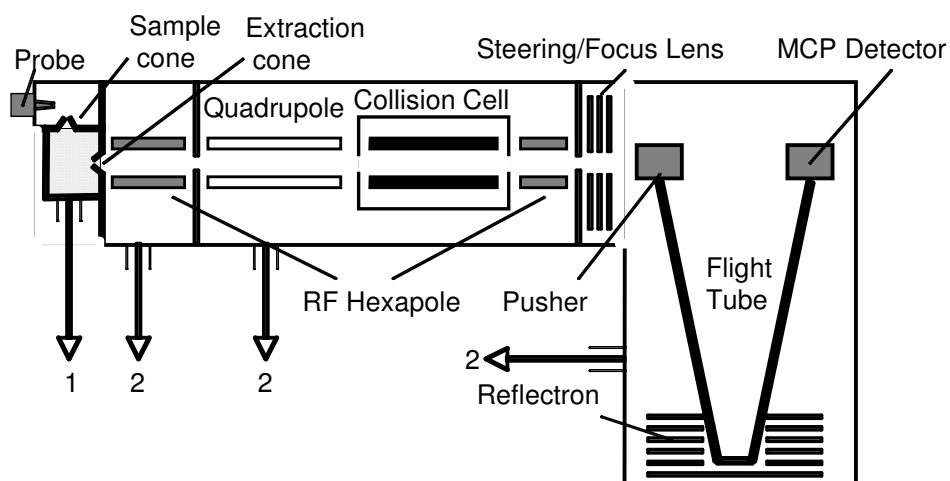


Figure 1.9: Schematic representation of an ESI-Q-ToF (Q-ToF II of Micromass) used for the analysis of non-covalent complexes. The atmospheric vacuum interface is represented between the sample cone and the extraction cone of the instrument. 1 and 2 are the source and turbomolecular pumps, respectively.

1.6 Hydrogen-Deuterium Exchange Mass Spectrometry (HDX-MS)

1.6.1 Development of HDX-MS

More than 50 years ago, Linderstrøm-Lang and co-workers used hydrogen exchange experiments in order to prove that protein conformations protect the amide protons from being exchanged with hydrogens from the solvent (85). Protein structure and dynamics were also probed by using tritium labelling and radiation counting experiments (86). Ultraviolet spectroscopy and neutron diffraction have also been used to study the hydrogen/deuterium exchange (87, 88). At present, there are two main techniques used to monitor hydrogen exchanges in proteins, multi-dimensional nuclear magnetic resonance (NMR) (89, 90) and mass spectrometry (MS) (91). Both methods can provide the localisation of the exchanged amide proton and the determination of the exchange rates in specific regions of the protein. The NMR technique enables the assignment of hydrogen exchange rates to single amides in the protein, but the complete assignment of all amides is arduous and often not reached. Further, high protein amounts are required by NMR to follow correctly the HDX rates of the assigned amide protons.

Alternatively, mass spectrometry can be used for the detection of deuterium uptake in peptides and proteins via the determination of their molecular masses. The advantages compared to NMR are multiple and include higher sensitivity, protein solubility (adapted for hydrophobic proteins) and no limitation to the size of the proteins. In 1991, Katta and Chait were the first to report the quantification of incorporated deuteriums into a protein using mass spectrometry (60). To measure the H/D exchange of localised regions of the target protein, the labelled macromolecule can be fragmented by proteolysis under isotopic quench conditions. Zhang and Smith combined protein fragmentation with HDX-MS using Fast-Atom-Bombardment (FAB) as ionisation source (91). Johnson and Walsh then improved the amide coverage with the use of LC-ESI-MS to study the stability of the myoglobin-heme complex (92). Later, the major challenge facing the HDX technique was to prevent the back exchange of incorporated deuteriums to hydrogens during the sample preparation for the MS analysis (93).

Matrix Assisted Laser Desorption Ionization (MALDI) is another ionisation technique, which can be used in combination with HDX. Although higher back exchange and lower sequence coverage is usually obtained compared to when using ESI-MS, the

absence of the HPLC step enables the data to be collected faster. The Komives group investigated the ligand binding sites in c-AMP-dependent protein kinase and in thrombin using HDX-MALDI-MS. Their HDX results were in good agreement with the X-ray data of the two proteins (94, 95).

1.6.2 Theory of the H/D exchange

The hydrogen/deuterium exchange acts on peptide amide bonds and can be both catalyzed by acids or bases. The rate constant for hydrogen exchange, k_{ex} can be expressed as the sum of the rate constants for acid (k_H) and base (k_{OH}) catalysed exchange, as indicated in the Equation 1.1.

$$k_{ex} = k_H [H^+] + k_{OH} [OH^-] \quad \text{Equation 1.1}$$

Studies on H/D techniques using polyalanine as a model peptide indicated that k_H and k_{OH} have values of 41.7 and $1.2 \times 10^{10} \text{ M}^{-1} \text{ min}^{-1}$ at 20 °C, respectively (96, 97). Isotopic exchange rates are pH and temperature dependent (97). The isotopic exchange rate, k_{ex} , for the model peptide polyalanine is shown in Figure 1.10 as a function of pH (98). The chemical exchange rate has been found to be the slowest at pH 2.3; further, the amide hydrogen exchange rate decreases 3-fold for each 10 °C. Additionally, adjacent amino acid side chains can also influence the exchange rate of a peptide amide proton by inductive and steric effects (97).

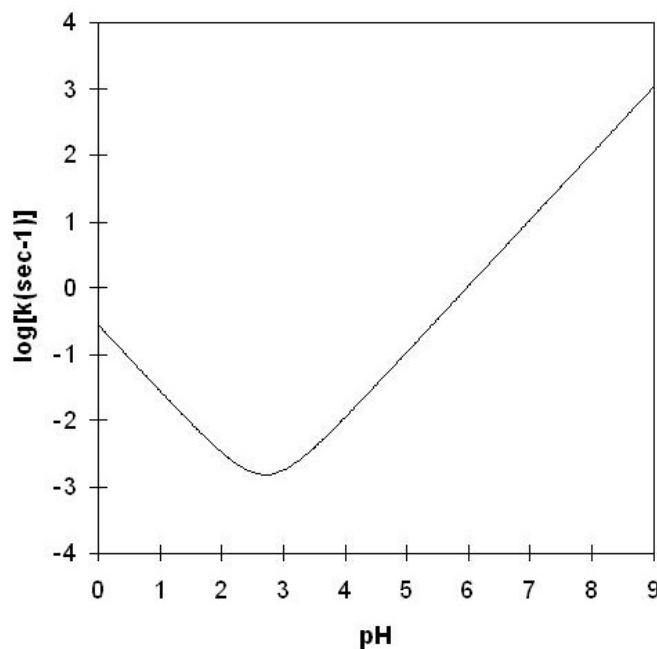


Figure 1.10: Rate constant for the isotopic exchange of hydrogen located on peptide amide linkages for a model polyalanine peptide presented as a function of pH (97).

The presence of secondary and tertiary structures in proteins decreases considerably the H/D exchange rates. This structural impact can be quantified using the protection factor value which is defined as the ratio between the exchange rate constant of a specific peptide amide proton located in the unfolded protein and the exchange rate constant for the same proton in the folded protein. Many reports determine the H/D exchange rates of single amide protons for an unstructured peptide in order to obtain the protection factors for the same amide protons in folded peptides (99, 100). Secondary and tertiary structures can decrease the H/D exchange rate by seven orders of magnitude compared to adjacent side chains in folded proteins. Consequently, a large reduction in H/D exchange rate is an excellent indicator of conformational changes in proteins.

Amide hydrogen exchange in folded proteins can essentially be explained by two different processes. The first one, described in Equation 1.2, reflects the hydrogen exchange on peptide bonds without the aid of structural changes, i.e for amide protons located on the surface or open channels within a folded protein (closed form).



M_{cl} refers to the closed form of the macromolecule (M) and H and D stand for hydrogen and deuterium, respectively. The rate constant for the H/D exchange by this process is k_f .

The second process of H/D exchange can be explained in combination with protein dynamics. In general, H/D exchange rates are slower when amide protons are located far from the solvent-protein interface or when the protons are involved in intramolecular hydrogen bonding such as in α -helices or β -sheet conformations. Shielded protons can only exchange with the solvent through local reversible unfolding-folding processes of small regions in the protein. Different models exist to explain these unfolding mechanisms. The “penetration model” postulates that the solvent enters the protein core through transiently formed channels and cavities (101). In the “local unfolding model”, small regions of a protein unfold cooperatively, which expose them to the solvent (99, 102). In both models, the hydrogen can then exchange with the solvent and can therefore be described by Equation 1.3.



M_{cl} and M_{op} refer to the closed and open forms of the macromolecule (M). Rate constants corresponding to the closure and the opening of the folded macromolecule are represented by k_{cl} and k_{op} , respectively, and the rate constant corresponding to the H/D exchange itself is represented by k_{ch} . In native proteins, $k_{op} \gg k_{cl}$ together with two extremes situations referred to as EX1 and EX2 exchange mechanisms are usually described (103, 104).

The observed H/D exchange rate (k_{obs}) is the deuteration level measured as a function of time. For most proteins at neutral pH and in absence of denaturants is $k_{cl} \gg k_{ch}$, which leads to the simplified expression of k_{obs} given by Equation 1.4. This extreme value of k_{obs} is also called the EX2 exchange mechanism.

$$k_{obs} = (k_{op} / k_{cl}) \times k_{ch} \quad \text{Equation 1.4}$$

where k_{op}/k_{cl} is the equilibrium between opened and closed form processes and k_{ch} is the exchange rate constant for the amide proton in the regions where the protein is unfolded (105, 106). Measuring k_{obs} and calculating k_{ch} leads to the direct determination of k_{op}/k_{cl} which enables the access to the ΔG value for the protein unfolding processes for specific regions of proteins or for the entire molecule (107-109).

If the local unfolding events are much slower than the chemical reaction ($k_{cl} \ll k_{ch}$), the k_{obs} is only dependent on the rate of protein unfolding k_{op} (110) as shown in Equation 1.5 and is referred to as the EX1 exchange mechanism.

$$k_{obs} = k_{op} \quad \text{Equation 1.5}$$

Generally the EX2 mechanism is preferred in native proteins, whereas the EX1 became favoured when significant amount of chaotropic agents are present in the system.

1.6.3 Measurement of H/D rates by mass spectrometry

There are two main strategies to label a protein using D_2O , the continuous labeling or the pulse-labeling. In the latter method the protein is incubated for a period of time (usually 30 min) in presence of chaotropic reagents and a short pulse of deuterium is then introduced to the reaction mixture subsequently followed by a quenching step. This technique is often used to detect kinetic intermediates in order to elucidate protein folding and unfolding mechanisms (111). In the continuous labeling method, the native protein is exposed to deuterium at time $t = 0$ and the reaction is quenched at different times during a period of one to two hours. This labeling technique is required for the study of conformational properties in native proteins. In both methods, the isotopic exchange rates can be determined by the mass increased on the whole labeled protein or on specific labeled regions in the protein using mass

spectrometry. While mass measurements of the whole protein enable the study of global changes in the protein, fragment analysis can pinpoint the actual location of these structural changes.

1.6.4 General procedure for HDX-MS experiments

In the present study, continuous labeling was used to monitor the conformational changes of the protein of interest. The general procedure used for the determination of amide hydrogen exchange rates in intact proteins is illustrated in Figure 1.11. Generally, the reaction is initiated by the addition of an excess of D_2O (10 fold) to the protein solution at physiological pH. After a number of exchange times, the reaction is quenched by rapidly decreasing both the temperature and the pH.

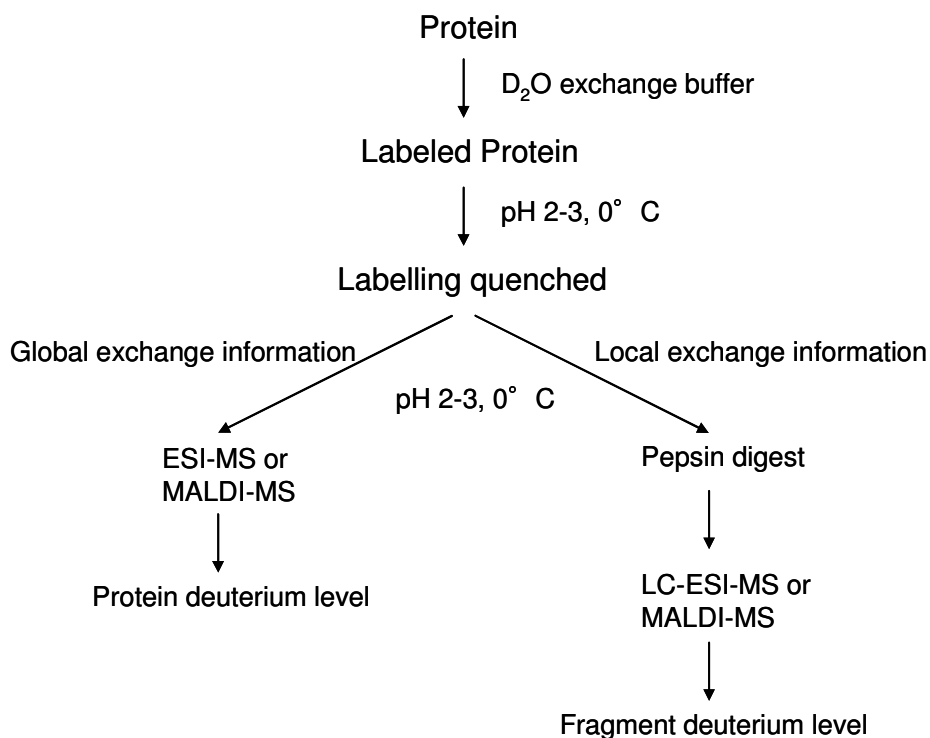


Figure 1.11: General procedure used for HDX exchange MS experiments. The protein is labeled using D_2O buffer and left standing for a pre-defined period time. The H/D exchange is quenched by decreasing pH and temperature. For the determination of the total amount of incorporated deuteriums in the protein, the mass of the labeled protein is directly measured by MS. For the determination of incorporated deuteriums in localised regions of the protein, the labeled protein is fragmented by pepsin proteolysis prior to the detection of the peptic peptide fragment by MS.

At pH 2.3 and 0 °C, the rate of the H/D reaction is significantly decreased. In case of the detection of global changes in the protein, the labeled macromolecule is then directly submitted to the mass spectrometer to minimize artifactual isotopic exchanges. For the localisation of structural changes, the labeled protein is first digested with an acid-stable protease, generally pepsin, which is added to the labeled protein and then submitted to the mass spectrometer for analysis.

1.6.5 Pepsin digestion

High pepsin concentration is generally added to the deuterated protein sample in order to speed up the digestion time, which is important to minimise the isotopic back-exchange. The ratio of protein:pepsin is often 1:1 (w/w). Pepsin is a protease with low specificity and usually produces many peptide fragments. The cleavage sites of pepsin can not be predicted with certainty, due to the possible cleavage at different residues both from the N-and C-terminal sides. The generation of many peptic peptides is necessary for a good sequence overlap in order to obtain a high sequence coverage. Presence of overlapping peptides can improve the structural resolution of the measurements to within 3-4 amino acids (112). Additionally, the structural resolution can also be optimised by using multiple acid stable proteases with different specificity (113). The use of a non-specific protease such as pepsin requires the sequencing of the product peptides and accurate peptide mass measurements. The sequencing of peptides is generally performed by tandem mass spectrometry experiments, which deliver the mass of several fragments originating from the same parent peptides.

1.6.6 Loss of deuterium during sample preparation for MS analysis

After labeling the protein using high amounts of D₂O buffer, the concentration of D₂O has to be decreased prior to digestion and MS analysis in order to avoid artificial deuterium incorporation through possible structural changes. This can be highly detrimental to the HDX experiments and lead to a major loss of structural information by uncontrolled back-exchange of the viable incorporated deuteriums with protons from the digestion buffer. This would then prompt to misleading conclusions since the distinction between deuterium not incorporated during kinetic analysis and those

back-exchanged during sample preparation is not possible anymore. Deuteriums located on the amino acid residue side chains and on the N- and C- terminus back-exchanged too rapidly to be detected. Consequently, only the deuteriums located at the backbone amide positions will be detected by mass spectrometry. The back-exchange rate constant of the amide bond deuterium can be drastically reduced by decreasing the pH to 2.3 and the temperature to 0 °C (96). Quantification of the back-exchange can be achieved by measuring the loss of incorporated deuteriums from fully labelled protein peptide fragments. 10-20 % back-exchange can usually be achieved by improvement of the MS protocols (93). When a LC separation is used prior to MS analysis, the application of a cooling and desalting system is required in order to minimise the back-exchange during the separation of the peptic peptide fragments. The use of MALDI as ionisation method, requires a fast preparation and an efficient target cooling techniques to further reduce the potential back-exchange during the sample preparation on the MALDI target (114).

1.6.7 Determination of hydrogen exchange rate constants

Structural differences between proteins exposed to various conditions (addition of ligands, post-translational modifications, pH variation, etc...) can be detected by the analysis of the fragments (peptides) generated from the labeled protein at specific times. However several time points of the H/D exchange experiment are required to obtain complete information about the conformational changes in the protein. By fitting the time courses to mono, bi- or tri-exponential equations, a range of isotopic exchange rate constants at peptide bonds in one segment can be determined. Ideally, the exchange rate constant for every single peptide linkage in the segment should be determined. However in practice, the determined rate constants are often the averaged values of a set of real rate constants.

1.6.8 HDX with MALDI-MS

Matrix Assisted Laser Desorption Ionization (MALDI) has been shown to be a soft ionisation method for the mass spectrometric analysis of biomolecules such as proteins, peptides and oligonucleotides (50, 51). Mandel *et al.*, 1998 have shown for the first time that MALDI can also be a powerful tool to monitor HDX experiments (115). Generally, the sample is co-crystallised with an excess of organic matrix on the

MALDI target and then is introduced into the high vacuum of the mass spectrometer. The matrix absorbs the energy of the laser light ($\lambda = 355 \text{ nm}$) and then induces the desorption and ionisation process of the analytes. The ionised analytes are then accelerated through a high voltage region and separated based on their mass to charge ratio inside the analyser. In most cases, a time of flight analyser is coupled to the MALDI technique (see paragraph 1.5.4).

In contrast to the ESI ionisation process, MALDI generates mainly single charge peptide ions $[M+H]^+$, which reduces the number of peaks observed in the mass spectrum. Moreover, by generating multiply charged ions, ESI requires the LC system to be connected upstream to the mass spectrometer to reduce peak overlapping. Due to complex deuteration states possibly occurring in a single peptide, deuterated peptides show more peak overlap compared to the non-deuterated ones, which leads to additional complication in the peak assignments of the ESI mass spectra, emphasising even more the advantage of using MALDI over ESI ionization.

CHAPTER II

EXPERIMENTAL PROCEDURES

2 EXPERIMENTAL PROCEDURES

2.1 Materials

2.1.1 Substrates and Inhibitors

Imipenem was a gift from Merck Sharp and Dohme (Haar, Germany). All tested inhibitors were provided by Benoît M. Liénard, Group of Prof. Christopher J. Schofield, Organic Chemistry Department, University of Oxford, UK.

2.1.2 Reagents and Chemicals

MALDI-matrix α -cyano-4-hydroxycinnamic acid (CCA), 5,5'-dithiobis-(2-nitrobenzoic acid) (DTNB), chelex-100 sodium form, metal ion salts (ZnCl_2 , CoCl_2 and CdSO_4) diaminoethanetetraacetic acid (EDTA), cesium iodide (CsI), sodium dodecyl sulphate (SDS), hydroxymethylaminomethane (TRIS) and dimethylsulfoxide (DMSO) were purchased from Sigma-Aldrich Chemical Co. (Steinheim, Germany). Trifluoroacetic acid (TFA), formic acid (FA), ammonium acetate ($\text{CH}_3\text{COONH}_4$), sodium chloride (NaCl) and ammonium hydroxide (NH_4OH) were provided by Fluka (Neu-Ulm, Germany). Acetonitrile (MeCN) and methanol (MeOH) were obtained from Riedel-de Haën (Seelze, Germany). Deuterated water (D_2O) (99.9 % deuterium) and deuterated sodium hydroxide NaOD (40 % in D_2O) were obtained from Deutero GmbH (Kastellaun, Germany). Pepsin immobilized on cross-linked 6 % beaded agarose was obtained from Pierce (Rockford, UK). Mag-fura-2 (MF) was provided by Molecular Probes, (Eugene, Oregon, USA). Calibration mixture containing des-Arg1-Bradykinin, Angiotensin I, Glu1-Fibrinopeptide B, ACTH 1-17, ACTH 18-39 was obtained by Applied Biosystems (Darmstadt, Germany). HEPES was purchased from Roth (Karlsruhe, Germany). Ammonium hydrogen carbonate (NH_4HCO_3) was provided by Merk (Darmstadt, Germany). Water was purified with a Millipore (Bedford, MA, USA) water purification system. Organic solvents were all of HPLC grade. All chemicals used were of analytical grade.

2.1.3 Membranes and columns

The dialysis tubing (16 mm Ø) was provided by Servapor, Boehringer Ingelheim Bioproducts, (Heidelberg, Germany). The Microcon YM-10 (cut off = 10,000 Da) centrifugal filters and the ZipTip_{C18} columns were obtained by Millipore (Bedford, MA, USA).

2.2 Methods

2.2.1 Production and characterization of Enzymes and Apo-Enzymes

Metallo-Enzymes

The metallo- β -lactamases BclI from *Bacillus cereus* 569/H/9, CphA from *Aeromonas hydrophilia* AE036 and L1 from *Stenotrophomonas maltophilia* were produced and purified as described in references (2, 116) and (117) respectively. The BclI preparation (2) was modified as follows: cells were grown at 37 °C in M9 minimal medium with 10 g/l of glucose and 1 g/l of NH₄Cl. Expression was induced by adding 1 mM isopropyl- β -D-thiogalactopyranoside (IPTG) at an absorbance at 600 nm of 0.6. After 16 h, cells were harvested by centrifugation, resuspended in MES buffer (10 mM, 1 mM ZnCl₂, pH 6) and broken using French Press. Cytosolic proteins were separated from cells debris and were loaded to purification columns (2).

Protein concentrations were determined with the following extinction coefficients: $\epsilon_{280(\text{BclI})} = 30,500 \text{ M}^{-1} \text{ cm}^{-1}$, $\epsilon_{280(\text{CphA})} = 38,000 \text{ M}^{-1} \text{ cm}^{-1}$ and $\epsilon_{280(\text{L1})} = 55,000 \text{ M}^{-1} \text{ cm}^{-1}$ (per monomer).

Apoenzymes

The apoenzyme of BclI was prepared by three dialysis steps of the corresponding enzyme (2 mg/ml) using dialysis tubing against a 250-fold excess of 15 mM HEPES, pH 7.0 containing 20 mM EDTA (24 h with stirring at 4 °C). EDTA was removed by three dialysis steps against the same buffer containing 1 M NaCl followed by two steps without salt. Apo-CphA and apo-L1 were obtained by three dialysis steps of the corresponding enzymes (2.5 mg/ml and 8.5 mg/ml respectively) against a 250-fold excess of 15 mM HEPES, pH 6.5 containing 20 mM EDTA and 0.15 mM NaCl. EDTA was removed by three dialysis steps against the same buffer containing 1M NaCl followed by two steps with 0.15 M NaCl and a last step without salt. All buffer

solutions were prepared in bidistilled water extensively stirred with Chelex in order to minimize zinc ion contamination. The final concentrations of apoBcII and apoCphA were determined using Ellman's reagent: 5,5'-dithiobis-(2-nitrobenzoic acid) (DTNB) quantifying the free sulfhydryl groups in the protein at an extinction coefficient of $\epsilon_{412(\text{DTNB})} = 13,600 \text{ M}^{-1} \text{ cm}^{-1}$.

2.2.2 Quantitation of sulfhydryl groups using Ellman's reagent

Desalting procedures can affect the sulfhydryl groups (cysteins) content in proteins by air oxidation. Therefore it was necessary to determine the exact active apoprotein concentration by quantifying the free sulfhydryl groups in the protein, since the number of cysteine residues in the protein is known (BcII and CphA contain only one cyteine residue). By addition of 5,5'-dithiobis-(2-nitrobenzoic acid) (DTNB) to the protein solution at pH 8, thiophenol anions are produced, where their concentration can be determined at a wavelength of 412 nm ($\epsilon_{412(\text{DTNB})} = 13,600 \text{ M}^{-1} \text{ cm}^{-1}$). In presence of an excess of DTNB, the amount of produced thiolphenol anions is dependent on the free sulfhydryl groups in the protein.

The reaction mixture was composed of 300 μM of DTNB and 10-50 μM protein solution in denaturing buffer (0.1 M TRIS, 1mM EDTA and 1% SDS, pH 8) at 22°C.

2.2.3 Determination of Metal ion Affinities

The dissociation constants for a first and second metal ion (K_{D1} and K_{D2} respectively) bound to apoenzymes (E) were determined in competition titration experiments with the chromophoric metal⁽²⁺⁾-chelator Mag-fura-2 (MF). The metal-free Mag-fura-2 (MF) has its absorption maximum at 363 nm and the metal-loaded Mag-fura-2 (Me-MF) at 335 nm (118). The dissociation constants of Zn-MF and Cd-MF and the absorption coefficient of MF at 363 nm were determined under the same conditions as in the competition titrations described below and resulted in $K_{\text{Zn-MF}} = 9.1 \text{ nM}$, $K_{\text{Cd-MF}} = 5.6 \text{ nM}$ and $\epsilon_{363(\text{MF})} = 28500 \text{ M}^{-1}\text{cm}^{-1}$. Their values were used to calculate the dissociation constants of metal ions bound to the apoenzymes.

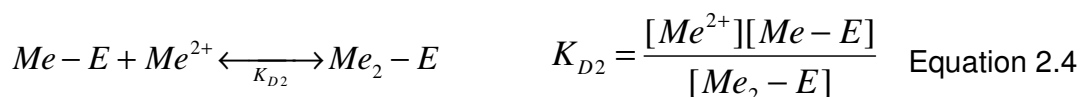
For the competition titrations experiments, a 1 ml solution of 3 μM of metal indicator and 3 μM of apoenzyme in 15 mM HEPES, pH 7 at 22 °C was titrated with a stock solution of 255 μM ZnCl_2 or 255 μM CdSO_4 . In presence of inhibitors, the 1 ml

solution contained also 6 μM of (*R,S*)-thiomandelate or 100 μM of *D*-captopril before titration with the metal ions. The total absorbance at 363 nm (A_{total}) corresponding to the sum of MF and Me-MF can be followed for each titration step (2 μl) according to Equation 2.1 using a Lambda 9 spectrophotometer (Perkin-Elmer instruments) equipped with thermostatically controlled cells.

$$A_{\text{total}} = \varepsilon_{\text{MF}}[\text{MF}] + \varepsilon_{\text{Me-MF}}[\text{Me-MF}] \quad \text{Equation 2.1}$$

where A_{total} is a function of the added volume of a metal ion stock solution $[\text{Me}]_{\text{stock}}$ to a defined starting volume (1 ml).

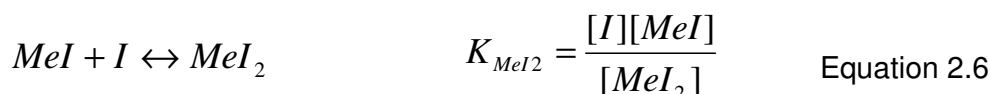
For numerical data analysis the program *Chemsim* was used calculating absorbance values for each titration step according to equation 2.1. For these calculations the laws of mass action (Equations 2.2-2.4) and the equations of mass conservation are used.



For data evaluation of competition experiments ε_{MF} , $K_{\text{Me-MF}}$, starting volume and $[\text{Me}]_{\text{stock}}$ were constrained. In a least squares procedure K_{D1} , K_{D2} , $[\text{E}]_{\text{start}}$ and $\varepsilon_{\text{Me-MF}}$ were simultaneously fitted and determined as described in (2).

The effect of the inhibitors on metal ion affinities of the different enzymes can be expressed in terms of variations in K_{D1} and K_{D2} . In presence of inhibitors (I), two additional equations were taken in account, representing the formation of 1:1

(Equation 2.5) and 2:1 inhibitor-metal complexes (Equation 2.6) in the case of (*R,S*)-thiomandelate and the formation of 1:1 complexes (Equation 2.5) in the case of *D*-captopril.



In titration experiments with the inhibitors *D*-captopril and (*R,S*)-thiomandelate Equation 2.5 or Equations 2.5 and 2.6 were included into the binding models, respectively. When competition experiments were carried out with enzymes, K_{MeI} and K_{MeI_2} were fixed to the experimentally determined values.

2.2.4 Determination of inhibition constants

Inhibition constants of the inhibitors were determined assuming competitive inhibition. Imipenem hydrolysis was followed by monitoring the change in absorbance at 300 nm ($\Delta\epsilon_{300} = 9000 \text{ M}^{-1} \text{ cm}^{-1}$) in 15 mM HEPES, pH 7 at 24 °C using a Lambda 9 spectrophotometer (Perkin-Elmer instruments) equipped with thermostatically controlled cells. The final BclI enzyme concentration was 10 nM. The substrate concentration (*S*) was 160 μM and equal to the Michaelis Menten constant value (K_M) of the enzyme for imipenem. The inhibitors were dissolved in 4-10 % DMSO, 15 mM HEPES pH 7 at 1-2 mg/ml and then diluted to the final concentration (*I*). Two different inhibitor concentrations were used to determine K_I values using the following Equation 2.7 for competitive inhibition:

$$v_o/v_i = \frac{K_M \cdot \left(1 + \frac{[I]}{K_I}\right) + [S]}{K_M + [S]} \quad \text{Equation 2.7}$$

where v_0 corresponds to the initial rate of hydrolysis in absence of inhibitor and v_i the initial rate of hydrolysis in presence of inhibitor.

2.2.5 Preparation of samples for “native”- ESI-MS

Desalting procedure of enzymes

Prior to analysis, all proteins were desalted using Microcon YM-10 (cut off = 10,000 Da) centrifugal filters in 15 mM ammonium acetate (pH 7.5). Seven dilution/concentration steps were performed at 4 °C and 14,000 g. Enzymes were diluted in 15 mM ammonium acetate buffer to a final concentration of 15 μ M.

Metal binding experiments

Zinc and cadmium enzymes were prepared at room temperature, by adding a volume of 1-10 μ l of 100 μ M $ZnCl_2$ or of 100 μ M $CdSO_4$ to 15 μ M apoenzyme BcII dissolved in 15mM CH_3COONH_4 (pH 7.5) to obtain $[Me^{2+}]:[E]$ ratios ranging between 0.3 and 2.

Inhibitor binding experiments

100 mM inhibitor stock solutions were prepared with ethanol. Subsequent dilutions to final concentration were done with 15 mM ammonium acetate and the pH was adjusted to 7.5. Unless otherwise stated, for the inhibitor binding experiments each metalloenzyme was mixed with 1.3 molar equivalents inhibitor to metalloenzyme at room temperature prior to mass analysis.

2.2.6 “Native”-ESI-MS analysis

All sample mixtures were analysed using an ESI-Q-TOF mass spectrometer (Q-TOFmicro Micromass, Altrincham, UK) interfaced with a NanoMate chip-based nano-ESI source (Advion Biosciences, Ithaca, NY, USA). Typically a spraying voltage of 1.68 kV and a sample pressure of 0.25 psi were applied. The instrument was equipped with a standard Z-spray source block. Each well was loaded with 5 μ l sample and was infused to the mass spectrometer. The estimated flow rate was ca. 100 nL/min. Clusters of $Cs_{(n+1)}I_n$ (1mg/ml CsI in 100 % methanol) were used for calibration. Calibration and sample acquisitions were performed in the positive ion mode in the mass range of m/z 500 – 5000. Operating conditions for the Q-TOF mass spectrometer were as followed: sample cone voltage (varied) between 15 to

200 V, source temperature 20 °C. Acquisition and scan time were 2 min and 1 s, respectively. The pressure at the interface between the atmospheric source and the high vacuum region was fixed at 6.7 mbar (measured with the roughing pump Pirani gauge) by throttling the pumping line using an Edwards Speedivalve to provide collisional cooling. Data were smoothed with the Savitzky Golay method (smooth windows: 20, number of smooth: 4) the background subtracted and the masses finally calculated by centering. The standard deviation reported for all the calculated masses represents the precision of the mass calculation from m/z values reported from the ESI mass spectrum. All data were processed using MassLynx software versions 4.0 and 3.5.

2.2.7 Preparation of samples for HDX-MS

Metal binding experiments

Zn₁ and Zn₂-BclI solutions were prepared by adding 0.7 and 2.3 equivalents of ZnCl₂ to the apoprotein, respectively. Cd₁ and Cd₂-BclI solutions were prepared by adding 0.9 and 6.6 equivalents to the apoprotein, respectively. Final metal-substituted protein and apoprotein stock solutions were 150 µM in 15 mM HEPES pH 7.

Inhibitor binding experiments

The inhibitor was dissolved in ethanol at 60 mM, and diluted in 15 mM HEPES pH 7.5. For all HDX experiments, 400 µM of the inhibitor were added to the protein stock solution.

2.2.8 Pepsin digestion

15 µM of apoenzyme in HEPES 15 mM pH 7 (10 µl) was diluted 1:11 with 0.1 % tri-fluoro acetic acid (TFA) solution to decrease the pH to 2.3. Protein digestion was performed by adding 30 µl of pepsin bead slurry (Pierce, Rockford, UK) (washed 4 times prior to use with 450 ml of 0.1 % TFA at 4°C) and incubated on ice for 10 min with occasional mixing. The resulting peptides were separated from the pepsin beads by centrifugation for 20 sec at 14.000 g at 4 °C. To desalt the sample 10 µl of digestion was loaded on a ZipTip_{C18} (Millipore Corp., Billerica, MA, USA) rinsed with 0.1 % TFA. Subsequently the peptides were eluted with 1 µl of α-cyano-4-

hydroxycinnamic acid matrix solution (5 mg/ml CCA in acetonitrile/ethanol/TFA 20/80/0.1) onto the MALDI plate and dried under compressed air stream.

2.2.9 Assignment of peptic peptides

Porcine pepsin is a non-specific acidic endopeptidase with broad substrate specificity. Therefore high mass accuracy and/or MS/MS sequencing are essential for the identification of pepsin-digested peptides. First, the mass of each measured peptide was verified using the Paws program (download free from Genomic Solutions Inc: <http://bioinformatics.genomicsolutions.com/paws.htm/>). Paws is a bioinformatic tool which permits the mapping of the measured peptides to the protein sequence of interest. In most of the cases, two or three theoretical peptides were found to fit with the mass of a detected peptide by assuming a mass accuracy of ≤ 20 ppm. In a second step, MS/MS was performed for each measured peptide and the resulting fragments were compared manually with the MS/MS fragments of the possible theoretical peptides to identify the peptides.

2.2.10 Hydrogen deuterium exchange (HDX) experiments

In-exchange experiments

For H/D exchange experiments, 1 μ l of 150 μ M apo-BcII or metal-substituted BcII stock solution was incubated 1: 10 with deuterated buffer (D_2O , 15 mM HEPES, pH 7, not corrected for isotope effects) at 22 °C. Deuterium labelling times varied between 50 and 5900 sec. Each in-exchange reaction was stopped by addition of 100 μ l of 0.1 % TFA on ice decreasing the pH to 2.3. The pepsin digestion and analysis of peptic-peptides were performed as described above for the non-deuterated digest. After spotting the deuterated digestion:matrix solution on the MALDI target, each exchange experiment was immediately measured by MALDI-MS with less than 1 min delay. All solutions and ZipTips were kept cold (on ice) before use. The MALDI plate was kept at room temperature in order to prevent condensation of water on the plate. All experiments were repeated in triplicate.

Back-exchange control experiments

Fully deuterated sample $m_{(100\%)}$ was prepared by incubating 10 μ l of pepsin digested apoBcII (15 μ M) in deuterated buffer (D_2O , 15 mM HEPES, pH 7 not corrected for

isotope effects) for 72 hours at 22 °C. Quenching and sample analysis were performed as described above.

2.2.11 Determination of deuterium content

The centroid mass of each isotope cluster was calculated using the MagTran software (119) by labelling the left side of the lowest deuterated peak and the right side of the highest deuterated peak. The deuterium in-exchange of amide groups (%D) of the peptic peptides was determined for each incubation time in D₂O using Equation 2.8. $m_{(t)}$ is the observed centroid mass of the deuterated peptide for each in-exchange time, and $m_{(0\%)}$ corresponds to the non-deuterated mass of the corresponding peptide. During sample preparation and transfer to the MALDI target, back exchange of incorporated deuteriums to hydrogens takes usually place. Therefore the experimental data were corrected for this back exchange using the experimentally obtained centroid mass of fully deuterated peptide $m_{(100\%)}$ after back exchange as the 100 % value (91).

$$\%D = \frac{(m_{(t)} - m_{(0\%)})}{(m_{(100\%)} - m_{(0\%)})} * 100\% \quad \text{Equation 2.8}$$

For data representation the experimentally obtained values were further processed. From the experimentally determined masses, the hypothetical values for 100 % D₂O in the incubation buffer were calculated. For the mononuclear samples, metal ion addition corrections for apo-enzyme content were introduced. Masses for Zn₁-BcII were calculated from the experimentally obtained centroid masses of Zn_{0.7}-BcII and apo-BcII according to $m(\text{Zn}_1\text{-BcII}) = 1.428[m(\text{Zn}_{0.7}\text{-BcII}) - 0.3m(\text{apo-BcII})]$. Masses for Cd₁-BcII were obtained from $m(\text{Cd}_1\text{BcII}) = 1.11[m(\text{Cd}_{0.9}\text{-BcII}) - 0.1m(\text{apo-BcII})]$.

2.2.12 Evaluation of HDX kinetics

All the deuteration versus time curves obtained can be described by mono-exponential curves. Equation 2.11 was used for fitting. A rapid HDX phase preceded the kinetic traces obtained for almost all the peptide fragments investigated. Since no

indication for the underlying rate constants can be derived from the data used, the amplitude of this phase is considered as a starting value of the fitted time course different from zero ($\%D_0$) in Equation 2.9. Fitting of Equation 2.9. to the data resulted in $\%D_0$, the rate constant k , and the amplitude of the process observed ($\%D_t$).

$$\%D(t) = \%D_0 + \%D_t(1 - e^{-kt}) \quad \text{Equation 2.9}$$

2.2.13 MALDI-MS analysis

Mass spectrometric analysis were performed using a 4800 MALDI TOF/TOFTM mass analyser (Applied Biosystems, Darmstadt, Germany) equipped with a 200-Hz Nd:YAG-Laser ($\lambda = 355$ nm, 3 to 7 ns pulse width). MS data were acquired in the positive ion reflectron mode with 470-ns delayed extraction, accumulating 500 laser shots using the 4000 Series ExplorerTM Remote Access Client software (version 3.5.1). A calibration mixture (Applied Biosystems) containing des-Arg1-Bradykinin [m/z 904.4681], Angiotensin I [m/z 1296.6853], Glu1-Fibrinopeptide B [m/z 1570.6774], ACTH 1-17 [m/z 2093.0867], ACTH 18-39 [m/z 2465.1989] was used for external calibration. Tandem mass spectrometry (post source decay with post acceleration) was performed for the sequencing of all detected peptic-peptides; no additional collision gas was used. For MS/MS measurements, the acceleration voltage was 8 kV, 4000 laser shots were accumulated for each MS/MS spectrum.

2.2.14 Circular Dichroism Spectroscopy

Circular dichroism spectra were recorded with a Jasco J740 at 20 °C. The CD spectra were recorded in 5 mM HEPES pH 7.0 at a protein concentration of 5 μ M in cuvettes with 1 mm light path. Due to a strong background signal the useful spectral range did not reach below 200 nm in the far UV region. Three spectral scans with a resolution of 1 nm were accumulated and a binary smoothing function for noise reduction was applied after subtraction of the blank spectrum obtained for the buffer.

CHAPTER III

METAL AND INHIBITOR STUDIES using “NATIVE”-ESI-MS and UV SPECTROSCOPY

3 METAL AND INHIBITOR BINDING STUDIES using „NATIVE“-ESI-MS and UV SPECTROSCOPY: RESULTS

3.1 Importance of the buffer system for the measurement of metal-protein complexes by ESI-MS

The analysis of metal-protein complexes using ESI-MS requires the conservation of the non-covalent interactions existing in solution. Therefore, different buffer systems, compatible with the ionisation process by electrospray, were tested on the binuclear zinc enzyme BcII (Zn_2 -BcII). The metalloprotein was first measured in an organic solvent (methanol acidified with formic acid, representing denaturing conditions) used for routine analysis of proteins by ESI-MS and later in volatile and aqueous buffers such as ammonium acetate and ammonium bicarbonate at neutral pH, i.e. “native” conditions.

Figure 3.1A and 3.1B show the ESI mass spectra of Zn_2 :BcII in methanol/0.2% formic acid and in aqueous ammonium acetate (pH 7.5), respectively. When Zn_2 -BcII was measured in the organic solvent, the corresponding spectrum displayed a number of ions carrying a high number of charges ranging between + 16 and + 32 with a broad charge states distribution at low m/z values (m/z between 800 and 1600). The determination of the deconvoluted mass for BcII in denaturing conditions (24960 ± 0.6 Da) revealed the loss of its two Zn(II) ions. In fact, the observed broad distribution of high charge states is typical for partially or fully unfolded proteins (120). When Zn_2 -BcII was dissolved in ammonium acetate-buffer, the ions carried a lower number of charges ranging between + 8 and + 10 at m/z values between 2500 and 3100. A deconvoluted mass of 25087 ± 0.2 Da was calculated which corresponds to the fully zinc-loaded enzyme Zn_2 :BcII. The narrow distribution of low charge states is consistent with a “native” conformation of the protein in solution (120). Similar results were obtained when Zn_2 -BcII was dissolved in ammonium bicarbonate (pH 7.5).

Thus, for the following metal titration experiments monitored by ESI-MS, the metal-substituted proteins were dissolved in aqueous buffer in order to preserve the metal-protein complex in solution.

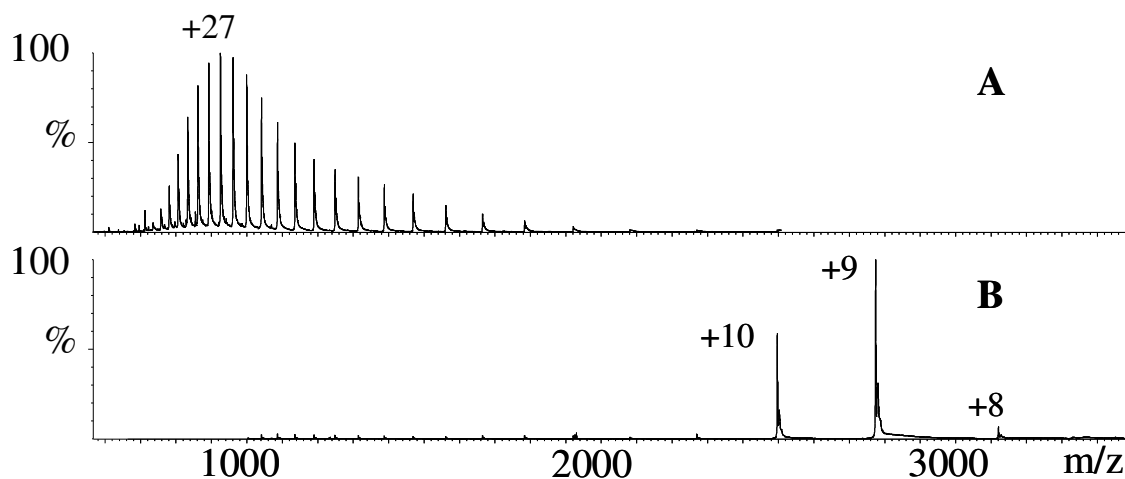


Figure 3.1: Influence of the solvent on the charge state repartition of the BcII MBL. ESI mass spectra of the binuclear zinc enzyme BcII (15 μ M) measured in methanol / 0.2 % formic acid (**A**) and in 15 mM ammonium acetate (pH 7.5) (**B**). Pressure at interface: 6.7 mbar, sample cone voltage: 100 V. The number of charges for the most relevant ions is specified in the figure.

3.2 Metal binding studies monitored using ESI-MS

To probe the zinc, cadmium and cobalt binding stoichiometry of the BcII enzyme, the addition of various concentrations of metal ions to the apoenzyme BcII was monitored by ESI-MS. The relative peak intensities of all the distinct protein species at different metal/apoenzyme ratios can then be compared.

3.2.1 Detection of the metal - protein complex by ESI-MS

In order for the results to have the potential to be biologically significant, the relative intensities displayed by the different protein species on the ESI mass spectra have to reflect exactly the distribution of these species in solution. Consequently, control experiments should be carried out in order to verify that certain protein structures or complexes are neither advantaged nor discriminated during the ionisation/desolvation process or later during their transfer through the interface of the instrument. The zinc titration of BcII was used for the validation of the method. ESI mass spectra (charge state $z = 9$ and $z = 10$) obtained by incubation of apo-BcII

In general, for titration methods monitored with ESI-MS it is assumed that the concentrations in solution of protein (P), ligand (L) and complex (PL) are proportional to the observed intensities (I) in the mass spectrometer. This can be expressed by equations 3.1 and 3.2, where the proportionality constants t_P and t_{PL} represent the transfer coefficient of P and PL, respectively. In the present work, only the intensities of PL and P were investigated.

$$[P] = t_P * I_P \quad \text{Equation 3.1}$$

$$[PL] = t_{PL} * I_{PL} \quad \text{Equation 3.2}$$

To ensure that the different protein species exhibit the same ionization efficiencies, equal amounts of the different protein forms can be mixed together and the ratio of intensities of the different species can deliver the ratio of the species transfer coefficient. The BclI zinc titration (Figure 3.2) reveals that at low $[Zn^{2+}]/[apoprotein]$ ratios, three protein species with identical charge state can be detected with a respective mass difference of 63.4 Da between the successive protein species corresponding to the binding of one zinc ion minus two protons. In this case, it was not possible to prepare the stock solutions, where only one BclI protein species occurred and consequently no relative ionization efficiencies could be determined independently.

However, when L is much smaller than P (e.g. the binding of metal ion to protein) the transfer coefficients are close to equal and the intensity ratio of I_{PL}/I_P is equal to the concentration ratio of $[PL]/[L]$ in solution (121). Therefore, in the following titration experiments it was assumed that apo, Zn_1 and Zn_2 species exhibit the same ionization efficiencies.

Furthermore the variation of the sample cone voltage (VC) can assess whether the protein species are abnormally represented on the mass spectrum, due to the possible dissociation via gas phase collisions at the atmospheric-vacuum interface (84). During all the titration experiments, the variation of the cone voltage from 30 to 200 V did not change the relative intensities of the protein species detected in the mass spectrum (data not shown). Therefore a high cone voltage was used for the

titration experiments to allow efficient ion desolvation and therefore a better mass accuracy.

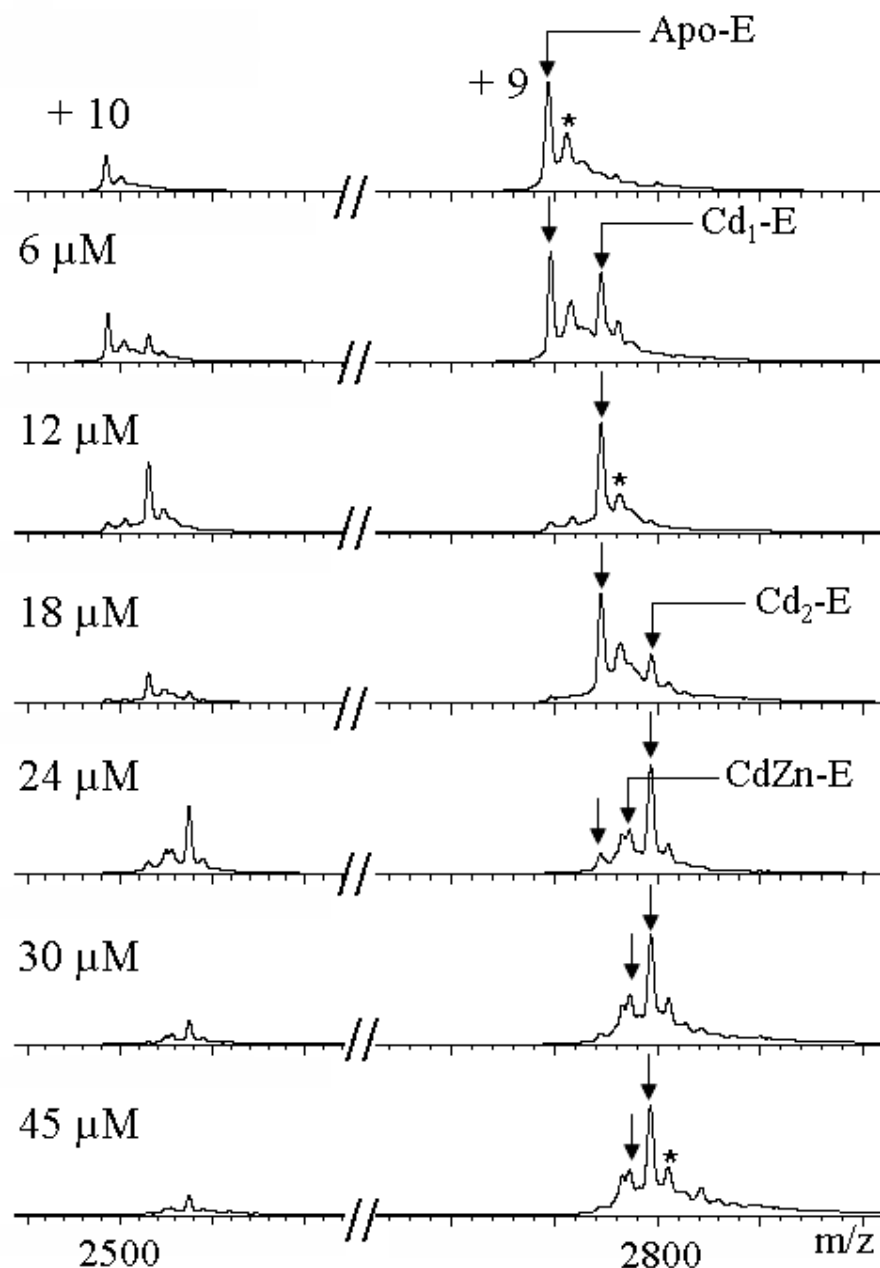


Figure 3.3: ESI mass spectra showing the result of the incubation of apo-BcII (11.7 μM in 15 mM ammonium bicarbonate, pH 7) with different concentrations of Cd(II) ions in solution (6 to 45 μM). The first recorded ESI mass spectrum corresponds to the apoenzyme just after the desalting procedure. (*) represented the salt adducts. The ions carrying the charges + 9 and + 10 are represented in the mass spectra. Experiments were carried out at sample cone voltage 200 V, pressure at interface 6.7 mbar.

3.2.2 Determination of the metal binding mode with ESI-MS

Table 3.1 summarises the relative peak intensities of the different protein species extracted from the ESI mass spectra of the zinc and cadmium titrations of BcII (Figure 3.2 and 3.3, respectively) as well as for the cobalt titration of BcII presented in appendix 1.

At low $[Cd^{2+}]/[apoprotein]$ ratios, only the signals for the apoenzyme and the Cd_1 -BcII species are observed. At $[Cd^{2+}]/[apoprotein]$ ratios > 1 , the Cd_2 -BcII species becomes the major signal in the ESI mass spectra. The results indicate that the active site of BcII accepts sequentially two Cd(II) ions, suggesting a negative cooperativity in metal binding.

Zinc and cobalt showed a different binding behaviour; Me_2 -BcII species are monitored already at low $[Me^{2+}]/[apoprotein]$ ratios, which can be explained by positive cooperativity of metal ion binding which means that the dissociation constant for the binding of the second metal ion is lower than the one for the binding of the first metal ion to the protein (K_{D2} (Equation 3.4) $<$ K_{D1} (Equation 3.3)).



The absolute values of the dissociation constants could not be measured accurately using this technique, but the ratio of both constants could be determined from the relative intensities of the apoenzyme and the metal-loaded BcII species according to Equation 3.5, which is derived from Equations 3.3 and 3.4.

$$\frac{K_{D1}}{K_{D2}} = \frac{[Me_2 - E][E]}{[Me_2 - E]^2} \quad \text{Equation 3.5}$$

Table 3.1 shows that at different zinc concentrations the determined K_{D1}/K_{D2} values

are > 1 , which is consistent with positive cooperativity for zinc binding to BcII. The ratios K_{D1}/K_{D2} obtained for the cobalt titration are close to 1.

Table 3.1: Relative abundances (%) (peak intensities of ions carrying the charge + 9 and + 10) of the different BcII complex species measured by ESI-MS during zinc, cadmium and cobalt titrations. The K_{D1}/K_{D2} ratios are calculated from the relative abundances of metal-free and metal-loaded enzyme species according to Equation 3.5. The apo-BcII concentration was estimated to be 11.7 μM .

[Me]tot (μM)	Relative peak intensities on the ESI mass spectrum (%)				K_{D1}/K_{D2}
	E	Zn ₁ -E	Zn ₂ -E		
Zn(II)					
5	61.5	18	20.5		3.9
10	39	19	42		4.5
12	24	22	54		2.7
14	9.5	14.5	76		3.5
30	/	/	100		
Cd(II)	E	Cd ₁ -E	Cd ₂ -E	CdZn-E	
6	60	40	/	/	
12	11	89	/	/	
18	/	70	30	/	
24	/	19	61.5	19.5	
30	/	24	57	19	
45	/	/	75	25	
Co(II)	E	Co ₁ -E	Co ₂ -E		
2.5	56	26.5	17.5		1.4
5	31	28	41		1.6
10	26	27	47		1.7
15	15	22	63		1.9
20	5	20	95		1.2
30	/	/	100		

3.3 Inhibitor binding studies performed by ESI-MS

3.3.1 Development/validation of the native ESI-MS technique for the screening of MBL inhibitors

The affinity of a number of mercaptocarboxylate compounds (Figure 3.4) towards the Zn_2 -BcII enzyme was investigated by “native” ESI-MS and was compared with those previously obtained by UV spectroscopy techniques (43). The affinity of the inhibitors was investigated by measuring the relative abundance of the Zn_2 -BcII-inhibitor complex compared to the free-inhibitor Zn_2 -BcII complex in the ESI mass spectra. Since the inhibitors have similar molecular masses, the comparison of the inhibitor affinities was performed from MS spectra containing a single inhibitor. Prior to run the first set of experiments, instrumental parameters for the detection of the metallo-enzyme-inhibitor complexes were first optimized. It was assumed that the different protein species reflect identical ionization efficiencies, as the mass of the ligand is much smaller than that of the protein.

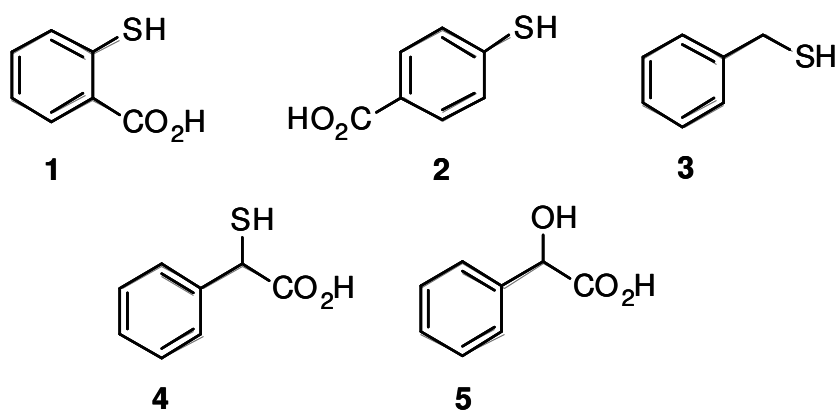


Figure 3.4: Mercaptocarboxylate compounds used in the screening for MBL inhibitors by nano-ESI-MS: Thiosalicylic acid (1), 4-mercaptobenzoic acid (2), benzylmercaptan (3), (*R,S*)-thiomandelic acid (4) and mandelic acid (5).

Influence of the cone voltage on the detection of metalloprotein-inhibitor complexes

Due to the possible dissociation of the non-covalent complexes in the interface of the instrument, the stability of the Zn_2 -BcII-inhibitor complexes was investigated at

different cone voltages by ESI-MS. Figure 3.5 shows the ESI mass spectra (charge state $z = 10$ and $z = 9$) obtained after incubation of $\text{Zn}_2\text{-BcII}$ with 1.3 molar equivalents of thiosalicylate measured at different cone voltages.

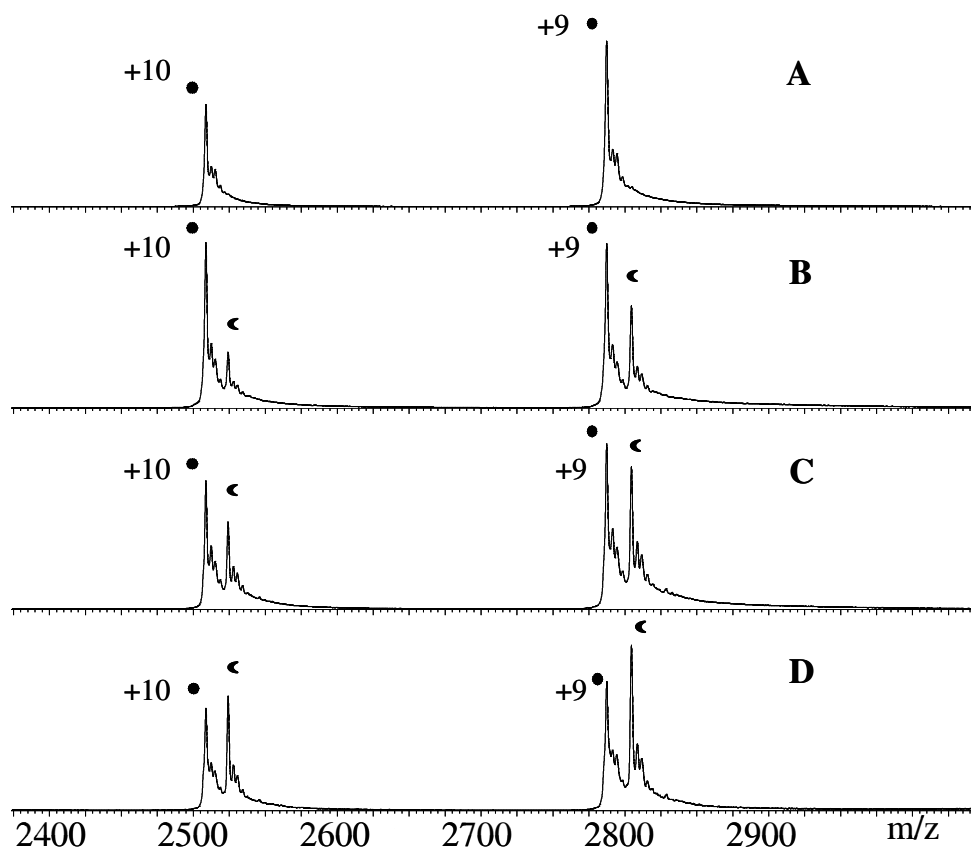


Figure 3.5: Influence of the cone voltage (VC) on the stability of the $\text{Zn}_2\text{-BcII}$ -thiosalicylate complex as observed by ESI-MS. $\text{Zn}_2\text{-BcII}$ ($15 \mu\text{M}$) incubated with 1.3 molar equivalents of thiosalicylic acid at sample cone voltage 120 V (**A**), 70 V (**B**), 50 V (**C**) and 20 V (**D**). All experiments were performed in ammonium acetate buffer (pH 7.5) with a pressure at the interface of 6.7 mbar . The ions carrying the charges $+9$ and $+10$ are represented in the mass spectra. Metalloenzyme and metalloenzyme-inhibitor-complex are represented by circle and crescent, respectively.

The binding of one molecule of thiosalicylate to $\text{Zn}_2\text{-BcII}$ led to a mass increase of 154 Da ; the charge state of the inhibited state is identical to the non-inhibited state. The results of the experiments indicated that the sample cone voltage dramatically influences the stability of the $\text{Zn}_2\text{-BcII}$ -thiosalicylate complex (Figure 3.5). By increasing the cone voltage from 20 to 120 V , the peak intensity of the $\text{Zn}_2\text{-BcII}$ -inhibitor complex decreased related to the peak corresponding to the $\text{Zn}_2\text{-BcII}$

complex and finally disappeared at 120 V (Figure 3.5A). Together with the solution data, the ESI-MS data exclude the formation of a covalent disulfide bridge between the inhibitor sulfhydryl group and the side chain of Cys168 present in the active site of the BclI enzyme (21), since a covalent interaction would not be expected to be disrupted by the higher collision energy induced by increase of the cone voltages.

Selection of the cone voltage for the study of BclI inhibitors by ESI-MS

In order to compare the relative affinities of different thiol inhibitors for BclI by ESI-MS, a single sample cone voltage has to be selected where the relative abundance of each Zn₂-BclI-inhibitor complex compared to the Zn₂-BclI is optimal. The relative abundance of Zn₂-BclI-inhibitor complexes compared to Zn₂-BclI at different cone voltages for (*R,S*)-thiomandelate, thiosalicylate and 4-mercaptobenzoate is illustrated in Figure 3.6. The abundance of the bound and unbound species were measured from the peak area of the two main charge states observed for the BclI enzyme (*z* = 9, *z* = 10). The data for the + 8 charge state were not used, due to its insignificant intensity.

The relative abundance of the Zn₂-BclI-thiomandelate complex compared to the Zn₂-BclI complex was constant (70.7 ± 2.5 %) from cone voltages 20 to 50 V, but decreased as the cone voltage was increased to 90 V, where only 20 % of the complex relative to that at 20 V was detected.

A similar behavior was revealed for the Zn₂:BclI:thiosalicylate and the Zn₂:BclI:4-mercaptobenzoate complexes; the effect was more apparent for 4-mercaptobenzoate where at 50 V only 20 % of its complex with Zn₂:BclI was observed and was undetectable at 90 V. Due to the effect of the cone voltage on the apparent relative stability of the Zn₂-BclI-inhibitor complexes, measurements for the comparison in the binding of different inhibitors to Zn₂-BclI were performed at a constant cone voltage of 50 V, thus enabling the observation of all complexes and therefore enabling their comparison. Use of lower cone voltages led to an inefficient desolvation resulting in a significantly lowered degree of mass accuracy.

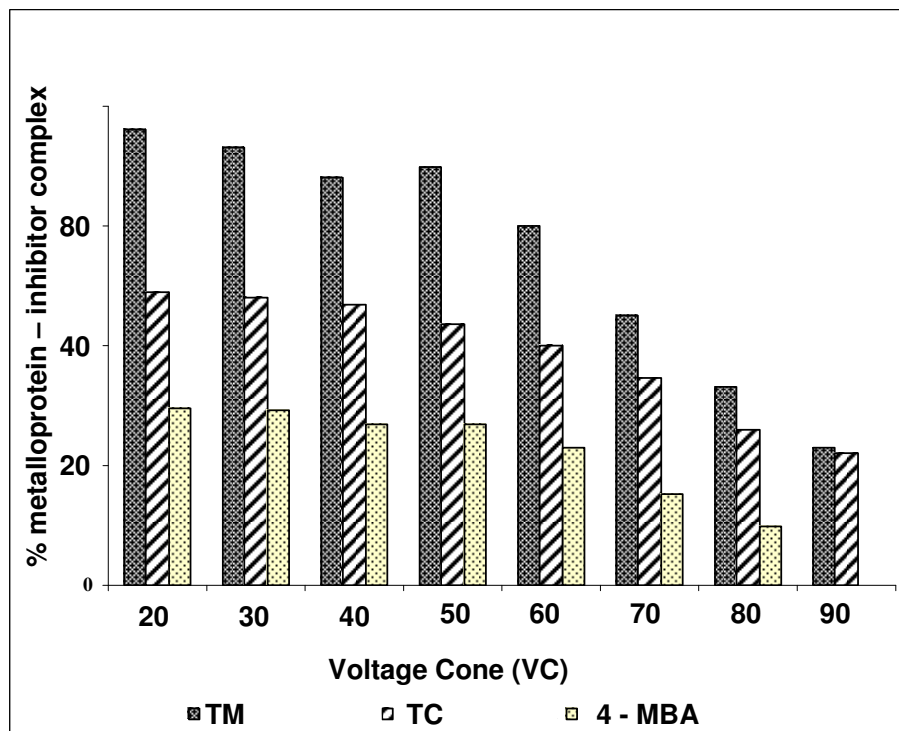


Figure 3.6: Relative abundance of Zn_2 -BcII-inhibitor complexes compared to the inhibitor – free Zn_2 -BcII complex (%) based on peak area integration at different sample cone voltages for (*R,S*)-thiomandelic acid (TM), thiosalicylic acid (TC) and 4-mercaptobenzoic acid (4-MBA). All experiments were performed in ammonium acetate buffer (pH 7.5) with a pressure at the interface of 6.7 mbar.

Determination of the relative affinities of thiol inhibitors on BcII using ESI-MS

Figure 3.7 shows the ESI mass spectra obtained for Zn_2 -BcII after incubation with 1.3 equivalents of (*R,S*)-thiomandelate (Figure 3.7A), thiosalicylate (Figure 3.7B), and 4-mercaptobenzoate (Figure 3.7C). Analysis of the spectra for the three inhibitors revealed that ca. 70 % of Zn_2 -BcII is associated with (*R,S*)-thiomandelate, compared to ca. 43 % for thiosalicylate and 27 % for 4-mercaptobenzoate. Inhibition constants K_i were previously determined in solution (43). In those experiments, K_i values of 0.34 μ M, 29 μ M and 346 μ M were determined for (*R,S*)-thiomandelic acid, thiosalicylic acid and 4-mercaptobenzoate, respectively. The authors explained that the compound affinity increased when the thiol and carboxylate groups are in close spatial proximity (43) which was in good agreement with the results obtained by ESI-MS. With 1.3 molar equivalents of inhibitor relative to metalloenzyme, two further

molecules of 4-mercaptobenzoate were observed to bind to the Zn_2 -BcII complex but at a stepwisely decreasing abundance relative to the first one, suggesting a non-specific binding for this inhibitor. A relative abundance of 33 % was observed for the Zn_2 -BcII-benzylmercaptan complex (Figure 3.7D), which is ca. 50 % less abundant than for thiomandelate acid, demonstrating that the presence of an appropriately positioned carboxylate group results in increased complex stability. Results previously obtained by spectrophotometric experiments in solution (43) are also consistent with the results obtained by ESI-MS in this work. A K_I of 9 μ M was obtained for benzylmercaptan.

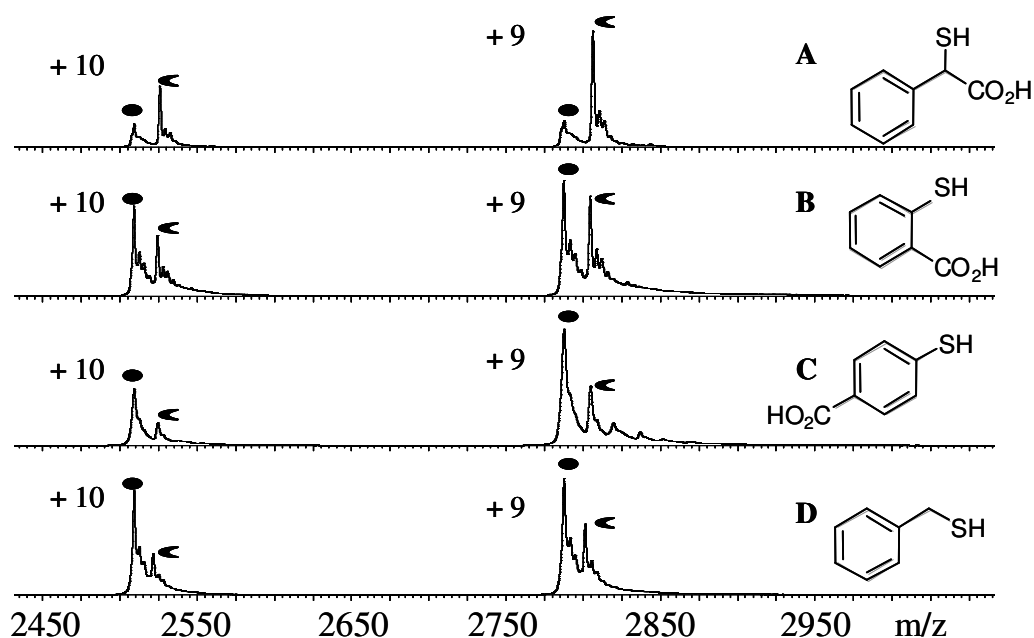


Figure 3.7: ESI mass spectra of Zn_2 -BcII (15 μ M) after incubation with 1.3 molar equivalents of (*R,S*)-thiomandelic acid (MW = 168.0 Da) (**A**), thiosalicylic acid (MW = 154.0 Da) (**B**), 4-mercaptobenzoic acid (MW = 154.0 Da) (**C**) and benzylmercaptan (MW = 124.0 Da) (**D**). Experiments were carried out in ammonium acetate (pH 7.5), sample cone voltage 50 V, pressure at interface 6.7 mbar. The ions carrying the charges + 9 and + 10 are represented in the mass spectra. Metalloenzyme and metalloenzyme-inhibitor-complex and represented by circle and crescent, respectively.

Replacing the thiol group of (*R,S*)-thiomandelate by a hydroxyl group, i.e. with mandelate (data not shown), resulted in a significant loss of affinity where less than 5 % of the Zn₂-BcII-inhibitor complex was formed even in the presence of 5.3 equivalents of inhibitor. This demonstrates that the presence of the thiol group is crucial for retaining the affinity with Zn₂-BcII, consistent with previously reported UV spectroscopy results (43). Thus the overall structure activity relationship (SAR) data obtained by mass spectrometry is consistent with SAR obtained previously in solution (122).

Determination of the dissociation constant K_D using ESI-MS

In order to obtain quantitative dissociation constant K_D data for a particular inhibitor, titration experiments, similar to the solution measurements, were carried out by mass spectrometry. The dissociation constant K_D value for the Zn₂-BcII-thiosalicylate complex was obtained by titrating the BcII metalloenzyme with different concentrations of the inhibitor. The calculation of the K_D value was performed by integrating the peak areas of the free metalloenzyme [E] and the BcII-inhibitor complex [EI]. The resulting ratio [EI]/[E] was used for the calculation of the absolute concentration of both species. Figure 3.8 shows the linear correlation between [EI]/[E] versus [I]_i-[EI] from 5 to 35 μM of thiosalicylate. The slope of the curve corresponds to 1/ K_D which was 35.3 ± 3.8 μM in this experiment. This value is in good agreement with the UV spectroscopy studies, where a value of 29 μM (SD ≤ 20 %) was determined (43).

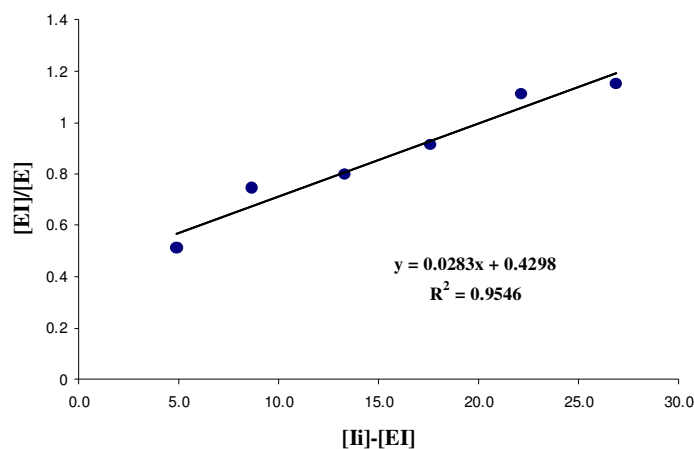


Figure 3.8 Graphic showing the correlation between [EI]/[E] versus [I]_i-[EI] obtained for the titration of BcII (15 μM) with thiosalicylic acid (10-35 μM). The K_i value calculated from the slope of the linear regression curve (in black) is 35.3 ± 3.8 μM.

3.3.2 Screening of new inhibitors using a dynamic chemistry approach combined with “native” ESI-MS

A dynamic combinatorial chemistry (DCC) approach combined with the above described “native”- ESI-MS technique was developed by B. M. Liénard in Oxford (Group of Prof. C. J. Schofield, Oxford, UK) to identify oligomers that can act as useful templates for MBL inhibitor discovery (123). The DCC method employs dithiols, derived from a selected lead inhibitor (compound A, Table 3.2), where one thiol group is designed to interact with the two active site zinc ions of BcII and the other as a tether to support the dynamic disulphide exchange with selected dynamic combinatorial library (DCL) members. With the use of “native”- ESI-MS and selected knockout experiments, two disulfides having the potential to improve the inhibition efficiency of the lead inhibitor were detected.

Since the two disulfides could not be synthesized, stable carba-analogues were synthesised (compounds B-F; Table 3.2). Analysis of the relative abundance of each of the Zn_2 -BcII-carbaanalogue complexes compared to the Zn_2 -BcII complex by “native” ESI-MS revealed that all synthesised carba-analogues display a better affinity for BcII: Zn_2 compared to the lead compound A, which is also in agreement with the inhibition constants (K_i) obtained by kinetic measurements in solution (Table 3.2).

Calculated K_i values indicated that the optimum linker chain length for mimicking the disulphide tether comprises two methylene groups as demonstrated by a K_i value of 6 μ M for compound C, which is also ca. 30 times more potent than the lead compound A. The highest K_i value corresponds to the analogue with the shortest linker chain i.e. only one methylene group (compound B, table 3.2). The small variation in K_i values observed with longer linker chains (compounds D and F, Table 3.2) may partly be due to the flexible nature of one of the BcII active site main loop, known for its participation in substrate recognition and catalysis by folding over the active site cavity (124).

The analysis of the relative ESI-MS affinity of compounds B-F for Zn_2 :BcII revealed that compounds with linkers comprising 2-4 methylene groups (a.k.a. C, D, F) are more potent than the compound B with the shortest linker chain. Moreover, in the gas phase the order of affinity potency is $D > F > C$, whereas the solution data gave $C > F > D$. Whilst the K_i values determined in solution are reasonably similar, it seems that small differences in inhibition potency are not differentiated by ESI-MS. Besides,

the relative abundance of the complex $Zn_2Bcll-E$ was found to be 51 % smaller than the compound with only one $-CH_2$ group. Compound E has the same linker length than compound D, but without the second carboxylate group. It could be concluded that the interaction between the second carboxylate group and Bcll are stronger in the gas phase compared to what was observed in solution.

3.4 Effect of inhibitors on the metal stoichiometry of MBLs determined by ESI-MS

As shown above, native ESI-MS is a suitable method for the evaluation of metal:enzyme:inhibitor ratios and therefore was further used to study the influence of two well known inhibitors (a.k.a *(R,S)*-thiomandelate and *D*-captopril: Figure 3.9) on the metal stoichiometry of MBLs.

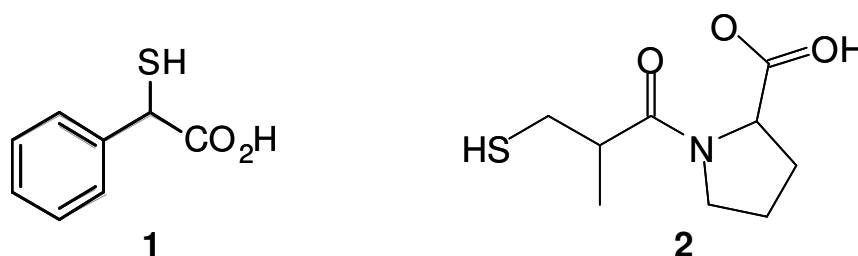
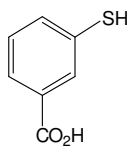
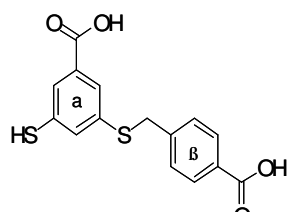
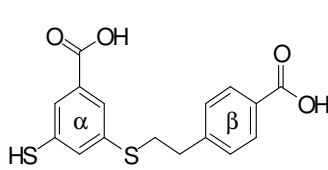
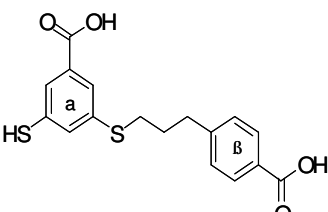
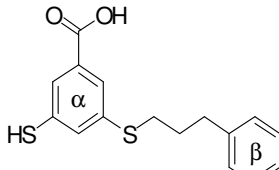
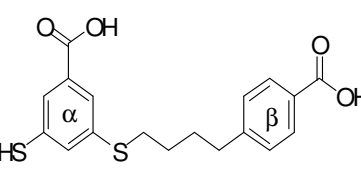


Figure 3.9: Structures of *(R,S)*-thiomandelic acid (1) and *D*-captopril (2).

Table 3.2: Inhibition constants (K_i) determined in solution of lead compound A for the DCC study and the synthesized carbaanalogue compounds (B-F) for BcII and relative abundances (sum of the peak intensities of ions carrying the charge + 9 and + 10) of the Zn_2BcII -inhibitor complexes (EI %) compared to the inhibitor-free Zn_2BcII monitored with ESI-MS. The final concentration of Zn_2 -BcII and of each compound was 15 μM and 45 μM , respectively in ESI-MS. Experiments were carried out in ammonium acetate (pH 7.5), cone voltage 50 V, pressure at interface 6.6 mbar.

Inhibitor	Structure	K_i (μM)	Complex EI (%)
A Lead structure 3-mercaptobenzoic acid		185	19
B 3-[(4-Carboxybenzyl) sulfanyl]-5-sulfanylbenzoic acid		102	62
C 3-[[2-(4-Carboxyphenyl) ethyl]sulfanyl]-5-sulfanylbenzoic acid		6	75
D 3-[[3-(4-Carboxyphenyl) propyl]sulfanyl]-5-sulfanylbenzoic acid		14	85
E 3-[[3-Phenylpropyl] sulfanyl]-5-sulfanylbenzoic acid		17	51
F 3-[[4-(4-Carboxyphenyl) butyl]sulfanyl]-5-sulfanylbenzoic acid		12	79

3.4.1 Binding of inhibitors to cadmium and zinc BclI enzyme

The case of (R,S)-thiomandelate

The binding of (*R,S*)-thiomandelate to Cd₁-BclI was investigated using ESI-MS (Figure 3.10). The Cd₁-BclI complex was first analysed without the presence of the inhibitor to assess the amount of any dinuclear species observable in the ESI mass spectra (Figure 3.10A). The addition of less than one molar equivalent of (*R,S*)-thiomandelate to the Cd₁-BclI complex led to the formation of five new peaks which correspond to the Cd₂-BclI-thiomandelate, Cd-Zn-BclI-thiomandelate, Zn₂-BclI-thiomandelate, apoBclI-thiomandelate and Cd₂-BclI complexes (Figure 3.10B). Thus, it seems that mainly dinuclear species have the ability to interact with (*R,S*)-thiomandelic acid, which may suggest that the inhibitor increases the affinity for binding of a second metal ion. The presence of the zinc-protein species can be explained by the presence of a residual amount of zinc in the apoprotein preparation and the inhibitor stock solution.

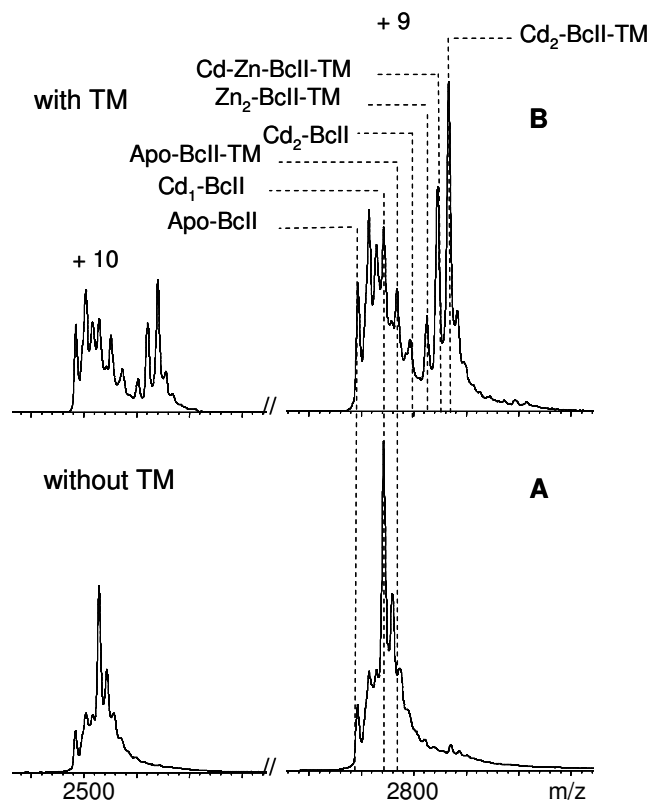


Figure 3.10: ESI mass spectra of the Cd₁-BclI complex in absence (**A**) and in presence of (*R,S*)-thiomandelate (**B**) in ammonium acetate pH 7.5. 8 μM of (*R,S*)-thiomandelate is added to 9.8 μM apoenzyme and 9.8 μM cadmium. Sample cone voltage 50 V, pressure at interface 6.7 mbar. The ions carrying the charges +9 and +10 are represented in the mass spectra.

The binding mode of (*R,S*)-thiomandelate to the zinc enzyme BclI at $[Zn^{2+}]/[apoprotein]$ ratios < 1 was then investigated. Figure 3.11 show that three protein species, namely apo-, Zn_1 - and Zn_2 -BclI are present and coexisting when less than one molar equivalent of zinc ion to the protein is present in solution and in absence of inhibitor (Figure 3.11A). The addition of less than one molar equivalent of (*R,S*)-thiomandelate to the zinc enzyme BclI at $[Zn^{2+}]/[apoprotein]$ ratios < 1 , resulted in the formation of a new peak which corresponded to the Zn_2 -BclI-thiomandelate complex, suggesting that the inhibitor binds preferentially to the dinuclear species of BclI (Figure 3.11B). Here the increase of the sample cone voltage to a value of 200 V shows that the Zn_2 -BclI-thiomandelate is a non-covalent complex, since it is disrupted at this cone voltage (Figure 3.11C).

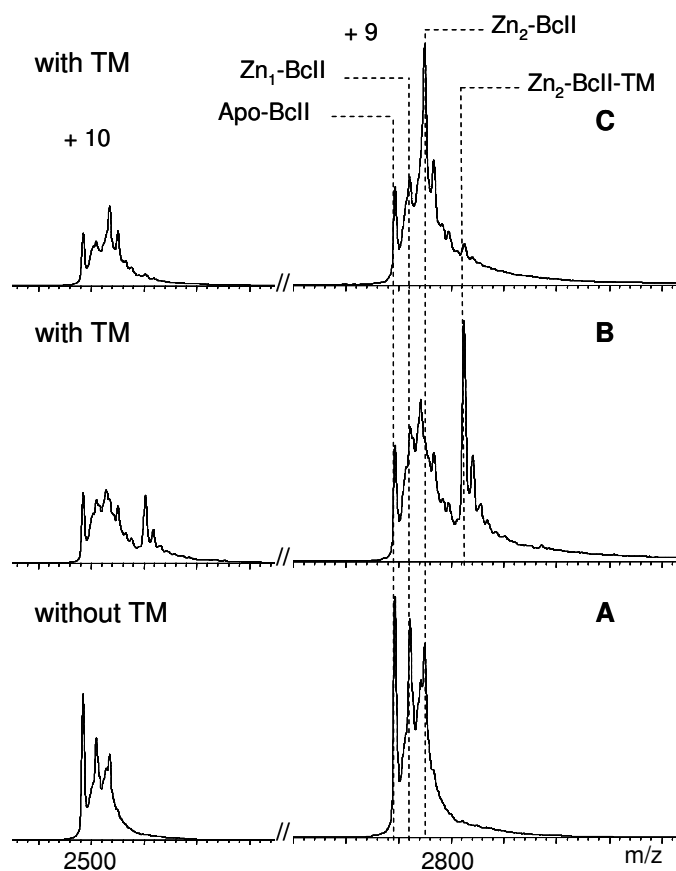


Figure 3.11: ESI mass spectra of the zinc enzyme BclI in absence (**A**) and in presence of (*R,S*)-thiomandelate (TM) in ammonium acetate pH 7.5 at a sample cone voltage of 50 V (**B**) and in presence of (*R,S*)-thiomandelate (TM) at sample cone voltage of 200 V (**C**). 8 μ M of (*R,S*)-thiomandelate is added to 9.8 μ M apoenzyme and 8.4 μ M zinc. Pressure at interface 6.7 mbar. The ions carrying the charges + 9 and + 10 are represented in the mass spectra.

D-Captopril versus (R,S)-thiomandelate

Table 3.3 shows the influence of *D*-captopril and (*R,S*)-thiomandelate on the metal stoichiometry of the zinc and cadmium BcII-enzymes. Incubation of *D*-captopril with the Cd₁-BcII complex resulted in the formation of a dinuclear protein species binding the inhibitor as already observed with (*R,S*)-thiomandelate, but with lower peak intensities. Thus, *D*-captopril also increases the affinity for the binding of a second cadmium ion in BcII. Incubation of *D*-captopril with the zinc-enzyme of BcII at [Zn²⁺]/[apoprotein] ratios < 1 led to the formation of a new peak which corresponded to the Zn₂-BcII-captopril complex.

Table 3.3: Relative peak intensities (sum of the intensities of ions carrying the charge + 9 and + 10) of the different protein BcII species as observed in ESI-MS when the zinc and cadmium enzyme BcII are incubated with (*R,S*)-thiomandelate (TM) or *D*-captopril (C) in ammonium acetate pH 7.5. ESI-MS spectra of the zinc enzyme are obtained by adding 8 μM (*R,S*)-thiomandelate or 15 μM *D*-captopril to 9.8 μM apoenzyme and 8.4 μM zinc. For the cadmium-enzyme, 8 μM (*R,S*)-thiomandelate or 15 μM *D*-captopril is added to 9.8 μM apoenzyme and 9.8 μM cadmium.

BcII species	Relative intensities of BcII-species by ESI-MS (%)					
	Cd(II)			Zn(II)		
		with TM	with C		with TM	with C
Apo-	16	15	16.5	39	21	12.5
Cd ₁ -	84	18	49	-	-	-
Cd ₂ -	-	-	-	-	-	-
Zn ₁ -	-	-	-	32	20.5	26
Zn ₂ -	-	-	-	29	22.5	37
Apo-l		7				
Zn ₁ -l	-		-	-	-	-
Zn ₂ -l	-	8	5	-	36	24.5
CdZn-l	-	21.5	10	-	-	-
Cd ₁ -l	-	-	-	-	-	-
Cd ₂ -l	-	30.5	19.5	-	-	-

3.4.2 Binding mode of (*R,S*)-thiomandelate to the CphA MBL

The binding mode of (*R,S*)-thiomandelate with the Zn₁-CphA complex was investigated (Figure 3.12). The addition of more than two molar equivalents of inhibitor to native mono-zinc CphA resulted in the formation of a new peak in the mass spectrum which could be assigned to the Zn₂-CphA-thiomandelate complex. The monozinc complex (Zn₁-CphA-thiomandelate) was not observed by ESI-MS under these experimental conditions. This observation suggests that the inhibitor induces the binding of the second metal ion. Moreover, the apo-CphA enzyme was not detected. Potentially, the formation of the Zn₂-CphA-thiomandelate complex is caused by the presence of Zn(II) is likely to originate from the inhibitor stock solution. Furthermore the results indicate that the inhibitor changes the charge state distribution of the protein ions in the ESI mass spectra, which is usually a reliable indication of the presence of conformational changes in the protein.

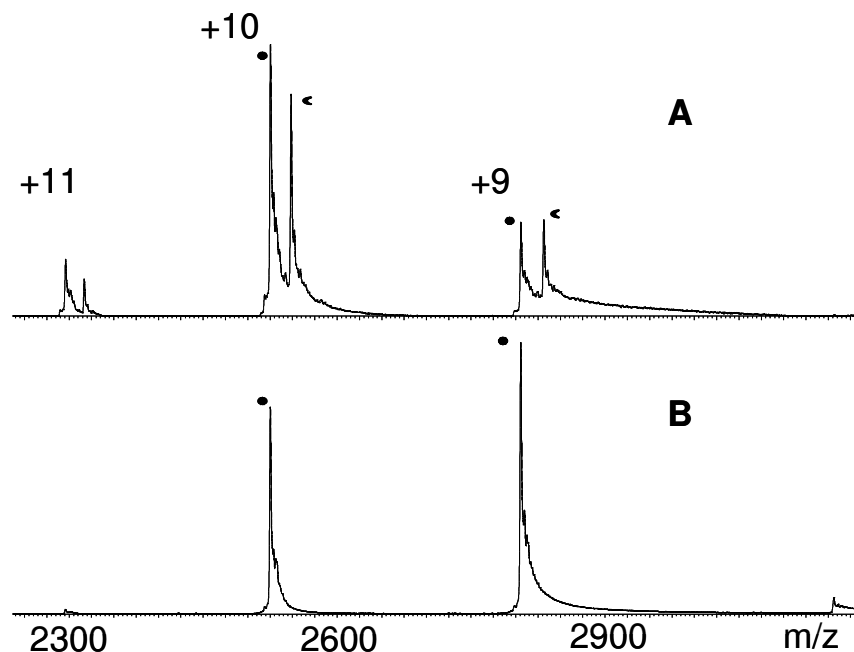


Figure 3.12: ESI mass spectra of Zn₁-CphA in presence (A) and in absence (B) of 2.6 molar equivalents of (*R,S*)-thiomandelate in ammonium acetate pH 7.5. The final concentration of Zn₁-CphA and (*R,S*)-thiomandelate was 15 μ M and 38 μ M, respectively. Sample cone voltage 50 V, pressure at interface 6.7 mbar. The ions carrying the charges + 9, + 10 and +11 are represented in the mass spectra. Metalloenzyme and metalloenzyme-inhibitor-complex are represented by circle and cresent, respectively.

3.5 Effect of inhibitors on the metal ion binding mode of MBLs using UV spectroscopy

In addition to ESI-MS, competition experiments with the chromophoric chelator Magfura-2 were performed to determine the dissociation constants for zinc and cadmium ions to the metal-free enzymes BcII, CphA and L1 in presence and in absence of (*R,S*)-thiomandelate and *D*-captopril. Figure 3.13 represents the experimental data (absorbance change at 363 nm) and fitting of the Zn(II) and Cd(II) binding to the three enzymes in presence and in absence of the inhibitors. One-step and two-step binding models (as described in paragraph 2.2.3) were fitted to the data in absence and in presence of apoenzymes, respectively. The resulting dissociation constants are summarized in Table 3.4.

The experimental data revealed that the zinc binding to the three enzymes is not drastically changed in presence of (*R,S*)-thiomandelate and *D*-captopril, whereas the cadmium binding is strongly affected. In fact, a higher concentration of Cd(II) ions is required for saturating the metal chelator with the inhibitors than without them.

Table 3.4 summarises the apparent dissociation constants for the three zinc and cadmium MBLs in presence or absence of the inhibitors.

The affinity for the binding of a second zinc ion increased slightly in presence of (*R,S*)-thiomandelate for all three zinc enzymes and is sufficient to induce positive cooperativity ($K_{D2} < K_{D1}$) in zinc binding for BcII. In contrast, the addition of (*R,S*)-thiomandelate to the three substituted cadmium-enzymes, led to the significant increase of the affinity for a second cadmium ion.

D-captopril had a smaller effect on the zinc enzymes compared to (*R,S*)-thiomandelate. The affinity recorded for the binding of a second zinc ion increased slightly for BcII and L1, whereas it became weaker for CphA. In contrast, *D*-captopril had a stronger effect on the Cd-enzyme L1. In the case of BcII and CphA, the dissociation constant for a second cadmium ion are slightly lower in presence of *D*-captopril.

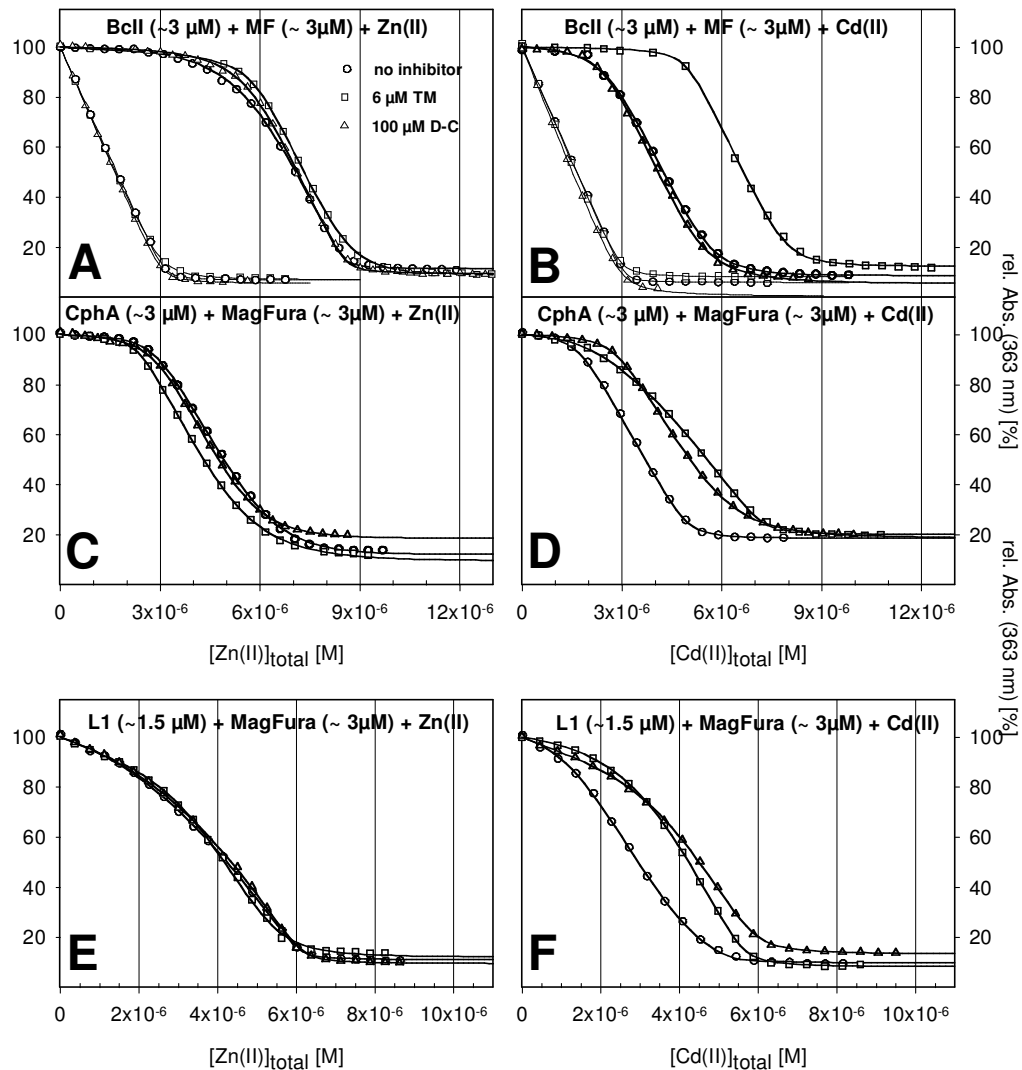


Figure 3.13: Determination of the affinity of the enzymes BclI, CphA, and L1 for Zn(II) and for Cd(II) in presence and in absence of (*R, S*)-thiomandelate and *D*-captopril by competition with Mag-fura-2 in 15 mM HEPES, pH 7 at 22 °C. The total absorbance change at 363 nm corresponding to the sum of metal-free Mag-fura-2 (MF) and metal-loaded Mag-fura-2 (Me-MF) is a function of the added volume of 255 μM Zn(II) ion stock solution (left) and 255 μM Cd(II) ion stock solution (right) to a defined starting volume (1ml) in absence of apoenzymes (○ in grey), where a one-step binding model was fitted to the data (grey line) (A, B); in presence of apoenzymes (○ in black), where a two-step binding model was fitted to the data (black lines) (A, B for BclI), (C, D for CphA) and (E, F for L1). The total absorbance change at 363 nm in presence of the inhibitors is represented as (□) for (*R, S*)-thiomandelate (6 μM) and (△) for *D*-captopril (100 μM).

Table 3.4: Apparent dissociation constants of Me₁ and Me₂ species of the three MBLs namely BcII, CphA and L1 in presence and in absence of (*R,S*)-thiomandelic acid (TM) and *D*-captopril (C). Data for Zn(II) and Cd(II) binding were obtained from competition titrations with Mag-fura-2 as described in Paragraph 2.2.3. K_{D1} and K_{D2} represent the dissociation constants of the Me-MBL and the Me₂-MBL complexes, respectively.

inhibitor	metal	BcII		CphA		L1	
		K_{D1} [nM]	K_{D2} [nM]	K_{D1} [nM]	K_{D2} [nM]	K_{D1} [nM]	K_{D2} [nM]
-	Zn(II)	<0.1	0.85	<0.1	160	0.9	4.8
-	Cd(II)	0.15	210	<0.1	~400	0.5	40
6 μ M TM	Zn(II)	~0.40	~0.16	<0.1	120	~1.3	~1.3
6 μ M TM	Cd(II)	<0.1	<0.1	~0.14	2.4	~0.25	~1.2
100 μ M C	Zn(II)	<0.1	~0.41	<0.1	190	~1.0	~4.0
100 μ M C	Cd(II)	~0.14	170	<0.1	110	~1	~1

3.6 DISCUSSION

3.6.1 Validity of the ESI-MS method for the study of MBLs

Relevance of the instrument parameters for the characterization of metallo- β -lactamases

The observation of biological complexes preserved in solution by a number of weak interactions can be achieved using “native” ESI-MS and has been demonstrated in the past as well as in the present work. The stoichiometry of complexes, the mode of binding and the binding strength of potential ligands can be assessed by this technique. This has only been proven viable if the network of interactions stabilizing the native complex is retained in the gas phase. Indeed, inappropriate experimental settings of the ESI interface can translate into artefacts in the MS spectra, which may lead to misinterpretations of the data.

An efficient ion desolvation usually requires the use of a counterflow of nitrogen gas, heat and collision induced dissociation (CID) in the atmosphere/vacuum interface. Variation of these parameters is known to affect the stability of complexes in the gas phase (84, 125, 126). In the present work, the influence of the accelerating voltage (VC) at the atmospheric/vacuum interface on the metal-enzyme BcII complex and the ternary metal-enzyme BcII-inhibitor complexes was evaluated.

Whilst studying the zinc-enzyme BcII interactions, three protein species were observed in the ESI mass spectra during the zinc titration of apoBcII i.e. the apo, Zn₁- and Zn₂-BcII species. Increasing the accelerating voltage to 200 V did not alter the relative abundance of the three protein species indicating that none of the three BcII species are advantaged or discriminated during their transfer through the vacuum/atmospheric interface.

In contrast, the accelerating voltage was shown to have a significant disrupting impact on the stability of the ternary metal-enzymes-inhibitor complexes. Progressive disruption of the non-covalent interactions between the inhibitor and the metalloenzyme were observed with increasing accelerating voltage value. Therefore, for comparing the binding strength of different inhibitors, this voltage value was kept constant throughout the study. The value of the appropriate accelerating voltage was determined by comparing the peak intensity corresponding to the different metalloprotein-inhibitor complexes at different accelerating voltages between 20 and

100 V. Below 30 V, low peak resolution due to inefficient ion desolvation was observed whereas at 90 V the peaks corresponding to a number of metalloprotein-inhibitor complexes disappeared. Thus, a compromise should be achieved between efficient desolvation and non-destructive gas-phase collisions in order to detect these types of complexes.

Specificity of the non-covalent complex: Observation of artefacts

A number of reports about the presence of non-specific interactions in “native” ESI mass spectra are available (127, 128). Smith and Light Wahl suggested that non-specific associations are rather formed in solution than in the gas phase. Aggregation leading to non-specific assembly through ion-ion or ion-molecule interactions in the gas phase is unlikely (128). During the ionization process, the ion concentrations and their presence in the gas phase remains relatively low; consequently, the probability that a charged molecule collides with a neutral molecule is very small (129). Furthermore, the aggregation of molecules with same polarity is not expected due to the coulombic repulsions (130). However, the hypothesis that non-specific aggregates are formed in the gas phase is not completely excluded. In fact, during the ionization process, the evaporation of the solvent leads to an increasing concentration of analytes in the small offspring droplets at the end of the Taylor cone. When the non-specific interactions survive the ionization process, they can be detected in the ESI mass spectra (128, 131).

To verify that the non-covalent interactions obtained in the ESI mass spectra are specific, a number of control experiments are required. This can be achieved by modifying the chemical equilibrium of the non-covalent complexes in solution. Variation of the experimental conditions (eg. pH, solvent, binding partners) can induce the formation of new signals in the ESI mass spectrum, demonstrating the specificity of the non-covalent complex obtained in the gas phase. In the case of the metal-protein interaction study, dissolving the metalloprotein in an organic solvent resulted in the observation of new peaks in the lower mass range corresponding to the metal-free species of BcII. Additionally, if the binding partner of the apoBcII is changed in solution as shown by replacing Zn(II) for Cd(II) ions, formation of new complexes such as Cd-bound species are observed in the ESI mass spectra. Furthermore, the saturation of apoBcII with Zn(II) ions resulted in the formation of the

expected metal : apoBcII binding stoichiometry only (i.e. 2:1). Any other metal-substituted protein complexes such as Zn_3 -, Zn_4 - or Zn_5 -BcII were not observed.

Control experiments were also carried out with the metalloprotein-inhibitor complexes. The addition of more than one molar equivalent of inhibitor to Zn_2 -BcII led to the formation of a Zn_2 BcII-inhibitor complex with a 1: 1 binding stoichiometry (except for 4-mercaptobenzoic acid, where a 1:3 binding stoichiometry was observed). Furthermore the addition of inhibitor to metal-free BcII did not produce any apoBcII-inhibitor complex (data not shown), which indicates that the inhibitor binds specifically to the active site metal ions.

Quantification of the different protein species from the ESI mass spectra

To determine the relative or absolute binding strength between an enzyme and a small molecule ligand using ESI-MS, the relative abundance of the different protein species observed in the mass spectra has to reflect that existent in solution. The distribution of the protein species in solution can be distorted during ion formation, ion desolvation and/or during transmission into the analyzer.

In fact, peptides and proteins are ionized in solution by protonation of the basic residues or by deprotonation of the acidic residues. The charge state depends on the relative values between the pI of the protein and the pH of the buffer in solution. Enzymes bearing a global positive net charge are more likely to yield intense signals when the measurement is performed in the positive ion mode (132).

During the ion desolvation, ionic interactions, hydrogen bonds and Van der Waals forces generally survive the ionization process but also the ionic bonds in particular are strengthened in the gas phase compared to the situation in solution (133). In contrast, hydrophobic interactions originating from the repulsion with water molecules, are not present in solvent-free environment. When hydrophobic interactions are the main forces involved in the cohesion of an enzyme-ligand complex, frequently no correlation is found between the binding strength in solution and the one observed in the gas-phase (134). In our metalloprotein-inhibitor studies, varying the distance between the thiol and the carboxylate groups of the mercaptocarboxylate compound has shown to significantly affect the binding affinity between the inhibitor and the enzyme as it was previously observed in solution (43). In the DCC-MS approach, ESI-MS data agreed reasonably well with the solution data, showing that a minimum of two methylene groups are required for efficient

inhibition of BcII. Therefore, it can be concluded that the major set of interactions between the metalloprotein BcII and the tested inhibitors are electrostatic forces. This is consistent with findings from crystal structures of MBLs with thiol-containing inhibitors, where both an interaction of the thiol group of the compounds with the metal ions in the active site of the protein (38) and an interaction of the carboxylate group with the side chain of a lysine residue (38) of BcII could be observed.

One significant anomaly between the solution phase and the gas phase data sets was observed in case of benzylmercaptan, where the relative abundance of the peak corresponding to the Zn_2 -BcII-benzylmercaptan complex was lower compared to that of the Zn_2 -BcII-thiosalicylate complex. This is in contrast to UV-spectroscopy data in solution, which indicated for a higher affinity of BcII for benzylmercaptan (9 μ M) than for thiosalicylate (29 μ M). The obvious chemical structure differences between the two inhibitors are the presence of a carboxylate group in thiosalicylate and the aromatic thiol versus the benzylic thiol function. Similar contradictory results between gas-phase data and solution data were also found when the DCC-MS approach was applied; here, the relative abundance of the BcII-compound E complex was lower than that of the BcII-compound B complex, whereas in solution the K_i values indicated that compound E (17 μ M) is approximately six times more potent than compound B (102 μ M). In this particular case, the chemical structure differences were the number of methylene groups constituting the proposed mimic arrangement for the disulfide bond and the presence of an additional carboxylate group on the second aromatic ring. One likely explanation for these discrepancies is that the interactions between BcII and benzylmercaptan or compound E are mainly hydrophobic whereas those involved between BcII and thiosalicylate or compound B have a more polar character.

3.6.2 Metal binding to MBLs

Despite having identical metal binding residues, namely 3-His for site 1 and DCH for site 2, the enzymes belonging to the B1 MBL subclass are known to have substantially different metal binding affinities. Indeed, the CCrA, Imp-1 and BlaB MBLs are known to bind tightly two Zn(II) ions (4, 135, 136), whereas very different affinities have been determined for the first zinc ion ($K_{D1} = 1.8$ nM) and the second zinc ion ($K_{D2} = 1.8$ μ M), respectively, in case of BcII (4). Negative cooperativity in zinc

binding was therefore concluded for this enzyme. Even when using cadmium or cobalt in place of zinc ions in BcII, the dissociation constant for the binding of a second metal ion was found to be significantly higher compared to the binding of a first metal ion ($K_{DCo1} = 93$ nM; $K_{DCo2} = 66.7$ μ M (39) and $K_{DCd1} = 12.5$ nM and $K_{DCd2} = 256$ nM (11)).

The present BcII metal binding study performing “native” ESI-MS revealed that two Zn(II) ions or two Co(II) ions bind tightly to BcII. Mag-fura-2 experiments revealed dissociation constants values for the binding of one and two zinc ions, which were found to be lower than 1 nM. The determined value K_{D2} was revised by a factor of 2000 compared to that previously reported (4). This difference in metal affinities with BcII is surprising and could not be explained up to now. The BcII enzyme used in this work was isolated from *E. coli* BL21(DE3). For cultivation, the cells were grown in minimal medium, whereas in all previous studies LB medium was used. LB-produced BcII samples showed a pink colouration (137), which was not observed in BcII samples isolated from cultivations on minimal medium. One reasonable explanation for the presence of this pink colouration could be the presence of a pigment in the case of the LB-produced BcII, which potentially possesses strong affinity for zinc (or cobalt) ions modifying the apparent metal:protein stoichiometry. Another possible reason for the difference in metal affinities is the presence of a small amount of N-terminally truncated BcII species, which has been observed by mass spectrometry in the LB-produced-BcII samples (data not shown). However, the BcII enzyme used in the present study was shown to be free of N-terminally truncated BcII species.

Furthermore, the analysis of the “non-denaturing” ESI mass spectra suggests that binding of the second Zn(II) ion to the apoenzyme BcII is positive cooperative. This conclusion is based on the observation that the ratio of $K_{D1}/K_{D2} \gg 1$ and that the Zn₁-BcII complex was not observed as the predominant protein species during the titration of apoBcII monitored by ESI-MS. In contrast, both K_D values obtained with the Mag-Fura titrations were not conclusive to determine the potential positive cooperativity in zinc binding to BcII. In fact, K_{D2} was found to be higher than K_{D1} .

In the ESI-MS experiments, it was assumed that the three protein forms i.e. apo, Zn₁ and Zn₂-BcII displayed the same ionization efficiencies, though it could not be proved experimentally, due to the presence of the three protein species at low ratios of $[Zn^{2+}]/[apoprotein]$. Therefore, these ESI-MS data have to be interpreted with care. In fact, a small difference in ionization efficiencies of the BcII protein species will have a

significant impact on the pre-existent equilibrium in solution.

Another parameter which has to be discussed is the determination of the concentration of the analytes in the gas phase. In fact, extensive evaporation of the charged droplets formed at the ESI spray tip increases the concentration of the analytes. A higher concentration of reactants in a droplet will shift the equilibrium of the reaction in solution: $P + L = PL$ towards more PL product. Therefore it has also to be proved that the kinetic rate of the equilibrium shift is slower than the evaporation rate (121).

When replacing zinc by cadmium ions, a sequential binding of the metal ion to BcII was observed by ESI-MS as well as in competition-titration experiments. These results were also consistent with the previously reported data using the BcII enzyme (4). Previous studies highlighted that the two binding sites require the same metal binding affinity, which led to the conclusion that the higher dissociation constant for a second metal ion could only be explained by negative cooperativity (39). Slow association rates for the formation of the Cd_2 -BcII enzyme determined by stopped-flow fluorescence measurements suggested that a fast metal exchange between the two sites of the mononuclear enzyme was inhibiting the binding of a second metal ion (39). A parallel investigation on the dynamics of cadmium binding to the mononuclear BcII enzyme used a combination of PAC and NMR spectroscopic experiments (11). The results revealed that the metal quickly jumped between the two metal binding sites in a μs time regime and thus inhibited the binding of a second cadmium ion, which is responsible for negative cooperativity. In the past, metal ion interchange was also suggested for zinc binding to BcII (39). In the present study, using purified BcII enzyme from cultivation on minimal medium, negative cooperativity for the zinc binding was not observed. It was therefore concluded that other parameters may be involved and that “zinc jumping” remains to be proven.

3.6.3 Inhibition of native and cadmium-substituted MBLs

1) D-Captopril

Captopril, a well-known angiotensin converting enzyme-blocking agent (140), was previously shown to inhibit metallo- β -lactamases (10). Kinetic studies have revealed that enzymes from the three MBL subclasses, loaded either partially or fully with metals, are inhibited by two of the captopril isomers. Furthermore, a combination of

several techniques including EXAFS, PAC and competition-titration experiments have shown that the mononuclear forms of BcII and CphA were preferentially inhibited by the inhibitor (10). The study demonstrated two different inhibitor binding modes: for the Cd₁-BcII enzyme, the thiolate group of *D*-captopril binds to the single metal ion when located at the 3H site and its carboxylate group potentially interacts with the metal when it is located in the DCH site. Moreover, for the Cd₁-CphA enzyme, only one binding mode was found i.e. the thiolate function of *D*-captopril coordinates the metal ion when it is located in the DCH site. CphA was also found to preferentially interact with the D- isomer of captopril.

In the present study, the binding of *D*-captopril to the native zinc BcII and CphA enzymes was investigated using titration experiments with the chelating agent Mag-fura-2 and “native”-ESI-MS. Additionally, the preference of *D*-captopril for the Cd₁-species of the BcII and CphA enzymes was verified. Besides, the inhibition of the enzyme L1, representative of subclass B3, was also investigated using Mag-Fura titrations.

Similar dissociation constants for the binding of the first ($K_{D1} = 0.9$ nM) and second zinc ion ($K_{D2} = 4.8$ nM) were found for the L1 enzyme, consistent with previously published reports (4). The L1 enzyme is considered as a di-zinc enzyme. The binding of *D*-captopril to the L1 enzyme had no influence on K_D values. L1 remained a Zn₂-form in presence of *D*-captopril. In the past, the crystal structure of the complex between another di-zinc enzyme of subclass B3, namely Fez-1 enzyme from *Legionella gormanii*, and *D*-captopril has been solved. The data revealed that the inhibitor is located close to the active site, but did not coordinate the two available zinc ions (45).

For the cadmium-bound L1 enzyme, two different dissociation constants were found, i.e. 4.8 nM for the first Cd(II) ion and 40 nM for the second Cd(II) ion. In presence of *D*-captopril, the second dissociation constant decreased by 40 fold approaching the dissociation constant of the first one. This indicates that the mode of inhibition of *D*-captopril may involve binding to the Cd₂-L1 to achieve efficient inhibition.

On the other hand, Mag-Fura titrations showed that *D*-captopril did not change the metal binding stoichiometry of the Cpha monozinc-enzyme. The strength of the interaction between *D*-captopril and Zn₁-CphA is likely to be rather weak. In fact, the zinc-CphA-*D*-captopril complex could not be observed in the ESI experiments. In the CphA monocadmium-enzyme, *D*-captopril slightly decreased the dissociation

constant for the second metal ion from 400 nM to 110 nM. The compound may bind to the Cd₁-CphA for efficient inhibition, which is consistent with previously reported EXAFS and PAC data (10).

In the zinc BcII enzyme, the two zinc ions bind very strong to the active site. In the presence of *D*-captopril, the dissociation constant for a second zinc ion was not significantly lower compared to the un-inhibited enzyme. *D*-captopril required two zinc ions for efficient binding to BcII, as clearly shown by the results of the ESI experiments. Despite the fact that the apo, Zn₁ and Zn₂-BcII species were present at low zinc concentrations, only the Zn₂-form was found to bind the inhibitor. In the crystal structure of the *D*-captopril complex with another MBL of subclass B1, namely BlaB enzyme from *Chryseobacterium meningosepticum*, it was found that the inhibitor interacts with the two active site zinc ions (44). BlaB is also considered a di-zinc enzyme.

Furthermore Mag-Fura titrations revealed that *D*-captopril did not significantly change the dissociation constant for a second cadmium ion in the BcII-enzyme i.e. 210 nM without inhibitor and 170 nM with inhibitor. Previous EXAFS and PAC data showed that the mononuclear form of BcII is the preferred target for inhibition (10). In contrast, the present ESI-MS analysis revealed only the presence of the dinuclear BcII species with bound *D*-captopril. One possible explanation is that the inhibitor exhibits two binding modes i.e. inhibition of the native Cd₁-form and to a certain extent induction of dinuclear-forms and that only the latter one survives the transfer from solution into the gas phase.

In conclusion, depending on the subclass of metallo- β -lactamase and the nature of the metal ion, *D*-captopril adopts different binding modes to convey its inhibitory effect, i.e. *D*-captopril seems to be able to interact with both mono- and di-zinc MBL. Whatever the nature of the metal ion is, *D*-captopril seems to interact with M₂-L1 only and Me₁-CphA only, whereas in the case of BcII, the metal stoichiometry, upon binding of *D*-captopril, depends on the nature of the metal ions itself, i.e. two metals when incubated with zinc and one or two metals with cadmium.

2) (*R,S*)-Thiomandelate

The inhibition by both enantiomers of thiomandelate has been previously assessed on different MBLs loaded with two zinc ions (43). (*R,S*)-thiomandelate was shown to be a potent inhibitor of subclasses B1 and B3 MBLs. Inhibition constants for the

dizinc BcII were 90 nM and 1280 nM for the *R*- and *S*-thiomandelate, respectively. Structure activity relationship (SAR) data in solution (43) and in ESI-MS (122) clearly showed that the thiol group is essential for inhibition and that the presence of the carboxylate group increases the inhibitory potency. A NMR/PAC study has also been performed with the Cd₂-BcII (9), showing that both enantiomers interact with the two cadmium ions via the thiol group and that the carboxylate group may interact with Arg91. This was observed previously for the complex between a mercaptocarboxylate ligand and the enzyme IMP-1 (38). In presence of one cadmium ion in the active site of BcII, the compound was shown to induce positive cooperativity in metal binding by PAC/NMR experiments (9).

In the present study, the interaction between zinc and cadmium-bound BcII, CphA and L1 enzymes and (*R,S*)-thiomandelate was investigated using competition titration experiments in solution. Native ESI-MS was only used for the study of BcII and CphA.

The titration-experiments revealed that the binding of (*R,S*)-thiomandelate to the zinc-L1 enzyme significantly decreased K_{D2} and slightly increased K_{D1} . (*R,S*)-Thiomandelate required the two zinc ions for efficient inhibition in the di-zinc-L1 enzyme. In the cadmium-bound L1 enzyme, (*R,S*)-thiomandelate had the same effect as *D*-captopril, i.e. it leads to a 40-fold decrease of K_{D2} . (*R,S*)-thiomandelate might also require two cadmium ions for efficient binding in the L1 enzyme.

The binding study carried out with (*R,S*)-thiomandelate and zinc-CphA monitored by ESI-MS indicated that the inhibitor induced the production of dinuclear zinc-species. The presence of the two zinc ions seems to be required for efficient binding of (*R,S*)-thiomandelate. However the Mag-Fura titrations revealed only a minor variation of the K_{D2} value in the zinc-CphA enzyme. This may be explained by the low amount of (*R,S*)-thiomandelate (6 μ M) added during the titrations experiments, which might not have been enough to inhibit the total amount of CphA enzyme present. In fact, the inhibition constant of (*R,S*)-thiomandelate for CphA has been found to be 144 μ M (43).

In cadmium-substituted CphA enzyme, (*R,S*)-thiomandelate decreased dramatically the dissociation constant for the binding of a second cadmium ion by 200-fold. Thus, this inhibitor produced the dinuclear form of CphA.

The inhibitory effect of (*R,S*)-thiomandelate on the cadmium-bound BcII enzyme decreased the K_{D2} value from 210 nM to less than 0.1 nM. The inhibitor required two

cadmium ions for binding to BcII. This was consistent with the ESI-MS results, where (*R,S*)-thiomandelate showed to induce only the formation of inhibited dinuclear protein species in the Cd₁-BcII enzyme. Moreover, the apparent K_D values determined in solution did not indicate any positive cooperativity of cadmium binding when incubated with the compound, which is not consistent with previous reports (9). On the other hand, positive cooperativity of zinc binding ($K_{D2} < K_{D1}$) was induced by (*R,S*)-thiomandelate when incubated with the zinc enzyme BcII, as determined by titration experiments in solution. Further on, the ESI-MS results show that (*R,S*)-thiomandelate only inhibited the dinuclear form of BcII at a metal: protein stoichiometry below 1.

In conclusion, it was found that the MBL inhibitor (*R,S*)-thiomandelate binds to BcII, CphA and L1 enzymes with a strong preference for binding to the dizinc species. This metal form may be induced upon inhibitor binding like it is the case for Zn- and Cd-CphA, Cd-L1 and Cd-BcII enzymes or native Zn-L1 and Zn-BcII enzymes.

CHAPTER IV

METAL AND INHIBITOR BINDING STUDIES STUDIES using HDX-MS

4 METAL AND INHIBITOR DEPENDENT PROTEIN FLEXIBILITY: RESULTS

4.1 Circular Dichroism (CD) spectroscopy

CD spectroscopy was used to measure the difference in secondary structure between the different metal-loaded species of BclI. The CD spectra of the apo, Zn₁, Zn₂, Cd₁ and Cd₂-BclI species are shown in Figure 4.1.

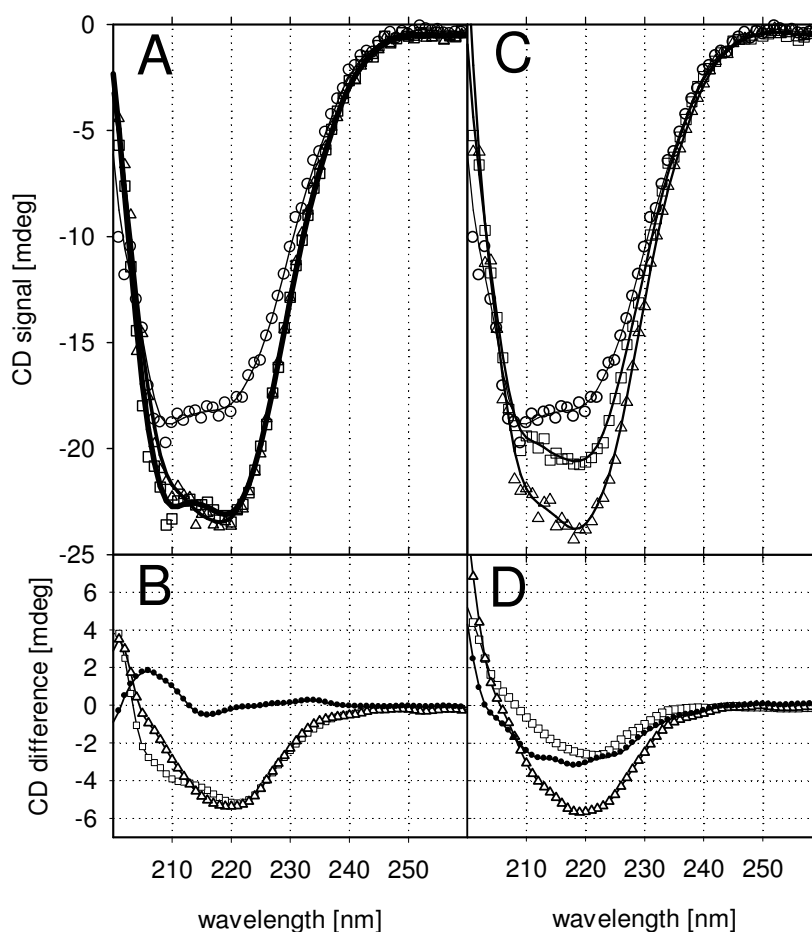


Figure 4.1: Circular dichroism spectra of BclI species. Experimental data are represented by symbols, smoothed spectra by lines. (A) Spectra of apo-BclI (open circles), Zn₁-BclI (open squares), and Zn₂-BclI (open triangles); (B) Difference spectra of Zn₁-BclI – apo-BclI (open squares), Zn₂-BclI – apo-BclI (open triangles), and Zn₂-BclI – Zn₁-BclI (filled circles); (C) Spectra of apo-BclI (open circles), Cd₁-BclI (open squares), and Cd₂-BclI (open triangles); (D) Difference spectra of Cd₁-BclI – apo-BclI (open squares), Cd₁-BclI – apo-BclI (open triangles), and Cd₂-BclI – Cd₁-BclI (filled circles).

A significant change in the 230-210 nm range of the spectrum was monitored when metals were added to the apoenzyme. Binding of two metals ions increased the intensities of the negative band at 220 nm compared to the metal-free enzyme, indicating an increase in secondary structure content. The addition of one zinc ion showed the same band intensity at 220 nm as for the Me₂-BcII species, an additional shoulder at 210 nm was observed. Thus, the binding of one Zn(II) ion had a more pronounced effect on the secondary structure than the addition of a second Zn(II) ion. The addition of one cadmium ion yielded a band intensity at 220 nm, which was between the apoenzyme and the Me₂-BcII proteins; the binding of only one Cd(II) might not be sufficient to reach the maximum of secondary structure elements.

4.2 Hydrogen/Deuterium Exchange-Mass Spectrometry

To follow and localize structural changes inside the BcII protein, HDX-MS combined with protein fragmentation was performed using the method described in paragraph 2.2.10: In the first step, the peptides generated by digestion of BcII with pepsin were identified and assigned to the protein. In a second step, the H/D exchange of the peptic-peptides was monitored in apo, Zn₁, Zn₂, Cd₁ and Cd₂-BcII species using MALDI-ToF/ToF/MS.

4.2.1 Assignment of the peptic-peptides to BcII protein

The identification of the peptic-peptides of BcII and their selection for the HDX experiments was performed after analysis of the peptide mass fingerprint (PMF) (see appendix 2).

In the PMF, 33 peptides in the mass range of m/z 800-3500 could be assigned to the BcII protein. A sequence coverage of 98 % was reached and all metal ligands could be identified. The average mass accuracy of identified peptides was 3.5 ppm. The amino acid sequence of all peptides was validated by tandem mass spectrometry using post source decay (PSD) with post-acceleration technique (see MS/MS spectrum in appendix 3 as an example). The same peptides could be assigned to the protein for all metal-substituted species namely Zn₁, Zn₂, Cd₁ and Cd₂-BcII species.

Due to peak overlapping caused by the different number of exchangeable protons, the extent of deuteration could not be unambiguously analyzed for all 33 peptic-

peptides after incubation of the protein in deuterated buffer; only 22 peptides covering almost 96 % of the protein sequence (Figure 4.2, Table 4.1) were accessible, again containing all residues belonging to the two metal binding sites were amongst the interpretable sequences. The three metal ion ligands of the C-terminal domain, namely His149, Cys168, and His210 were found in the peptide fragments P[139-155], P[165-188], and P[205-219], respectively. The typical MBL superfamily sequence motif HxHxD was found in P[82-110] from the N-terminal domain.

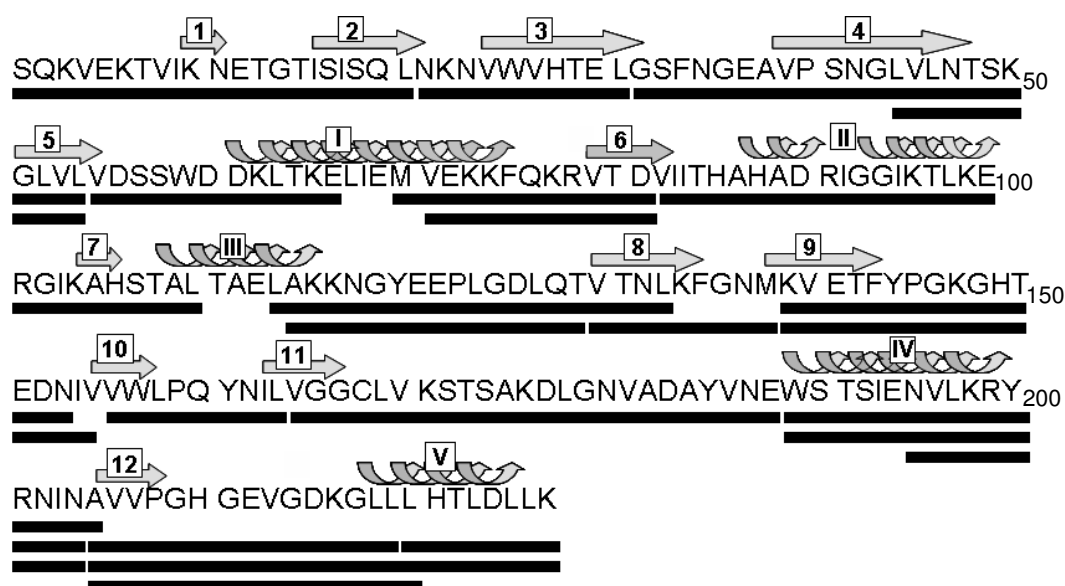


Figure 4.2: Sequence coverage of the BclI enzyme reached in PMF analysis of a 10 minutes-pepsin-digested apoenzyme BclI. Each bar corresponds to a peptic peptide, which was identified by tandem mass spectrometry and further on analysed by HDX-MS. Secondary structures are labelled by an arrow for the β -sheets and a spring for the α -helices. Metal ligands for the first binding site are His86, His88, His149 (His116, His118 and His196 in the class B β -lactamase (BBL) numbering (20)). Metal ligands of the second binding site are Asp90, Cys168, His210 (BBL: Asp120, Cys221, His263).

4.2.2 Determination of the deuterium uptake for one in-exchange time

In order to follow the deuterium uptake of the 22 peptic peptides for the different metal-substituted species, the centroid mass of each isotope cluster of the 22 deuterated peptides was calculated for each in-exchange time (Figure 4.3). Subsequently their masses were subtracted from the centroid mass of the non-deuterated one and corrected as described in Paragraph 2.2.11. In the following study, the data are shown for selected peptides after an incubation time of 2000 sec.

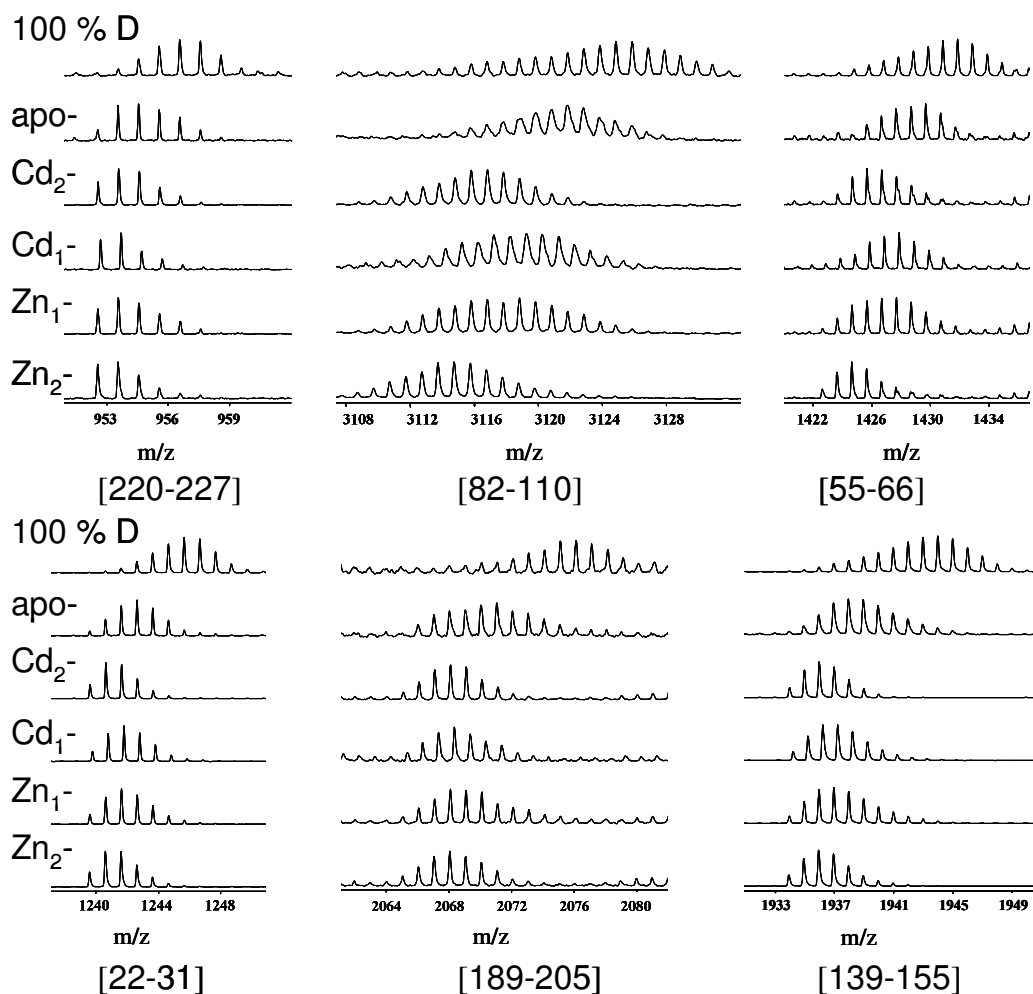


Figure 4.3: MALDI-mass spectra of selected peptic-peptides P[220-227], $m/z = 952.581$; P[82-110], $m/z = 3106.751$; P[55-66], $m/z = 1422.675$; P[22-31], $m/z = 1239.650$; P[189-205], $m/z = 2064.100$; P[139-155], $m/z = 1933.965$ in deuterated buffer after 2000 sec for apo-, Cd₂⁻, Cd₁⁻, Zn₁⁻, Zn₂⁻-BcII species and after a 100 % deuteration (100 %D).

Table 4.1: Deuterium uptake within selected peptic-peptides after 2000 sec. In column 1 and 2, the sequence of the analysed peptides and their corresponding experimental mass are given. In column 3, the number of peptide amide protons in the peptide is represented. In the columns 4-8, the number of deuteriums incorporated in the peptide for apo, Zn₁, Zn₂, Cd₁ and Cd₂-BclI species are shown.

Sequence of identified peptides	[MH] ⁺	NH	apo-BclI	Zn ₁ -BclI	Zn ₂ -BclI	Cd ₁ -BclI	Cd ₂ -BclI
N-term. tail (β1, β2) ¹ SQKVEKTVIKNETGTISISQL ²¹	2303.280	20	17.7 ± 1.0	15.1 ± 0.6	15.1 ± 0.6	16.6 ± 0.04	15.6 ± 0.8
β3, loop 32-39, β4, β5							
⁴⁴ LVLNTSKGLVL ⁵⁴	1156.737	11	5.8 ± 0.2	4.4 ± 0.6	4.8 ± 0.4	5.0 ± 0.2	4.9 ± 0.4
²² NKNVWVHTEL ³¹	1239.650	10	5.1 ± 0.1	3.3 ± 0.1	2.4 ± 0.2	3.0 ± 0.2	2.5 ± 0.2
³² GSENGEAVPSNGLV-LNTSKGLVL ⁵⁴	2273.196	22	13.5 ± 0.6	9.2 ± 1.6	11.5 ± 0.8	11.6 ± 0.5	11.9 ± 0.9
loop 56-60							
⁵⁵ VDSSWDDKLTKE ⁶⁶	1422.675	12	8.5 ± 0.1	5.9 ± 0.3	3.7 ± 0.6	7.1 ± 0.4	5.5 ± 0.3
αI, β6							
⁷¹ VEKKFQKRVTD ⁸¹	1377.788	11	7.1 ± 0.6	5.9 ± 0.1	6.1 ± 0.7	6.5 ± 0.03	5.7 ± 0.3
⁷⁰ MVEKKFQKRVTD ⁸¹	1508.827	12	7.3 ± 0.4	6.2 ± 0.1	6.3 ± 0.6	6.4 ± 0.2	5.8 ± 0.3
αII, β7							
⁸² VIITHAHADRIGGIKTLKER-GIKAHSTAL ¹¹⁰	3106.751	29	27.3 ± 1.5	18.3 ± 0.3	14.4 ± 1.1	21.3 ± 0.9	17.3 ± 0.3
Connecting Loop, β8							
¹³⁰ VTNLKFGNM ¹³⁸	1023.534	9	7.6 ± 0.2	5.9 ± 0.9	6.4 ± 0.7	7.1 ± 0.4	6.7 ± 0.3
¹¹⁵ AKKNGYEEPLGDLQT ¹²⁹	1662.828	14	11.0 ± 0.7	7.7 ± 0.7	8.5 ± 0.9	9.6 ± 0.5	8.5 ± 0.8
¹¹⁴ LAKKNGYEEPLGDLQVTNL ¹³³	2203.161	19	16.5 ± 0.7	12.7 ± 1.1	13.2 ± 0.5	14.6 ± 0.7	13.0 ± 0.5
β9							
¹³⁹ KVETFYPGKGHTEDN ¹⁵³	1721.815	14	8.0 ± 1.0	5.6 ± 0.2	3.4 ± 0.4	3.6 ± 0.7	3.3 ± 0.3
¹³⁹ KVETFYPGKGHTEDNIV ¹⁵⁵	1933.965	16	9.1 ± 0.7	4.8 ± 0.04	3.3 ± 0.5	3.6 ± 0.1	2.9 ± 0.2
β10							
¹⁵⁶ VWLPPQYNIL ¹⁶⁴	1145.637	8	2.5 ± 0.1	1.4 ± 0.3	1.8 ± 0.02	1.7 ± 0.1	1.8 ± 0.1
β11, Loop 174-185							
¹⁶⁵ VGGCLVKSTSAKD-LGNVADAYVNE ¹⁸⁸	2410.205	24	17.1 ± 1.1	14.0 ± 0.2	14.4 ± 1.1	16.4 ± 0.3	14.9 ± 0.6
αIV							
¹⁹⁵ NVLKRYRNIN ²⁰⁴	1289.751	10	7.2 ± 0.8	5.7 ± 0.1	5.2 ± 0.4	5.2 ± 0.1	4.7 ± 0.6
¹⁸⁹ WSTSIENVLKRYRNIN ²⁰⁴	1993.058	16	9.9 ± 0.7	7.1 ± 0.2	5.7 ± 0.4	5.2 ± 0.04	5.1 ± 0.4
¹⁸⁹ WSTSIENVLKRYRNINA ²⁰⁵	2064.100	17	10.7 ± 1.1	8.0 ± 0.2	6.0 ± 0.3	6.0 ± 0.1	5.6 ± 0.7
C-term. tail, β12, αV							
²²⁰ LHTLDLLK ²²⁷	952.581	8	5.5 ± 0.4	3.1 ± 0.3	1.6 ± 0.4	1.1 ± 0.2	2.8 ± 0.4
²⁰⁵ AVVPGHGEVGDKGLL ²¹⁹	1447.793	14	10.5 ± 0.2	6.8 ± 1.5	8.3 ± 0.4	8.0 ± 0.3	7.7 ± 0.7
²⁰⁵ AVVPGHGEVGDKGLL ²²⁰	1560.880	15	10.9 ± 1.0	8.0 ± 0.8	9.1 ± 0.4	8.5 ± 0.7	8.4 ± 0.7
²⁰⁵ AVVPGHGEVGDKG-LLLHTLDLLK ²²⁷	2381.349	22	17.3 ± 0.8	13.2 ± 0.1	11.8 ± 0.5	11.7 ± 0.2	12.7 ± 0.8

The average back exchange for 22 peptic-peptides was around 45 %, but individual values for each peptide were determined and used for data correction (see appendix 4). Depending on the total number of exchanged amide protons in a peptide the resulting standard deviations were highly variable, ranging between 2 and 12 %. In Table 4.1 a comparison of H/D exchange of apo-BcII and the metal-substituted species after 2000 sec is listed. The total number of exchangeable amide protons and the experimentally observed exchange are compared. Some sequence sections are found in several peptides, which is caused by the occurrence of alternative cleavage sites of pepsin.

4.2.3 Quantification and structural interpretation of the Hydrogen/Deuterium Exchange kinetics

14 peptides mapped in Figure 4.4, covering almost 96 % of the protein sequence, were used to probe the influence of metal and inhibitor binding on HDX kinetics between 50 sec and 5900 sec. After analysis of the HDX kinetics, only a part of the totally possible HDX was time resolved. In fact, for most peptides, the H/D exchange has already begun in the dead time prior to the first measurement. The crystal structure of the Zn₂-BcII enzyme is available from the protein data bank (PDB accession code: 1BVT), which allows for the determination of the solvent accessibility of the amide protons from the 14 peptides. 216 amide protons were covered in total by these peptides.

Three types of amide protons were classified as follows: First, the amide protons involved in main chain - main chain (mc-mc) hydrogen bonds. They comprise spatially neighbouring peptide bonds found in α -helices, β -sheets or turns (126 in total). They are protected against solvent and thus show generally slow HDX. The same might hold true for amide protons involved in hydrogen bonds to side chains (mc-sc) of spatially neighbouring amino acids (15 in total). Best solvent accessibility and highest rates of HDX are expected for amide protons not involved in hydrogen bonds.

In Table 4.2, the total number of exchangeable amide protons is presented together with the numeric values for mc-mc and mc-sc hydrogen bonds determined from the crystal structure (1BVT). For the representation in Figure 4.4 these structural parameters are used to derive the %HDX expected when the amide protons not

involved in hydrogen bonds were exchanged. Generally, the percentage of non-hydrogen-bonded amide protons correlated well with the first data points obtained of the HDX kinetics of Zn₂BcII (Figure 4.4). Thus it might be concluded that at least all hydrogen-bonded amide protons are largely protected against HDX for incubation times < 50 s. The %D₀ values resulting from data evaluation (Table 4.2) thus represented the non-hydrogen bonded amide protons. In fact, enzyme species showing considerably higher percental HDX at t = 50 s might have structures with a decreased number of hydrogen-bonded amide protons for the respective peptides.

4.2.4 Hydrogen/Deuterium Exchange in the N-terminal domain of BcII

Three peptides of the N-terminal domain revealed higher %D₀ values for the apo and Me₁-species than for the di-zinc form of BcII. These peptides are P[82-110], P[115-129] and P[55-66].

In the crystal structure of the di-zinc BcII (1BVT), P[82-110] spans the metal ion-binding HxHxD motif and two secondary structure elements; the α -helix II and the β -sheet 7. In this peptide, 20 out of 29 amide protons are involved in 16 mc-mc and 4 mc-sc interactions. Thus only 9 out of 29 amide protons (31 %) are accessible to the solvent, explaining the low %D₀ value (i.e. 30 %) obtained from the HDX-MS data for the Zn₂-BcII. In the case of the apoenzyme and Me₁-BcII, %D₀ values of 80 and 45 % were found for this peptide, respectively. This can only be explained by a decreased number of hydrogen-bonded amide protons. In the case of the apoenzyme, the secondary structure elements existing in this peptide should be partially unfolded.

Similar effects of metal ion loading were observed for the peptide P[115-129]. In the crystal structure of the di-zinc BcII (1BVT), P[115-129] covers the loop connecting the N- and C-terminal domains. In this peptide, 11 out of 14 amide protons from P[115-129] are involved in 9 mc-mc and 2 mc-sc interactions. Thus only 3 out of 14 amide protons (21 %) are accessible to the solvent, which is close to the %D₀ value (i.e. 30 %) evaluated from the HDX-MS data for the Zn₂-BcII. In the case of the apo-BcII and Me₁-species, %D₀ values of 63 % and 45 % were obtained, respectively. Here, the connecting loop is more flexible in the apo- and Me₁-species than in the di-zinc BcII.

In the crystal structure of di-zinc BcII (1BVT), the peptide P[55-66] contains the loop 56-60. In this peptide, 9 of 12 amide protons are involved in 7 mc-mc and 2 mc-sc

interactions. Thus 3 out of 12 amide protons (20 %) are not protected against the solvent, which is consistent with the %D₀ value of 18 % obtained from the HDX-MS data for the Zn₂-BcII. Here also higher %D₀ values were found with apo-BcII and the Me₁-species.

Although the %D₀ values of the three peptides (P[82-110], P[115-129] and P[55-66]), were similar for the Me₁-species, the Zn₁-species showed shorter half life for the kinetically resolved reaction phase than the Cd₁-species (Table 4.2). Furthermore, the number of non-exchanged amide protons (%H_{end}) was lower for the Cd₁- than for the Zn₁-species. In case of the Me₂ species, the %H_{end} value was also lower for the Cd₂-species, revealing more flexibility.

The kinetic analysis of HDX resulted in the highest %D₀ and/or %D_t values and short half life for most of the peptides in the N-terminal domain of apo-BcII compared to the other species (Table 4.2). Only one peptide was found to reflect similar exchange patterns in all protein forms, namely the peptide P[70-81] covering regions of the C-terminus of α 1 and the N-terminus of β 6 .

Another peptide, P[32-54], showed longer half life in the Zn₁-species ($t_{1/2} = 37$ min) than in the di-zinc form of BcII ($t_{1/2} = 6$ min). This peptide spans the loop 32-39 (a.k.a substrate binding loop) and β 4.

4.2.5 Hydrogen/Deuterium Exchange in the C-terminal domain of BcII

Most of the peptides in the C-terminal domain revealed similar %D₀ values for the different metal loading states, but indicated different numbers of non-exchanged amide protons at the end of the HDX process (%H_{end}). The metal-free BcII form was always the most solvent accessible form for these regions. Generally the resulting %D_t values were higher for apo-BcII. One exception was observed in case of the peptide P[165-188]: the %D_t value and the rate constant of the process of the H/D exchange were both higher in the Cd₁-enzyme (%D_t = 24.8 and $k = 1.52 \text{ min}^{-1}$) than in the apoenzyme (%D_t = 14.6 and $k = 0.02 \text{ min}^{-1}$). This peptide covers the metal ligand Cys168 and the minor loop 174-185, which flanks the active site of the protein. Two peptides P[189-205] and P[220-227], covering the α -helices IV and V of the protein, respectively showed higher stability against HDX for the Cd₁-form compared to Zn₂-BcII (Figure 4.4). Similar results were found for P[139-155], which contains the 147-152 loop and the metal ligand His149.

Four peptides of the C-terminal domain spanning the residues 156-219 showed more stability with one zinc ion than with two zinc ions. This is most pronounced for P[205-219] containing the metal ligand His210 from the metal-binding site 2 (Figure 4.4).

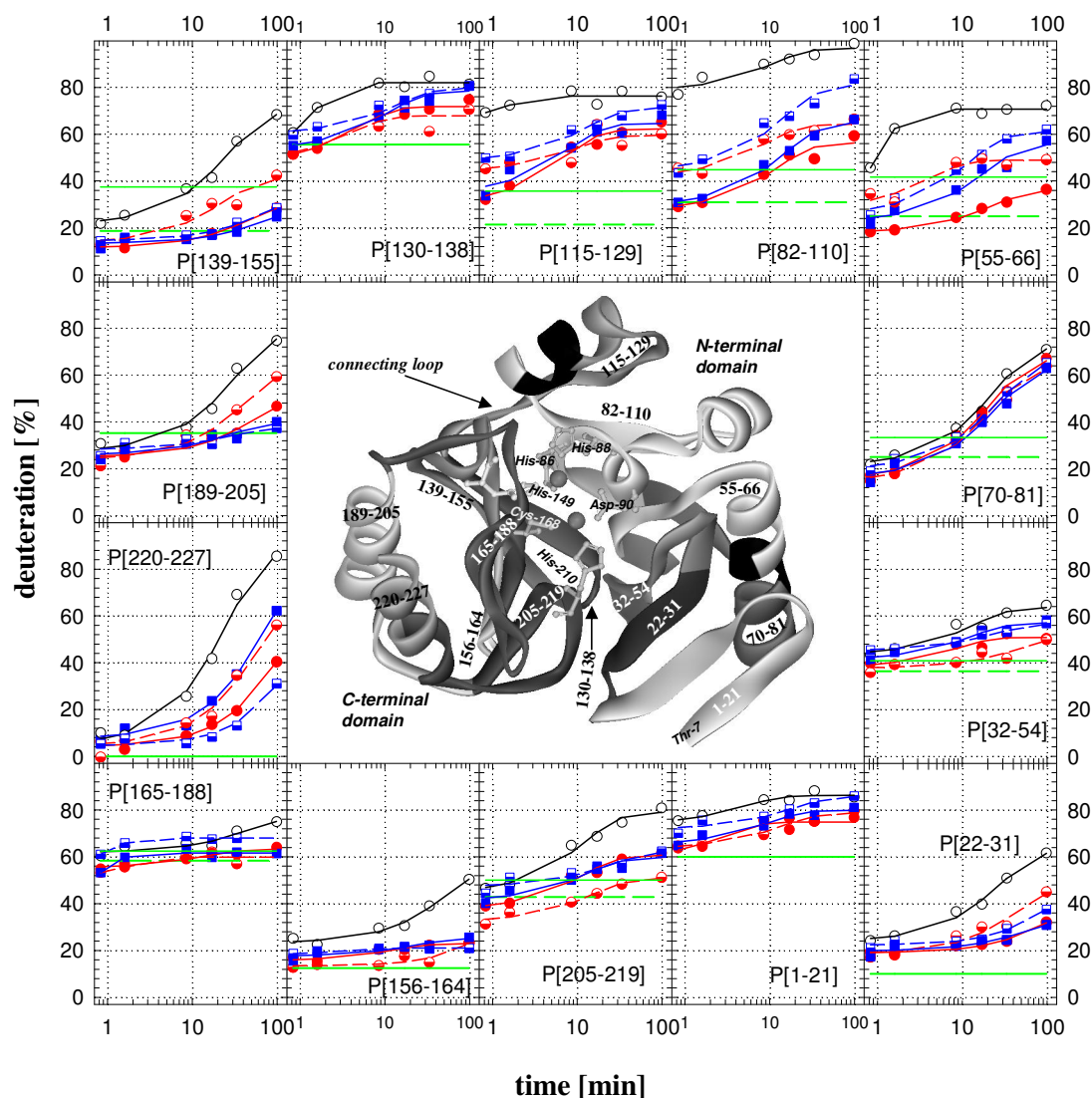


Figure 4.4: HDX kinetics of BclI. The time courses of percentage deuterium in-exchange are given on a logarithmic time scale. Experimental data for the different enzyme species are presented as follows: apo-BclI (black circles), Zn_1 -BclI (half-filled red circles), Zn_2 -BclI (filled red circles), Cd_1 -BclI (half-filled blue squares), Cd_2 -BclI (filled blue squares). The theoretical curves are represented by lines through the data points and were obtained from fitting equation 2.11 to the data. The percentage of amide hydrogens not involved in main chain - main chain (mc-mc) hydrogen bonds is indicated by full green lines, the percentage of amide hydrogens involved in neither main chain - main chain nor main chain - side chain hydrogen bonds is represented by broken green lines. The latter data were obtained from an inspection of the crystal structure of Zn_2 -BclI (1BVT).

Table 4.2: Results of the kinetic analysis of HDX data from Fig. 4.4. %D, %D_t (amplitude of the process), and *k* (rate constant) result from fitting Equation 2.11 to the data; %H_{end} = ΣNH - %D₀ - %D_t; t_{1/2} = ln2/*k*. Percental deuterium in-exchange is given together with the standard deviation resulting from the fits. The corresponding number of protons (ΣHX) is given in brackets.

peptide - ΣNH - mc-mc H- bonds - mc-sc H- bonds	metal	%D ₀ (ΣHX)	%D _t (ΣHX)	%H _{end} (ΣH)	<i>k</i> [min ⁻¹]	t _{1/2} [min] approx.
P[1-21] 20 8 0	0	74.0±1.2 (16)	12.3±1.5 (3)	13.7 (3)	0.190±0.080	4
	1Zn	63.7±1.3 (13)	15.0±2.1 (3)	21.3 (4)	0.072±0.028	10
	2Zn	59.0±2.3 (12)	15.9±2.5 (3)	25.1 (5)	0.332±0.177	2
	1Cd	71.9±1.3 (15)	13.9±2.3 (3)	14.2 (3)	0.055±0.023	13
	2Cd	65.2±1.4 (14)	14.7±1.9 (3)	20.1 (4)	0.104±0.041	7
P[22-31] 10 9 0	0	24.0±1.1 (2)	38.3±2.5 (4)	37.2 (4)	0.035±0.006	20
	1Zn	18.6±1.8 (2)	29.5±6.6 (3)	51.9 (5)	0.022±0.011	32
	2Zn	19.0±0.7 (2)	23.0±1.5 (2)	58.0 (6)	0.0083±0.0081	84
	1Cd	22.2±0.8 (2)	30.1±24.7 (3)	47.7 (5)	0.0071±0.0081	98
	2Cd	19.8±1.2 (2)	13.7±6.7 (1)	66.5 (7)	0.016±0.016	43
P[32-54] 22 13 1	0	43.5±1.9 (10)	20.1±3.0 (5)	36.4 (8)	0.072±0.030	9
	1Zn	37.7±1.5 (9)	13.9±6.6 (3)	48.4 (11)	0.019±0.019	37
	2Zn	37.9±1.5 (9)	12.9±2.0 (3)	49.2 (11)	0.117±0.058	6
	1Cd	45.2±0.5 (10)	11.5±1.0 (3)	43.3 (10)	0.040±0.009	17
	2Cd	41.4±1.2 (9)	15.7±1.9 (4)	42.9 (10)	0.075±0.025	9
P[55-66] 12 7 2	0	-5.4±1.4 (0)	76.1±1.6 (9)	23.9 (3)	1.351±0.067	0.5
	1Zn	27.9±2.7 (3)	21.0±3.0 (3)	51.1 (6)	0.243±0.126	3
	2Zn	18.0±0.6 (2)	18.3±1.1 (2)	63.7 (8)	0.043±0.006	16
	1Cd	25.8±1.7 (3)	35.3±2.5 (4)	38.9 (5)	0.082±0.017	8
	2Cd	22.9±2.3 (3)	32.7±4.1 (4)	44.4 (5)	0.054±0.018	13
P[70-81] 12 8 1	0	21.4±1.2 (3)	50.7±2.3 (6)	27.9 (3)	0.041±0.005	17
	1Zn	14.5±1.6 (2)	48.8±3.1 (6)	36.7 (4)	0.047±0.007	15
	2Zn	15.8±1.3 (2)	51.0±2.5 (6)	33.2 (4)	0.045±0.006	15
	1Cd	19.9±1.2 (2)	46.8±2.7 (6)	33.3 (4)	0.036±0.005	19
	2Cd	16.5±2.1 (2)	46.7±4.3 (6)	36.8 (4)	0.039±0.009	18
P[82-110] 29 16 4	0	78.8±2.1 (23)	18.0±3.1 (5)	3.2 (1)	0.092±0.047	7
	1Zn	41.9±2.0 (12)	22.4±2.7 (6)	35.7 (10)	0.114±0.044	6
	2Zn	27.5±2.4 (8)	28.8±3.6 (8)	43.7 (13)	0.081±0.030	9
	1Cd	44.5±2.8 (13)	36.7±4.6 (11)	18.8 (5)	0.065±0.022	10
	2Cd	29.5±1.2 (9)	35.7±2.0 (10)	35.5 (10)	0.066±0.010	10
P[115-129] 14 9 2	0	62.6±2.7 (9)	13.7±3.0 (2)	23.7 (3)	0.786±0.386	0.9
	1Zn	44.2±4.0 (6)	15.3±5.6 (2)	40.5 (6)	0.105±0.117	7
	2Zn	30.1±2.4 (4)	32.1±3.0 (4)	37.8 (5)	0.139±0.044	5
	1Cd	48.6±1.3 (7)	22.8±2.0 (3)	28.6 (4)	0.076±0.019	9
	2Cd	34.8±3.3 (5)	29.8±4.4 (4)	35.4 (5)	0.126±0.060	6
P[130-138] 9 4 0	0	37.0±1.9 (3)	45.0±2.1 (4)	18.0 (2)	0.901±0.096	0.8
	1Zn	48.6±4.7 (4)	19.2±5.3 (2)	32.2 (3)	0.245±0.245	3
	2Zn	47.6±2.0 (4)	24.3±2.3 (2)	28.1 (3)	0.203±0.070	3
	1Cd	60.4±1.8 (5)	19.6±2.9 (2)	20.0 (2)	0.069±0.028	10
	2Cd	53.7±1.6 (5)	24.9±2.3 (2)	21.4 (2)	0.091±0.025	8

P[139-155] 16 10 3	0	21.7±1.4 (3)	48.1±2.9 (8)	30.2 (5)	0.0368±0.0056	19
	1Zn	13.6±2.4 (2)	27.6±4.7 (4)	58.8 (9)	0.0429±0.0184	16
	2Zn	11.6±0.6 (2)	19.4±2.5 (3)	69.0 (11)	0.0202±0.0061	34
	1Cd	14.5±0.6 (2)	19.6±5.6 (3)	65.9 (11)	0.0129±0.0068	54
	2Cd	13.4±1.2 (2)	15.6±10 (2)	71.0 (11)	0.0130±0.0157	53
P[156-164] 8 7 0	0	23.3±1.1 (2)	32.2±4.7 (3)	44.5 (4)	0.0188±0.0061	37
	1Zn	13.3±1.1 (1)	n.d. (<1)	76.5 (6)	n.d.	n.d.
	2Zn	15.6±0.7 (1)	n.d. (<1)	77.0 (6)	n.d.	n.d.
	1Cd	18.1±0.3 (1)	n.d. (<1)	79.0 (6)	n.d.	n.d.
	2Cd	17.6±1.2 (1)	n.d. (<1)	74.7 (6)	n.d.	n.d.
P[165-188] 24 9 1	0	61.9±1.2 (15)	14.6±3.9 (4)	23.5 (6)	0.0235±0.0152	30
	1Zn	48.8±2.5 (12)	11.1±2.8 (3)	40.1 (10)	0.6163±0.3824	1
	2Zn	55.4±0.8 (13)	7.9±1.4 (2)	37.6 (9)	0.0698±0.0332	10
	1Cd	45.3±0.6 (11)	24.8±0.6 (6)	29.9 (7)	1.5200±0.0966	0.5
	2Cd	18.9±1.5 (5)	42.8±1.7 (10)	39.2 (9)	1.9540±0.2255	0.4
P[189-205] 17 11 0	0	27.5±1.6 (5)	50.4±3.8 (9)	22.1 (4)	0.0307±0.0058	23
	1Zn	24.0±2.0 (4)	39.3±6.5 (7)	36.7 (6)	0.0230±0.0091	30
	2Zn	25.2±1.1 (4)	25.2±5.2 (4)	49.6 (8)	0.0186±0.0085	37
	1Cd	28.2±1.6 (5)	9.4±3.6 (2)	62.4 (11)	0.0338±0.0324	21
	2Cd	26.0±1.6 (4)	13.7±3.4 (2)	60.3 (10)	0.0371±0.0230	19
P[205-219] 14 7 1	0	44.7±1.8 (6)	34.4±2.7 (5)	20.9 (3)	0.0808±0.0181	9
	1Zn	32.4±1.1 (5)	18.5±1.8 (3)	49.1 (7)	0.0641±0.0171	11
	2Zn	37.6±1.3 (5)	23.2±2.0 (3)	39.2 (5)	0.0851±0.0210	8
	1Cd	47.4±1.7 (7)	14.8±3.5 (2)	37.8 (5)	0.0406±0.0241	17
	2Cd	41.3±1.9 (6)	18.5±3.0 (3)	40.2 (6)	0.0751±0.0339	9
P[220-227] 8 8 0	0	4.8±2.2 (0)	83.9±4.6 (7)	11.3 (1)	0.0375±0.0052	19
	1Zn	4.5±1.8 (0)	63.6±9.3 (5)	31.9 (3)	0.0171±0.0053	40
	2Zn	4.2±1.0 (0)	64.2±20.8 (5)	31.6 (3)	0.0084±0.0041	83
	1Cd	4.5±1.2 (0)	100±200 (8)	0 (0)	0.0030±0.0073	230
	2Cd	7.8±1.3 (1)	74.5±10.9 (6)	17.7 (1)	0.0133±0.0037	52
Σ [1-227] 216 126 15	0	(97)	(74)	(50)	-	-
	1Zn	(75)	(49)	(90)		
	2Zn	(68)	(47)	(97)		
	1Cd	(83)	(56)	(78)		
	2Cd	(67)	(57)	(90)		

4.2.6 Effect of the inhibitor thiomandelate on HDX-MS for the different BclI protein species

To determine the influence of (*R,S*)-thiomandelate on the flexibility of the different regions of the metal-substituted species namely Zn₁, Zn₂, Cd₁ and Cd₂-BclI species, the degree of H/D exchange of the inhibitor-free protein species were compared with their inhibited forms (see Table 4.3). The results show that only for the Cd₂-BclI form of BclI, the H/D exchange decreases in presence of the inhibitor for the following regions: the H-X-H-X-D motif of P[82-110], the loop 56-60 of P[55-66] and the α -helix

V of P[220-227]. For all other metal-species, (*R,S*)-thiomandelate increases the H/D exchange of the different peptides.

Table 4.3: Effects of binding of (*R,S*)-thiomandelic acid (TM) to Cd₁-, Cd₂-, Zn₁-, and Zn₂-BcII. Comparison of un-inhibited and inhibited enzyme species (-). Percent deuteration is shown for a reaction time of 2000 s.

Residues	% Deuteration							
	Cd ₁ -BcII		Cd ₂ -BcII		Zn ₁ -BcII		Zn ₂ -BcII	
	-	TM	-	TM	-	TM	-	TM
1-21	83,0	86,4	77,7	81,8	75,1	84,8	75,2	83,5
22-31	29,2	42,4	24,6	26,4	30,4	44,6	23,9	29,5
32-54	52,7	60,3	53,7	55,4	41,8	59,3	52,2	60,7
55-66	57,5	58,9	45,9	30,5	44,9	53,9	30,9	35,7
70-81	53,0	59,3	47,8	53,8	49,5	60,4	53,2	59,1
82-110	73,2	75,0	59,4	53,0	61,5	71,1	49,4	59,4
115-129	68,1	79,5	60,5	71,0	55,2	80,6	60,7	75,6
130-138	77,3	82,8	74,1	78,9	61,1	81,0	70,6	89,6
139-155	22,3	42,8	18,2	21,5	29,8	46,1	20,3	27,0
156-164	21,4	30,5	22,3	27,3	18,1	29,5	22,3	28,7
165-188	67,9	70,1	62,0	71,3	57,0	72,0	61,0	67,6
189-205	34,9	50,3	32,9	38,0	45,1	49,4	35,2	40,4
205-219	57,3	66,0	55,1	59,3	48,3	66,6	59,0	64,4
220-227	13,1	44,6	35,1	22,7	34,5	50,4	19,4	23,2

To determine the binding mode of (*R,S*)-thiomandelate with the Cd₁ and Zn₁-BcII-species, the theoretical H/D exchange (calculated from Equation 4.1) of the peptides of the inhibited species were compared with the experimental H/D exchange. In case of theoretical H/D exchange, positive cooperativity in metal binding was assumed.

Equation 4.1:

$$\%D = [0.5 * \%D(Me_2 - BcII - TM) + 0.5 * \%D(apo - BcII)] - \%D(Me_1 - BcII)$$

Figure 4.5 shows the difference of the percentage of deuteration for Zn₁- (Figure 4.5A) and for Cd₁-BcII species (Figure 4.5B) with and without the presence of the

inhibitor respectively. The values obtained for the inhibitor-bound form were subtracted from those of the ligand free form of the protein, thus positive values indicate an increased H/D-exchange for the (*R,S*)-thiomandelate containing species. The theoretical values of the H/D exchange are similar with to experimental ones for both metals, revealing that (*R,S*)-thiomandelate might induce positive cooperativity in metal binding for Cd(II) and Zn(II) ions in BcII.

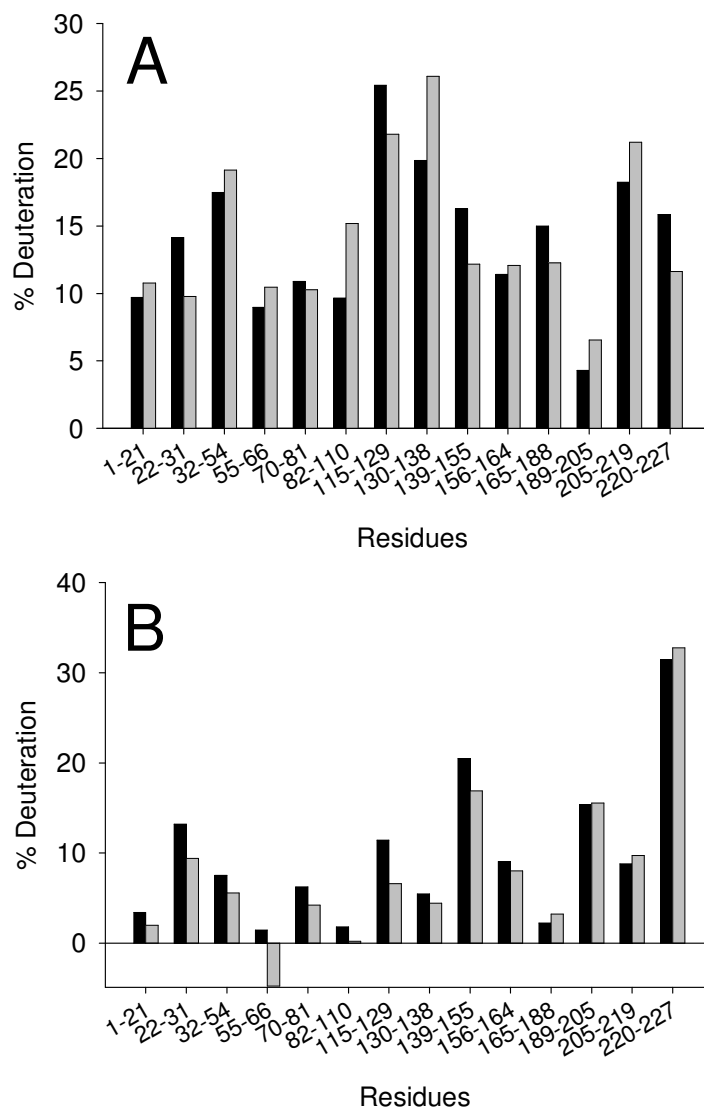


Figure 4.5: Influence of (*R,S*)-thiomandelic acid binding on HDX of Me₁-BcII. Experimental (black bars) and theoretical (grey bars) HDX data for Zn₁BcII (**A**) and Cd₁BcII (**B**) in presence of excess (*R,S*)-thiomandelic acid are compared. Changes of the percental deuterium incorporation after addition of the inhibitor to the Me₁-species are shown for a reaction time of 2000 s. Theoretical data were calculated assuming that all added metal ions were finally bound to inhibited Me₂-enzyme (see equation 4.1).

4.3 DISCUSSION

4.3.1 Metal-dependent protein structure and flexibility of BcII

4.3.1.1 Comparison of the apo-BcII and Me₂-enzyme

Differences in secondary structures between the metal-free and the Me₂-species of BcII were observed with CD spectroscopy and HDX-MS. For the CD spectra, the addition of two metal ions to the apoenzyme strongly increased the intensities of the negative band at 220 nm, indicating an increased content of secondary structure within the protein. One can conclude that parts of the secondary structure are not yet formed or sufficiently stabilized in metal-free BcII; potentially binding of the two metals either contributes to the stabilization of such structures or the binding of the metal ions induces conformational changes bringing residues in closer proximity thus finally enabling the formation of secondary structures. HDX-MS of pepsin-digested proteins permitted to localize the structural changes. The peptide P[82-110] containing the metal ion-binding HxHxD motif and its surrounding α -helix II showed very high solvent accessibility at early time HDX measurements for the metal-free enzyme. Together with CD spectra it can be concluded that the α -helical part must be partially unfolded in the apoprotein. This destabilization of secondary structure in this region would have a direct impact on the solvent accessibility of the neighbouring peptides. Indeed this was observed for the two peptides P[55-66] and P[115-129] containing the buried loop 56-60 and the loop connecting the N- and C-terminal domains, respectively. Both peptides showed high solvent accessibility in the metal free enzyme. In the crystal structure of Zn₂-BcII (1BVT), P[115-129] is bound to P[82-110] via 1 mc-mc and 3 mc-sc hydrogen bonds and P[55-66] forms 3 mc-mc and 3 sc-sc hydrogen bonds including salt bridges of the guanidinium group of Arg91 to Asp 90 and Asp56. A strained conformation of the main chain at position 56 is induced which may be relevant for the structural organization of the metal binding site. This structural feature is strictly conserved among the MBLs (23). P[55-66] also contains Trp59 which was suggested to contribute to the binding of the phenyl group of penicillin via formation of a hydrophobic pocket with Phe34 .

The absence of metal ions had also shown to influence regions far from the active site, as observed for the two peptides P[189-205] and P[220-227] which contain the α -helices IV and V, respectively, in the C-terminal tail of the protein. In the crystal

structure of the di-zinc form of BcII, a low B-factor was determined for the α -helix V, meaning that the position of its atoms have been determined with high precision. This can be due to the crystal packing of the BcII protein; two molecules are stacked against each other by their C-terminal α -helices (α V) (1BVT). However, in solution this region can be less stable especially in absence of metal ions. For all conditions tested HDX-MS analysis revealed a strong correlation between the flexibility of the fragments covering the α -helices IV and V and the peptide P[139-155] containing the metal ligand His149.

Generally most regions of metal-free BcII showed faster HDX kinetics during 50 sec and 5900 sec than the metal-loaded states. This higher solvent accessibility of metal-free BcII reflects a solution structure, which appears different from the known crystal structure of the Zn₂-form. Previous NMR studies of backbones amide resonances by ¹H-¹⁵N-HSQC-experiments already resulted in significant differences between apo- and metal-loaded forms of BcII (11).

Thus it can be assumed that metal ion binding strongly contributes to the stabilization of the protein fold observed in the crystal structure. The metal-free enzyme in solution might be partly unstructured at the interface site of N- and C-terminal domain and it might be concluded that the metal ion binding site is not pre-formed by the protein fold. By comparison of the crystal structure of the di-zinc and the metal-free form it was observed that the metal ions fulfill not only catalytic but also structural functions in the *B. cereus* metallo- β -lactamase (141). The main differences in the C α -positions were found close to the active site: in the absence of metal, the minor loop and the N-terminus of the α -helix II (residues 87-93) showed larger distances between each other. Thus, in the metal-free form the connection between both regions, which is formed by the interaction between Asp183 and the side chain of the metal ligand His86 in case of the metal enzyme was disrupted.

Thus binding of metal ions introduces additional bonds between N- and C-terminal domains which might be necessary to keep the domains connected. If the metal is absent, the N- and C terminal domains will be separated from each other, which can lead to an increased flexibility of the connecting loop, finally also influencing regions situated far from the active site. High flexibility of the apo-enzyme might also explain the ease of metal ion transfer from e.g. EDTA to the protein (4).

4.3.1.2 Comparing Cd₂-and Zn₂-BclI enzymes

The analysis of the Me₂-species using CD spectroscopy did not indicate significant differences between the secondary structure contents of the cadmium and the zinc enzymes. In contrast, the HDX-MS study revealed that the regions in the interface domain of the protein were more flexible for the Cd₂-than for the Zn₂-form of BclI. In fact, the two structurally coupled peptides namely P[55-66] and P[82-110] showed higher solvent accessibilities in case of the Cd₂-form.

The X-ray structure of *B. fragilis* zinc- β -lactamase, another member of the subclass B1 enzymes, revealed a bridging solvent molecule between the two metals, which was assumed to exist as a hydroxide ion (27, 36). In the structure of the Zn₂-BclI at pH 7.5, a similar bridging water molecule was found (33). This hydroxide ion may be involved in the nucleophile attack to the carbonyl carbon atom of the β -lactam ring (21, 27, 30). Moreover, the distance of the shared solvent molecule to the cations was found to be higher in the Cd₂-form compared to the Zn₂-form of the *B. fragilis* enzyme (34). A higher distance between the two cadmium ions compared to the two zinc ions could have an influence on the stability of surrounding regions, as observed for the two peptides P[55-66] and P[82-110] in the BclI enzyme.

4.3.1.3 Me₁-BclI enzymes

Metal jumping/flexibility of active site in the Cd₁-BclI enzyme

Previous NMR and PAC spectroscopic experiments demonstrated a fast exchange (jumping) of the single Cd²⁺ ion between the two metal binding sites in a time regime between 0.1 and 10 μ s (11). De Seny et al., 2001 determined the dissociation rate k_{off} for cadmium at 0.22 sec⁻¹ for the BclI enzyme by combination of the association rates with the corresponding dissociation constants (39). The fast exchange of the Cd²⁺ ion between the two binding sites via a dissociation/association mechanism, where the metal ion is first transferred to the bulk water before binding again, however, would require a dissociation rate constant between 7x10⁴ s⁻¹ and 7x10⁶ s⁻¹. Consequently, the experimental k_{off} is by 5-7 orders of magnitude too low for such a mechanism. Thus an alternative explanation for the rapid transfer between both binding sites can be given by the movement of the N- and C-terminal domain relative to each other. In fact, this movement enables a site-to-site metal ion transfer without the requirement to break all metal-protein bonds at the same time, thus indicating an intra-molecular

ligand exchange reaction. This would afford a rather flexible and highly dynamic protein structure, especially at the metal ion binding site. The observations of a less structured Cd₁-enzyme in the CD spectra and highly labile protein regions at the domain interface with peptide (P[115-129]) and metal binding site (P[82-110] and P[55-66]) strongly support such a mechanism.

Flexibility of BcII at [Zn²⁺]/[apoprotein] ratio of 1

Based on the NMR/PAC results for the Cd₁-BcII enzyme, a rapid exchange of the Zn²⁺ ion was also suggested in the zinc enzyme at [Zn²⁺]/[apoprotein] ratio of 1 using stopped-flow methods (39). In the past, the BcII enzyme was considered as a native monozinc enzyme, due to one high affinity (K_{D1}) (nM) and one low affinity (K_{D2}) (μM) dissociation constant for the binding of metal ions. In this case, only one metal-bound species, the mono-zinc form, can exist at a [Zn²⁺]/[apoprotein] ratio of 1. In the present study, competition titrations revealed that the K_{D2} value was revised by a factor of 2000 in BcII and the ESI-MS data detected the presence of three protein species, i.e. apo, Zn₁- and Zn₂ forms at low [Zn²⁺]/[apoprotein] ratios. Therefore the H/D kinetics obtained for each peptide at the investigated metal binding stoichiometry resulted from the superposition of the three coexisting species. In fact, the H/D exchange into the Zn₁-form can not be followed separately from that of the other two protein species. Thus conclusions can not be drawn to explain a possible intramolecular exchange of the Zn²⁺ ion in the Zn₁-enzyme.

When one molar equivalent of zinc was added to the apoprotein the CD spectra indicated a modification of secondary structures compared to the situation found with two molar equivalents of zinc. Furthermore, it was found that certain regions revealed the best protection against H/D exchange, e.g. in the fragments P[156-164], P[205-219] and P[32-54] at [Zn²⁺]/[apoprotein] ratio of 1. This was most pronounced for the peptide P[205-219] containing the metal ligand His210. These three fragments are spatial neighbouring regions in the crystal structure of the Zn₂-BcII. Here, the formation of metal ion-bridged dimers of the protein at low [Zn²⁺]/[apoprotein] ratios might be responsible for the increase of protein stability, but has to be proved in further investigations.

4.3.2 The influence of the inhibitor thiomandelate on the protein flexibility of BcII

4.3.2.1 Me₂-species

HDX-MS experiments presented in this work revealed that (*R,S*)-thiomandelate stabilized the Cd₂-enzyme in the metal binding site, especially in the region of the H-X-H-D motif and the coupled segment P[55-66]. Studying the Cd₂-enzyme-inhibitor complex by NMR experiments revealed that the inhibitor binds to the two metals via its sulphur donating function (9). This has an impact on the stabilization of the two cadmium ions in the active site, which might explain a lower percentage of deuteration of P[55-66] in Cd₂-BcII compared to the Zn₂-BcII. The fragment P[55-66] contains also W59, whose side chain extends toward the β 3- β 4 loop. A shift of this residue was found in NMR experiments for the di-Zn₂-BcII enzyme after the binding of the inhibitor (43). It was concluded that after binding of the inhibitor to the Zn₂-enzyme, the closing of the β 3- β 4 loop might cause the shift of the tryptophane residue. In the present study, an increased stability of the loop after inhibitor binding was not observed.

In the Zn₂-BcII enzyme the HDX-MS showed that no region of the protein was stabilized by (*R,S*)-thiomandelate. Indeed, in presence of the inhibitor all regions in the Zn₂-BcII protein present similar or higher H/D exchanges compared to the inhibitor-free state. One possible explanation is that the high amount of inhibitor added to the Zn₂-BcII enzyme might induce the formation of Zn₁- or apo-enzyme. The inhibitor is known to have strong affinity for zinc ions in solution.

4.3.2.2 Me₁-species

After binding of thiomandelate to the Me₁-BcII species, the percentage of deuteration increased for all parts of the protein. It was concluded that the formation of apoenzyme, due to the positive cooperativity in metal binding of thiomandelate, was responsible for this high level of H/D exchange. Positive cooperativity in metal binding was also shown for the cadmium enzyme in NMR studies (9) as well as for the zinc enzyme in the presented competition titrations experiments. Thus, it was not possible to identify the regions in the Me₂- species stabilized by the inhibitor, due to the high level of deuteration of the produced apoenzyme.

5 CONCLUSION AND OUTLOOK

When combining miniaturization and automation in a nano-electrospray (nanoESI) device, such as the Nanomate® system, direct high-throughput screening can be easily reached for small-molecule protein interactions as it is the case in metalloenzyme-inhibitor complexes. The results obtained by ESI-MS for the binding of the inhibitors to the metallo-beta-lactamases via analysis of the relative abundance of the metalloprotein-inhibitor complexes were generally in good agreement with SAR data obtained in solution (43). In only one case, the order of binding strengths obtained in the gas phase was different from that obtained in solution. A different impact of non-covalent forces between inhibitors and proteins in the gas phase and in solution might explain the deviating results. In fact, electrostatic and hydrogen bonding interactions might be emphasized during ion transfer from solution into the gas phase, whereas the strength of hydrophobic interactions is reduced. Thus different equilibrium constants can be expected.

The technique is also well suited for the rapid detection of metal:enzyme:inhibitor ratios, and in particular for the detection of the metal:protein stoichiometry. This information is often difficult to obtain by other methods, which are generally time-consuming and demand high sample amounts. Besides that, the metal loading state of proteins is usually ignored in high-throughput studies on the inhibition of metallo-enzymes.

Competition titration experiments in combination with ESI-MS revealed that the inhibitor *D*-captopril preferentially binds to the dinuclear forms of zinc BcII and L1 enzymes and the mononuclear form of the CphA enzyme. For (*R,S*)-thiomandelate two metal ions are required for efficient binding to BcII and L1 and unexpectedly to CphA, where formation of the dinuclear form was induced. In the CphA enzyme, the affinity for a second metal ion can only be increased by introducing a new metal ligand (i.e. the thiol group from (*R,S*)-thiomandelate. However, the increase of the affinity for a second metal ion might not be sufficient to inactivate the MBLs completely, due to the presence of catalytically active mononuclear species. One exception is BcII where positive cooperativity of zinc binding is induced by the presence of (*R,S*)-thiomandelate. To address the mononuclear forms of MBLs might be a major challenge in the design of new and clinically useful inhibitors.

HDX-MS was used to study the effect of metal ion binding on the flexibility of BclI, with special emphasis on the mononuclear forms. The data revealed a high flexibility at the active site and the interdomain region of the monocadmium enzyme, which might facilitate the known metal exchange between the two available ligand binding sites. This intramolecular exchange of the metal ion was also suggested for the mononuclear zinc enzymes. A highly flexible active site architecture of Zn₁-MBLs might explain the difficulty to inhibit such enzymes.

6 REFERENCES

1. Heinz, U., and Adolph, H. W. (2004) Metallo-beta-lactamases: two binding sites for one catalytic metal ion?, *Cell Mol Life Sci* 61, 2827-2839.
2. Paul-Soto, R., Bauer, R., Frere, J. M., Galleni, M., Meyer-Klaucke, W., Nolting, H., Rossolini, G. M., de Seny, D., Hernandez-Valladares, M., Zeppezauer, M., and Adolph, H. W. (1999) Mono- and binuclear Zn²⁺-beta-lactamase. Role of the conserved cysteine in the catalytic mechanism, *J Biol Chem* 274, 13242-13249.
3. Paul-Soto, R., Hernandez-Valladares, M., Galleni, M., Bauer, R., Zeppezauer, M., Frere, J. M., and Adolph, H. W. (1998) Mono- and binuclear Zn-beta-lactamase from *Bacteroides fragilis*: catalytic and structural roles of the zinc ions, *FEBS Lett* 438, 137-140.
4. Wommer, S., Rival, S., Heinz, U., Galleni, M., Frere, J. M., Franceschini, N., Amicosante, G., Rasmussen, B., Bauer, R., and Adolph, H. W. (2002) Substrate-activated zinc binding of metallo-beta-lactamases: physiological importance of mononuclear enzymes, *J Biol Chem* 277, 24142-24147.
5. Siemann, S., Brewer, D., Clarke, A. J., Dmitrienko, G. I., Lajoie, G., and Viswanatha, T. (2002) IMP-1 metallo-beta-lactamase: effect of chelators and assessment of metal requirement by electrospray mass spectrometry, *Biochim Biophys Acta* 1571, 190-200.
6. Hernandez Valladares, M., Felici, A., Weber, G., Adolph, H. W., Zeppezauer, M., Rossolini, G. M., Amicosante, G., Frere, J. M., and Galleni, M. (1997) Zn(II) dependence of the *Aeromonas hydrophila* AE036 metallo-beta-lactamase activity and stability, *Biochemistry* 36, 11534-11541.
7. Crawford, P. A., Sharma, N., Chandrasekar, S., Sigdel, T., Walsh, T. R., Spencer, J., and Crowder, M. W. (2004) Over-expression, purification, and characterization of metallo-beta-lactamase ImiS from *Aeromonas veronii* bv. *sobria*, *Protein Expr Purif* 36, 272-279.
8. Moran-Barrio, J., Gonzalez, J. M., Lisa, M. N., Costello, A. L., Peraro, M. D., Carloni, P., Bennett, B., Tierney, D. L., Limansky, A. S., Viale, A. M., and Vila, A. J. (2007) The metallo-beta-lactamase GOB is a mono-Zn(II) enzyme with a novel active site, *J Biol Chem* 282, 18286-18293.
9. Damblon, C., Jensen, M., Ababou, A., Barsukov, I., Papamichael, C., Schofield, C. J., Olsen, L., Bauer, R., and Roberts, G. C. (2003) The inhibitor thiomandelic acid binds to both metal ions in metallo-beta-lactamase and induces positive cooperativity in metal binding, *J Biol Chem* 278, 29240-29251.
10. Heinz, U., Bauer, R., Wommer, S., Meyer-Klaucke, W., Papamichaels, C., Bateson, J., and Adolph, H. W. (2003) Coordination geometries of metal ions in d- or l-captopril-inhibited metallo-beta-lactamases, *J Biol Chem* 278, 20659-20666.
11. Hemmingsen, L., Damblon, C., Antony, J., Jensen, M., Adolph, H. W., Wommer, S., Roberts, G. C., and Bauer, R. (2001) Dynamics of mononuclear cadmium beta-lactamase revealed by the combination of NMR and PAC spectroscopy, *J Am Chem Soc* 123, 10329-10335.
12. Waley, S. G. (1988) Beta-lactamases: a major cause of antibiotic resistance, *Sci Prog* 72, 579-597.

13. Bush, K., Jacoby, G. A., and Medeiros, A. A. (1995) A functional classification scheme for beta-lactamases and its correlation with molecular structure, *Antimicrob Agents Chemother* 39, 1211-1233.
14. Nordmann, P., and Poirel, L. (2002) Emerging carbapenemases in Gram-negative aerobes, *Clin Microbiol Infect* 8, 321-331.
15. Sabath, L. D., and Abraham, E. P. (1966) Zinc as a cofactor for cephalosporinase from *Bacillus cereus* 569, *The Biochemical journal* 98, 11C-13C.
16. Payne, D. J. (1993) Metallo-beta-lactamases--a new therapeutic challenge, *J Med Microbiol* 39, 93-99.
17. Chen, Y., Succi, J., Tenover, F. C., and Koehler, T. M. (2003) Beta-lactamase genes of the penicillin-susceptible *Bacillus anthracis* Sterne strain, *J Bacteriol* 185, 823-830.
18. Walsh, T. R., Toleman, M. A., Poirel, L., and Nordmann, P. (2005) Metallo-beta-lactamases: the quiet before the storm?, *Clin Microbiol Rev* 18, 306-325.
19. Garau, G., Garcia-Saez, I., Bebrone, C., Anne, C., Mercuri, P., Galleni, M., Frere, J. M., and Dideberg, O. (2004) Update of the standard numbering scheme for class B beta-lactamases, *Antimicrob Agents Chemother* 48, 2347-2349.
20. Galleni, M., Lamotte-Brasseur, J., Rossolini, G. M., Spencer, J., Dideberg, O., and Frere, J. M. (2001) Standard numbering scheme for class B beta-lactamases, *Antimicrobial agents and chemotherapy* 45, 660-663.
21. Carfi, A., Pares, S., Duee, E., Galleni, M., Duez, C., Frere, J. M., and Dideberg, O. (1995) The 3-D structure of a zinc metallo-beta-lactamase from *Bacillus cereus* reveals a new type of protein fold, *Embo J* 14, 4914-4921.
22. Neuwald, A. F., Liu, J. S., Lipman, D. J., and Lawrence, C. E. (1997) Extracting protein alignment models from the sequence database, *Nucleic Acids Res* 25, 1665-1677.
23. Daiyasu, H., Osaka, K., Ishino, Y., and Toh, H. (2001) Expansion of the zinc metallo-hydrolase family of the beta-lactamase fold, *FEBS Lett* 503, 1-6.
24. Aravind, L. (1999) An evolutionary classification of the metallo-beta-lactamase fold proteins, *In Silico Biol* 1, 69-91.
25. Callebaut, I., Moshous, D., Mornon, J. P., and de Villartay, J. P. (2002) Metallo-beta-lactamase fold within nucleic acids processing enzymes: the beta-CASP family, *Nucleic Acids Res* 30, 3592-3601.
26. Moshous, D., Callebaut, I., de Chasseval, R., Poinsignon, C., Villey, I., Fischer, A., and de Villartay, J. P. (2003) The V(D)J recombination/DNA repair factor artemis belongs to the metallo-beta-lactamase family and constitutes a critical developmental checkpoint of the lymphoid system, *Ann N Y Acad Sci* 987, 150-157.
27. Concha, N. O., Rasmussen, B. A., Bush, K., and Herzberg, O. (1996) Crystal structure of the wide-spectrum binuclear zinc beta-lactamase from *Bacteroides fragilis*, *Structure* 4, 823-836.
28. Carfi, A., Duee, E., Paul-Soto, R., Galleni, M., Frere, J. M., and Dideberg, O. (1998) X-ray structure of the ZnII beta-lactamase from *Bacteroides fragilis* in an orthorhombic crystal form, *Acta Crystallogr D Biol Crystallogr* 54, 45-57.
29. Fast, W., Wang, Z., and Benkovic, S. J. (2001) Familial mutations and zinc stoichiometry determine the rate-limiting step of nitrocefin hydrolysis by metallo-beta-lactamase from *Bacteroides fragilis*, *Biochemistry* 40, 1640-1650.
30. Bounaga, S., Laws, A. P., Galleni, M., and Page, M. I. (1998) The mechanism of catalysis and the inhibition of the *Bacillus cereus* zinc-dependent beta-

- lactamase, *Biochem J* 331 (Pt 3), 703-711.
31. Orellano, E. G., Girardini, J. E., Cricco, J. A., Ceccarelli, E. A., and Vila, A. J. (1998) Spectroscopic characterization of a binuclear metal site in *Bacillus cereus* beta-lactamase II, *Biochemistry* 37, 10173-10180.
 32. Fabiane, S. M., Sohi, M. K., Wan, T., Payne, D. J., Bateson, J. H., Mitchell, T., and Sutton, B. J. (1998) Crystal structure of the zinc-dependent beta-lactamase from *Bacillus cereus* at 1.9 Å resolution: binuclear active site with features of a mononuclear enzyme, *Biochemistry* 37, 12404-12411.
 33. Paul-Soto, R., Zeppezauer, M., Adolph, H. W., Galleni, M., Frere, J. M., Carfi, A., Dideberg, O., Wouters, J., Hemmingsen, L., and Bauer, R. (1999) Preference of Cd(II) and Zn(II) for the two metal sites in *Bacillus cereus* beta-lactamase II: A perturbed angular correlation of gamma-rays spectroscopic study, *Biochemistry* 38, 16500-16506.
 34. Concha, N. O., Rasmussen, B. A., Bush, K., and Herzberg, O. (1997) Crystal structures of the cadmium- and mercury-substituted metallo-beta-lactamase from *Bacteroides fragilis*, *Protein Sci* 6, 2671-2676.
 35. Carfi, A., Duee, E., Galleni, M., Frere, J. M., and Dideberg, O. (1998) 1.85 Å resolution structure of the zinc (II) beta-lactamase from *Bacillus cereus*, *Acta crystallographica* 54, 313-323.
 36. Fitzgerald, P. M., Wu, J. K., and Toney, J. H. (1998) Unanticipated inhibition of the metallo-beta-lactamase from *Bacteroides fragilis* by 4-morpholineethanesulfonic acid (MES): a crystallographic study at 1.85-Å resolution, *Biochemistry* 37, 6791-6800.
 37. Toney, J. H., Fitzgerald, P. M., Grover-Sharma, N., Olson, S. H., May, W. J., Sundelof, J. G., Vanderwall, D. E., Cleary, K. A., Grant, S. K., Wu, J. K., Kozarich, J. W., Pompliano, D. L., and Hammond, G. G. (1998) Antibiotic sensitization using biphenyl tetrazoles as potent inhibitors of *Bacteroides fragilis* metallo-beta-lactamase, *Chem Biol* 5, 185-196.
 38. Concha, N. O., Janson, C. A., Rowling, P., Pearson, S., Cheever, C. A., Clarke, B. P., Lewis, C., Galleni, M., Frere, J. M., Payne, D. J., Bateson, J. H., and Abdel-Meguid, S. S. (2000) Crystal structure of the IMP-1 metallo beta-lactamase from *Pseudomonas aeruginosa* and its complex with a mercaptocarboxylate inhibitor: binding determinants of a potent, broad-spectrum inhibitor, *Biochemistry* 39, 4288-4298.
 39. de Seny, D., Heinz, U., Wommer, S., Kiefer, M., Meyer-Klaucke, W., Galleni, M., Frere, J. M., Bauer, R., and Adolph, H. W. (2001) Metal ion binding and coordination geometry for wild type and mutants of metallo-beta -lactamase from *Bacillus cereus* 569/H/9 (BcII): a combined thermodynamic, kinetic, and spectroscopic approach, *J Biol Chem* 276, 45065-45078.
 40. Lienard, B. M., Horsfall, L. E., Galleni, M., Frere, J. M., and Schofield, C. J. (2007) Inhibitors of the FEZ-1 metallo-beta-lactamase, *Bioorg Med Chem Lett* 17, 964-968.
 41. Horsfall, L. E., Garau, G., Lienard, B. M., Dideberg, O., Schofield, C. J., Frere, J. M., and Galleni, M. (2007) Competitive inhibitors of the CphA metallo-beta-lactamase from *Aeromonas hydrophila*, *Antimicrob Agents Chemother* 51, 2136-2142.
 42. Toney, J. H., Hammond, G. G., Fitzgerald, P. M., Sharma, N., Balkovec, J. M., Rouen, G. P., Olson, S. H., Hammond, M. L., Greenlee, M. L., and Gao, Y. D. (2001) Succinic acids as potent inhibitors of plasmid-borne IMP-1 metallo-beta-lactamase, *J Biol Chem* 276, 31913-31918.

43. Mollard, C., Moali, C., Papamicael, C., Damblon, C., Vessilier, S., Amicosante, G., Schofield, C. J., Galleni, M., Frere, J. M., and Roberts, G. C. (2001) Thiomandelic acid, a broad spectrum inhibitor of zinc beta-lactamases: kinetic and spectroscopic studies, *J Biol Chem* 276, 45015-45023.
44. Garcia-Saez, I., Hopkins, J., Papamicael, C., Franceschini, N., Amicosante, G., Rossolini, G. M., Galleni, M., Frere, J. M., and Dideberg, O. (2003) The 1.5-A structure of *Chryseobacterium meningosepticum* zinc beta-lactamase in complex with the inhibitor, D-captopril, *J Biol Chem* 278, 23868-23873.
45. Garcia-Saez, I., Mercuri, P. S., Papamicael, C., Kahn, R., Frere, J. M., Galleni, M., Rossolini, G. M., and Dideberg, O. (2003) Three-dimensional structure of FEZ-1, a monomeric subclass B3 metallo-beta-lactamase from *Fluoribacter gormanii*, in native form and in complex with D-captopril, *J Mol Biol* 325, 651-660.
46. Berg, J. M., Tymoczko, J. L., and Stryer, L. (2007) *Biochemie, 6. Auflage*, Elsevier, München.
47. Tanaka, K., Waki, H., Ido, Y., Akita, S., Yoshida, Y., and Yoshida, T. (1987) in *Second Japan-China Joint Symposium on Mass Spectrometry*, pp 185-188.
48. Karas, M., and Hillenkamp, F. (1988) Laser desorption ionization of proteins with molecular masses exceeding 10,000 daltons, *Anal Chem* 60, 2299-2301.
49. Fenn, J. B., Mann, M., Meng, C. K., Wong, S. F., and Whitehouse, C. M. (1989) Electrospray ionization for mass spectrometry of large biomolecules, *Science (New York, N.Y)* 246, 64-71.
50. Chait, B. T., and Kent, S. B. (1992) Weighing naked proteins: practical, high-accuracy mass measurement of peptides and proteins, *Science* 257, 1885-1894.
51. Dai, Y., Whittal, R. M., Li, L., and Weinberger, S. R. (1996) Accurate mass measurement of oligonucleotides using a time-lag focusing matrix-assisted laser desorption/ionization time-of-flight mass spectrometer, *Rapid Commun Mass Spectrom* 10, 1792-1796.
52. Fukai, T., Kuroda, J., and Nomura, T. (2000) Accurate mass measurement of low molecular weight compounds by matrix-assisted laser desorption/ionization time-of-flight mass spectrometry, *J Am Soc Mass Spectrom* 11, 458-463.
53. Nelson, R. W., Dogruel, D., and Williams, P. (1994) Mass determination of human immunoglobulin IgM using matrix-assisted laser desorption/ionization time-of-flight mass spectrometry, *Rapid Commun Mass Spectrom* 8, 627-631.
54. Biemann, K. (1990) Sequencing of peptides by tandem mass spectrometry and high-energy collision-induced dissociation, *Methods in enzymology* 193, 455-479.
55. Spengler, B., Kirsch, D., Kaufmann, R., and Jaeger, E. (1992) Peptide sequencing by matrix-assisted laser-desorption mass spectrometry, *Rapid Commun Mass Spectrom* 6, 105-108.
56. Belghazi, M., Bathany, K., Hountondji, C., Grandier-Vazeille, X., Manon, S., and Schmitter, J. M. (2001) Analysis of protein sequences and protein complexes by matrix-assisted laser desorption/ionization mass spectrometry, *Proteomics* 1, 946-954.
57. Borchers, C., and Tomer, K. B. (1999) Characterization of the noncovalent complex of human immunodeficiency virus glycoprotein 120 with its cellular receptor CD4 by matrix-assisted laser desorption/ionization mass spectrometry, *Biochemistry* 38, 11734-11740.
58. Davis, R. G., J., A. R., and Blanchard, S. G. (1997) Iterative size-exclusion

- chromatography coupled with liquid chromatography - mass spectrometry to enrich and identify tight-binding ligands from complex mixtures, *Tetrahedron*, 1653-1667.
59. Ganem, B., Li, Y.T, and Henion, J.D. (1991) Detection of noncovalent receptor-ligand complexes by mass spectrometry, *J Am Chem Soc* 113, 6294-6296.
 60. Katta, V., and Chait, B. T. (1991) Conformational changes in proteins probed by hydrogen-exchange electrospray-ionization mass spectrometry, *Rapid Commun Mass Spectrom* 5, 214-217.
 61. Loo, J. A. (1997) Studying noncovalent protein complexes by electrospray ionization mass spectrometry, *Mass spectrometry reviews* 16, 1-23.
 62. Shields, S. J., Oyeyemi, O., Lightstone, F. C., and Balhorn, R. (2003) Mass spectrometry and non-covalent protein-ligand complexes: confirmation of binding sites and changes in tertiary structure, *J Am Soc Mass Spectrom* 14, 460-470.
 63. Loo. (2001) Probing protein-metal interactions by ESI-MS : enolase and nucleocapsid protein, *International Journal of Mass Spectrometry* 204, 113-123.
 64. Tang, X., Callahan, J. H., Zhou, P., and Vertes, A. (1995) Noncovalent protein-oligonucleotide interactions monitored by matrix-assisted laser desorption/ionization mass spectrometry, *Anal Chem* 67, 4542-4548.
 65. Hillenkamp, F. (1988) In new methods for the study of biomolecular complexes; Ens W., Standing K.G., Chernushevich I.V., Eds.; NATO ASI Series C: Mathematical and Physiological Sciences, pp 181-191, Kluwer Academic, Dordrecht.
 66. Schaumlöffel, D., Prange, A., Marx, G., Heumann, K. G., and Bratter, P. (2002) Characterization and quantification of metallothionein isoforms by capillary electrophoresis-inductively coupled plasma-isotope-dilution mass spectrometry, *Anal Bioanal Chem* 372, 155-163.
 67. Yu, X., Wojciechowski, M., and Fenselau, C. (1993) Assessment of metals in reconstituted metallothioneins by electrospray mass spectrometry, *Anal Chem* 65, 1355-1359.
 68. Hu, P., Ye, Q. Z., and Loo, J. A. (1994) Calcium stoichiometry determination for calcium binding proteins by electrospray ionization mass spectrometry, *Anal Chem* 66, 4190-4194.
 69. Loo, J. A., Hu, P. F., and Smith, R. D. (1994) Interaction of angiotensin peptides and zinc metal-ions probed by electrospray-ionization mass-spectrometry, *J Am Soc Mass Spectrom* 5, 959-965.
 70. Cheng, X., Chen, R., Bruce, J. E., Schwartz, B. L., Anderson, G. A., Hofstadler, S. A., Gale, D. C., and Smith, R. D. (1995) Using electrospray ionization FTICR mass spectrometry to study competitive binding of inhibitors to carbonic anhydrase, *J Am Chem Soc* 117, 8859-8860.
 71. Gao, J., Cheng, X., Chen, R., Sigal, G. B., Bruce, J. E., Schwartz, B. L., Hofstadler, S. A., Anderson, G. A., Smith, R. D., and Whitesides, G. M. (1996) Screening derivatized peptide libraries for tight binding inhibitors to carbonic anhydrase II by electrospray ionization-mass spectrometry, *Journal of medicinal chemistry* 39, 1949-1955.
 72. Kempen, E. C., and Brodbelt, J. S. (2000) A method for the determination of binding constants by electrospray ionization mass spectrometry, *Anal Chem* 72, 5411-5416.

73. De Vriendt, K., Sandra, K., Desmet, T., Nerinckx, W., Van Beeumen, J., and Devreese, B. (2004) Evaluation of automated nano-electrospray mass spectrometry in the determination of non-covalent protein-ligand complexes, *Rapid Commun Mass Spectrom* 18, 3061-3067.
74. Dole, M., Mack, L. L., Hines, R. L., Mobley, R. C., Ferguson, L. D., and Alice, M. B. (1968) Molecular beams of macroions, *J Chem Phys* 49.
75. Clegg, G. A., and Dole, M. (1971) Molecular beams of macroions. 3. Zein and polyvinylpyrrolidone, *Biopolymers* 10, 821-826.
76. Yamashita, M., and Fenn, J. B. (1984) Electrospray ion source. Another variation on the free-jet theme, *J Chem Phys* 88, 4451-4459.
77. Yamashita, M., and Fenn, J. B. (1984) Negative ion production with the electrospray ion source *J Chem Phys* 88, 4671-4675.
78. Irbane, J. V., and Thomson, B. A. (1976) On the evaporation of small ions from charged droplets, *J Chem Phys* 64, 2287-2294.
79. Thompson, B. A., and Irbane, J. V. (1979) Field-induced ion evaporation from liquid surfaces at atmospheric pressure, *J Chem Phys* 71, 4451-4463.
80. Wim, M., and Mann, M. (1994) Electrospray and Taylor-cone theory, Dole's beam of macromolecules at least ?, *Int J Mass Spectrom Ion Proc* 136, 167-180.
81. Juraschek, R., Dülcks, T., and Karas, M. (1999) Nanoelectrospray-More than just a minimized-flow elctrospray ionization source, *J Am Soc Mass Spectrom* 10, 300-308.
82. Schultz, G. A., Corso, T. N., Prosser, S. J., and Zhang, S. (2000) A fully integrated monolithic microchip electrospray device for mass spectrometry, *Anal Chem* 72, 4058-4063.
83. Loo, J. A., Udseth, H. R., and Smith, R. D. (1988) Collisional effects on the charge distribution of ions from large molecules formed by elctrospray-ionization mass spectrometry of larges molecules, *Rapid Commun Mass Spectrom* 2, 207-210.
84. Pramanik, B. N., Bartner, P. L., Mirza, U. A., Liu, Y. H., and Ganguly, A. K. (1998) Electrospray ionization mass spectrometry for the study of non-covalent complexes: an emerging technology, *J Mass Spectrom* 33, 911-920.
85. Hvidt, A., and Linderstrom-Lang, K. (1954) Exchange of hydrogen atoms in insulin with deuterium atoms in aqueous solutions, *Biochimica et biophysica acta* 14, 574-575.
86. Englander, S. W. (1963) A Hydrogen Exchange Method Using Tritium and Sephadex: Its Application to Ribonuclease, *Biochemistry* 2, 798-807.
87. Bentley, G. A., Delepierre, M., Dobson, C. M., Wedin, R. E., Mason, S. A., and Poulsen, F. M. (1983) Exchange of individual hydrogens for a protein in a crystal and in solution, *Journal of molecular biology* 170, 243-247.
88. Englander, J. J., Calhoun, D. B., and Englander, S. W. (1979) Measurement and calibration of peptide group hydrogen-deuterium exchange by ultraviolet spectrophotometry, *Anal Biochem* 92, 517-524.
89. Englander, J. J., Rogero, J. R., and Englander, S. W. (1985) Protein hydrogen exchange studied by the fragment separation method, *Anal Biochem* 147, 234-244.
90. Baldwin, R. L. (1995) The nature of protein folding pathways: the classical versus the new view, *Journal of biomolecular NMR* 5, 103-109.
91. Zhang, Z., and Smith, D. L. (1993) Determination of amide hydrogen exchange by mass spectrometry: a new tool for protein structure elucidation, *Protein Sci* 2, 522-531.

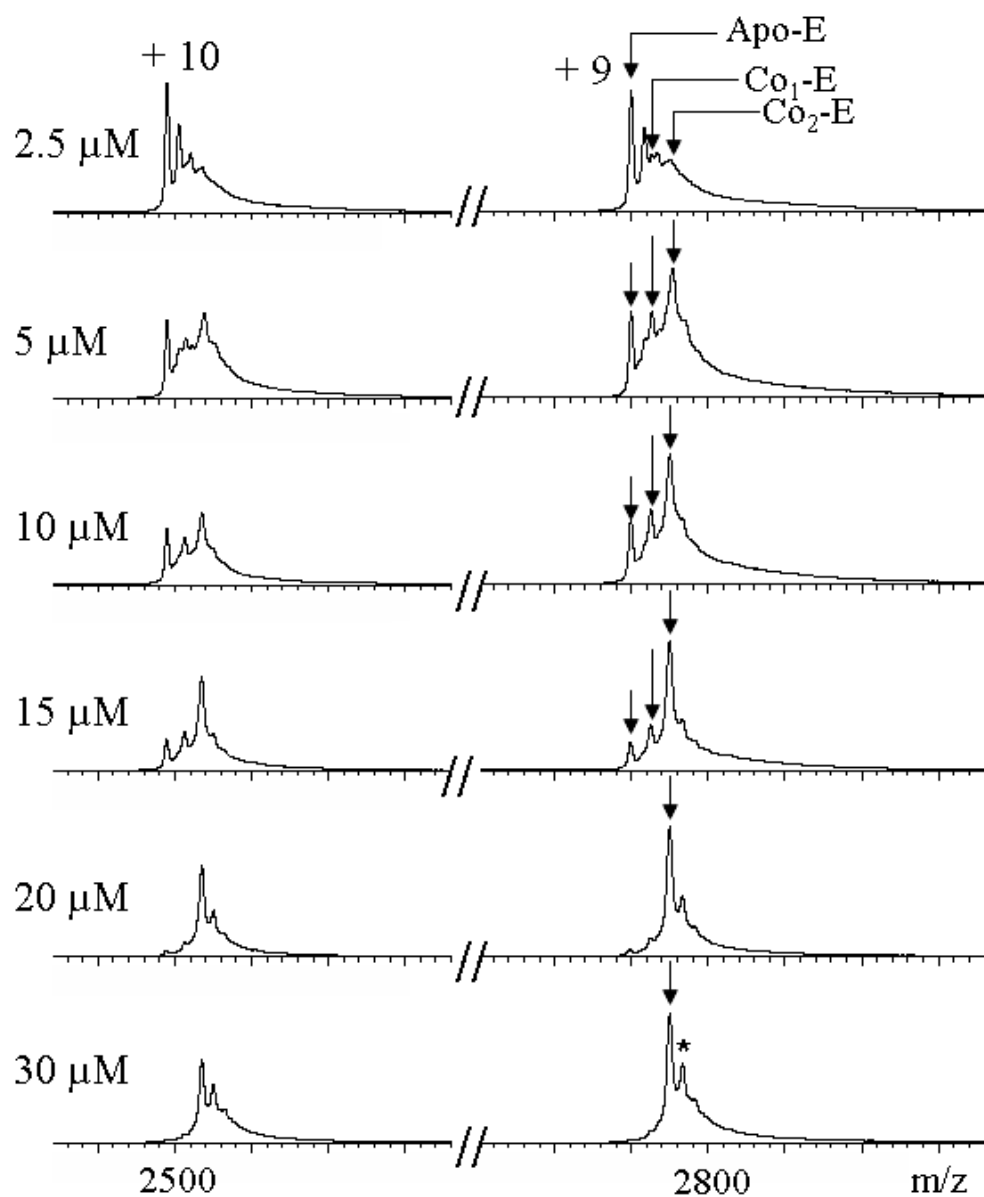
92. Johnson, R. S., and Walsh, K. A. (1994) Mass spectrometric measurement of protein amide hydrogen exchange rates of apo- and holo-myoglobin, *Protein Sci* 3, 2411-2418.
93. Hoofnagle, A. N., Resing, K. A., Goldsmith, E. J., and Ahn, N. G. (2001) Changes in protein conformational mobility upon activation of extracellular regulated protein kinase-2 as detected by hydrogen exchange, *Proceedings of the National Academy of Sciences of the United States of America* 98, 956-961.
94. Mandell, J. G., Baerga-Ortiz, A., Akashi, S., Takio, K., and Komives, E. A. (2001) Solvent accessibility of the thrombin-thrombomodulin interface, *Journal of molecular biology* 306, 575-589.
95. Mandell, J. G., Falick, A. M., and Komives, E. A. (1998) Identification of protein-protein interfaces by decreased amide proton solvent accessibility, *Proceedings of the National Academy of Sciences of the United States of America* 95, 14705-14710.
96. Molday, R. S., Englander, S. W., and Kallen, R. G. (1972) Primary structure effects on peptide group hydrogen exchange, *Biochemistry* 11, 150-158.
97. Bai, Y., Milne, J. S., Mayne, L., and Englander, S. W. (1993) Primary structure effects on peptide group hydrogen exchange, *Proteins* 17, 75-86.
98. Smith, D. L., Deng, Y., and Zhang, Z. (1997) Probing the non-covalent structure of proteins by amide hydrogen exchange and mass spectrometry, *J Mass Spectrom* 32, 135-146.
99. Englander, S. W., and Kallenbach, N. R. (1983) Hydrogen exchange and structural dynamics of proteins and nucleic acids, *Quarterly reviews of biophysics* 16, 521-655.
100. Marmorino, J. L., Auld, D. S., Betz, S. F., Doyle, D. F., Young, G. B., and Pielak, G. J. (1993) Amide proton exchange rates of oxidized and reduced *Saccharomyces cerevisiae* iso-1-cytochrome c, *Protein Sci* 2, 1966-1974.
101. Woodward, C., Simon, I., and Tuchsén, E. (1982) Hydrogen exchange and the dynamic structure of proteins, *Molecular and cellular biochemistry* 48, 135-160.
102. Englander, S. W., Mayne, L., and Rumbley, J. N. (2002) Submolecular cooperativity produces multi-state protein unfolding and refolding, *Biophysical chemistry* 101-102, 57-65.
103. Clarke, J., and Itzhaki, L. S. (1998) Hydrogen exchange and protein folding, *Current opinion in structural biology* 8, 112-118.
104. Englander, S. W., Downer, N. W., and Teitelbaum, H. (1972) Hydrogen exchange, *Annual review of biochemistry* 41, 903-924.
105. Hvidt, A., and Nielsen, S. O. (1966) Hydrogen exchange in proteins, *Advances in protein chemistry* 21, 287-386.
106. Miller, D. W., and Dill, K. A. (1995) A statistical mechanical model for hydrogen exchange in globular proteins, *Protein Sci* 4, 1860-1873.
107. Englander, S. W., and Kallenbach, N. R. (1984) Hydrogen -exchange and structural dynamics of proteins and nucleic acids, *Quarterly reviews of biophysics* 16, 521-655.
108. Bai, Y., Sosnick, T. R., Mayne, L., and Englander, S. W. (1995) Protein folding intermediates: native-state hydrogen exchange, *Science* 269, 192-197.
109. Mayo, S. L., and Baldwin, R. L. (1993) Guanidinium chloride induction of partial unfolding in amide proton exchange in RNase A, *Science* 262, 873-876.

110. Roder, H., Wagner, G., and Wuthrich, K. (1985) Amide proton exchange in proteins by EX1 kinetics: studies of the basic pancreatic trypsin inhibitor at variable p2H and temperature, *Biochemistry* *24*, 7396-7407.
111. Englander, S. W. (2000) Protein folding intermediates and pathways studied by hydrogen exchange, *Annual review of biophysics and biomolecular structure* *29*, 213-238.
112. Hoofnagle, A. N., Resing, K. A., and Ahn, N. G. (2003) Protein analysis by hydrogen exchange mass spectrometry, *Annual review of biophysics and biomolecular structure* *32*, 1-25.
113. Cravello, L., Lascoux, D., and Forest, E. (2003) Use of different proteases working in acidic conditions to improve sequence coverage and resolution in hydrogen/deuterium exchange of large proteins, *Rapid Commun Mass Spectrom* *17*, 2387-2393.
114. Kipping, M., and Schierhorn, A. (2003) Improving hydrogen/deuterium exchange mass spectrometry by reduction of the back-exchange effect, *J Mass Spectrom* *38*, 271-276.
115. Mandell, J. G., Falick, A. M., and Komives, E. A. (1998) Measurement of amide hydrogen exchange by MALDI-TOF mass spectrometry, *Anal Chem* *70*, 3987-3995.
116. Hernandez Villadares, M., Galleni, M., Frere, J. M., Felici, A., Perilli, M., Franceschini, N., Rossolini, G. M., Oratore, A., and Amicosante, G. (1996) Overproduction and purification of the *Aeromonas hydrophila* CphA metallo-beta-lactamase expressed in *Escherichia coli*, *Microb Drug Resist* *2*, 253-256.
117. Crowder, M. W., Walsh, T. R., Banovic, L., Pettit, M., and Spencer, J. (1998) Overexpression, purification, and characterization of the cloned metallo-beta-lactamase L1 from *Stenotrophomonas maltophilia*, *Antimicrob Agents Chemother* *42*, 921-926.
118. Simons, T. J. (1993) Measurement of free Zn²⁺ ion concentration with the fluorescent probe mag-fura-2 (furaptra), *Journal of biochemical and biophysical methods* *27*, 25-37.
119. Zhang, Z., and Marshall, A. G. (1998) A universal algorithm for fast and automated charge state deconvolution of electrospray mass-to-charge ratio spectra, *J Am Soc Mass Spectrom* *9*, 225-233.
120. Konermann, L., and Douglas, D. J. (1997) Acid-induced unfolding of cytochrome c at different methanol concentrations: electrospray ionization mass spectrometry specifically monitors changes in the tertiary structure, *Biochemistry* *36*, 12296-12302.
121. Peschke, M., Verkerk, U. H., and Kebarle, P. (2004) Features of the ESI mechanism that affect the observation of multiply charged noncovalent protein complexes and the determination of the association constant by the titration method, *Journal of the American Society for Mass Spectrometry* *15*, 1424-1434.
122. Selevsek, N., Tholey, A., Heinzle, E., Lienard, B. M., Oldham, N. J., Schofield, C. J., Heinz, U., Adolph, H. W., and Frere, J. M. (2006) Studies on ternary metallo-beta lactamase-inhibitor complexes using electrospray ionization mass spectrometry, *J Am Soc Mass Spectrom* *17*, 1000-1004.
123. Lienard, B. M., Selevsek, N., Oldham, N. J., and Schofield, C. J. (2007) Combined Mass Spectrometry and Dynamic Chemistry Approach to Identify Metalloenzyme Inhibitors, *ChemMedChem* *2*, 175-179.
124. Moali, C., Anne, C., Lamotte-Brasseur, J., Gros Lambert, S., Devreese, B., Van Beeumen, J., Galleni, M., and Frere, J. M. (2003) Analysis of the importance

- of the metallo-beta-lactamase active site loop in substrate binding and catalysis, *Chem Biol* 10, 319-329.
125. Robinson, C. V., Chung, E. W., Kragelund, B. B., Knudsen, J., Aplin, R. T., Poulsen, F. M., and Dobson, C. M. (1996) Probing the nature of noncovalent interactions by mass spectrometry. A study of protein-CoA ligand binding and assembly, *J Am Chem Soc* 118, 8646-8653.
126. Samalikova, M., Matecko, I., Muller, N., and Grandori, R. (2004) Interpreting conformational effects in protein nano-ESI-MS spectra, *Anal Bioanal Chem* 378, 1112-1123.
127. Winger, B. E., Light-Wahl, K. J., Ogorzalek Loo, R. R., Udseth, H. R., and Smith, R. D. (1993) Observation and implications of high mass-to-charge ratio ions from electrospray ionization mass spectrometry, *J Am Soc Mass Spectrom* 4, 536-545.
128. Smith, R. D., and Light-Wahl, K. J. (1993) The observation of non-covalent interactions in solution by electrospray ionization mass spectrometry: promise, pitfalls and prognosis, *Biol Mass Spectrom* 22, 493-501.
129. Ogorzalek Loo, R. R., Loo, J. A., Udseth, H. R., and Smith, R. D. (1992) A new approach for the study of gas-phase ion-ion reactions using electrospray ionization, *J Am Soc Mass Spectrom* 3, 695-705.
130. Rockwood, A. L., Busman, M., and Smith, R. D. (1991) Coulombic effects in the dissociation of large highly charged ions, *Int J Mass Spectrom Ion Proc* 111, 103-129.
131. Busman, M., Knapp, D. R., and Schey, K. L. (1994) Observation of large multimers in the electrospray ionization mass spectrometry of peptides, *Rapid Commun Mass Spectrom* 8, 211-216.
132. Lemaire, D., Marie, G., Serani, L., and Laprevote, O. (2001) Stabilization of gas-phase noncovalent macromolecular complexes in electrospray mass spectrometry using aqueous triethylammonium bicarbonate buffer, *Anal Chem* 73, 1699-1706.
133. Feng, R. (1995) Unusually strong binding of a noncovalent gas-phase spermine-peptide complex and its dramatic temperature dependence, in *Proceedings of the 43rd ASMS Conference of Mass Spectrometry and Allied Topics*, p 1264, Atlanta, GA.
134. Wu, Q., Gao, J., Joseph-McCarthy, D., Sigal, G. B., Bruce, J. E., Whitesides, G. M., and Smith, R. D. (1997) Carbonic anhydrase-inhibitor binding: From solution to the gas phase, *J Am Chem Soc* 119, 1157-1158.
135. Crowder, M. W., Wang, Z., Franklin, S. L., Zovinka, E. P., and Benkovic, S. J. (1996) Characterization of the metal-binding sites of the beta-lactamase from *Bacteroides fragilis*, *Biochemistry* 35, 12126-12132.
136. Laraki, N., Franceschini, N., Rossolini, G. M., Santucci, P., Meunier, C., de Pauw, E., Amicosante, G., Frere, J. M., and Galleni, M. (1999) Biochemical characterization of the *Pseudomonas aeruginosa* 101/1477 metallo-beta-lactamase IMP-1 produced by *Escherichia coli*, *Antimicrob Agents Chemother* 43, 902-906.
137. de Seny, D., Prosperi-Meys, C., Bebrone, C., Rossolini, G. M., Page, M. I., Noel, P., Frere, J. M., and Galleni, M. (2002) Mutational analysis of the two zinc-binding sites of the *Bacillus cereus* 569/H/9 metallo-beta-lactamase, *Biochem J* 363, 687-696.
138. De Vriendt, K., Van Driessche, G., Devreese, B., Bebrone, C., Anne, C., Frere, J. M., Galleni, M., and Van Beeumen, J. (2006) Monitoring the zinc affinity of

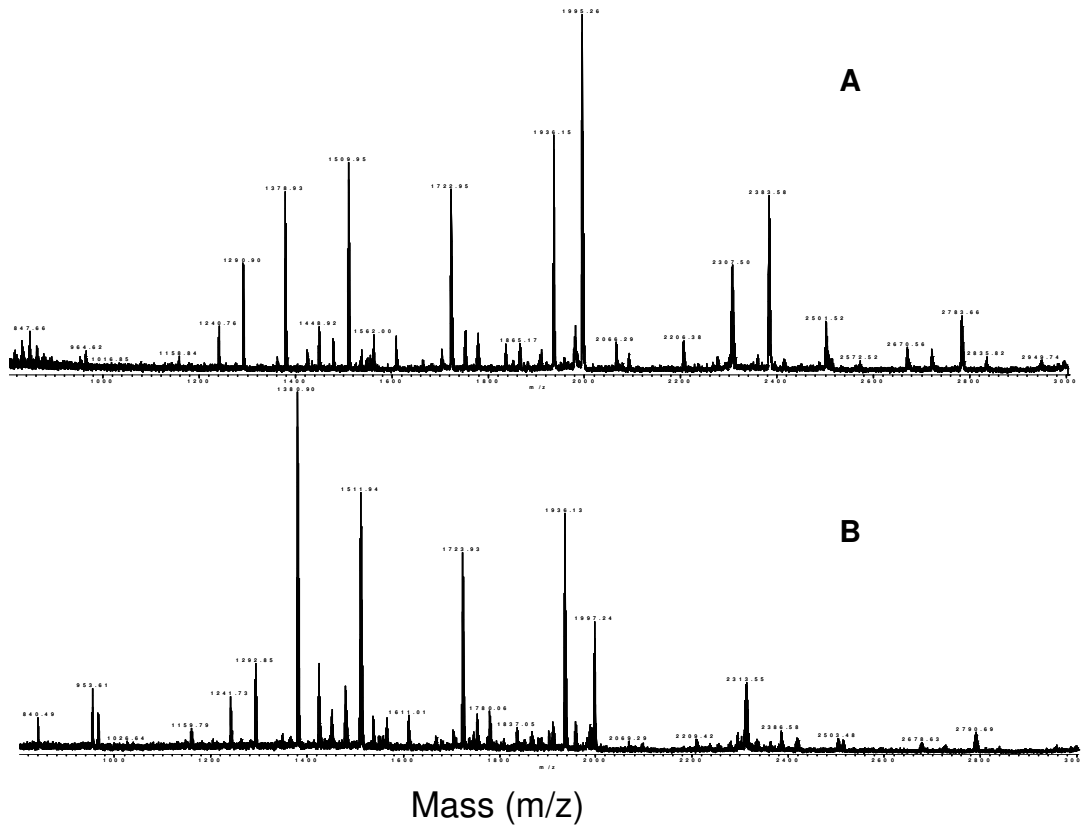
- the metallo-beta-lactamase CphA by automated nanoESI-MS, *Journal of the American Society for Mass Spectrometry* 17, 180-188.
139. Hernandez Valladares, M., Kiefer, M., Heinz, U., Soto, R. P., Meyer-Klaucke, W., Nolting, H. F., Zeppezauer, M., Galleni, M., Frere, J. M., Rossolini, G. M., Amicosante, G., and Adolph, H. W. (2000) Kinetic and spectroscopic characterization of native and metal-substituted beta-lactamase from *Aeromonas hydrophila* AE036, *FEBS Lett* 467, 221-225.
140. Antonaccio, M. J. (1982) Angiotensin converting enzyme (ACE) inhibitors, *Annual review of pharmacology and toxicology* 22, 57-87.
141. Carfi, A., Duee, E., Galleni, M., Frere, J. M., and Dideberg, O. (1998) 1.85 Å resolution structure of the zinc (II) beta-lactamase from *Bacillus cereus*, *Acta Crystallogr D Biol Crystallogr* 54 (Pt 3), 313-323.

APPENDIX 1:



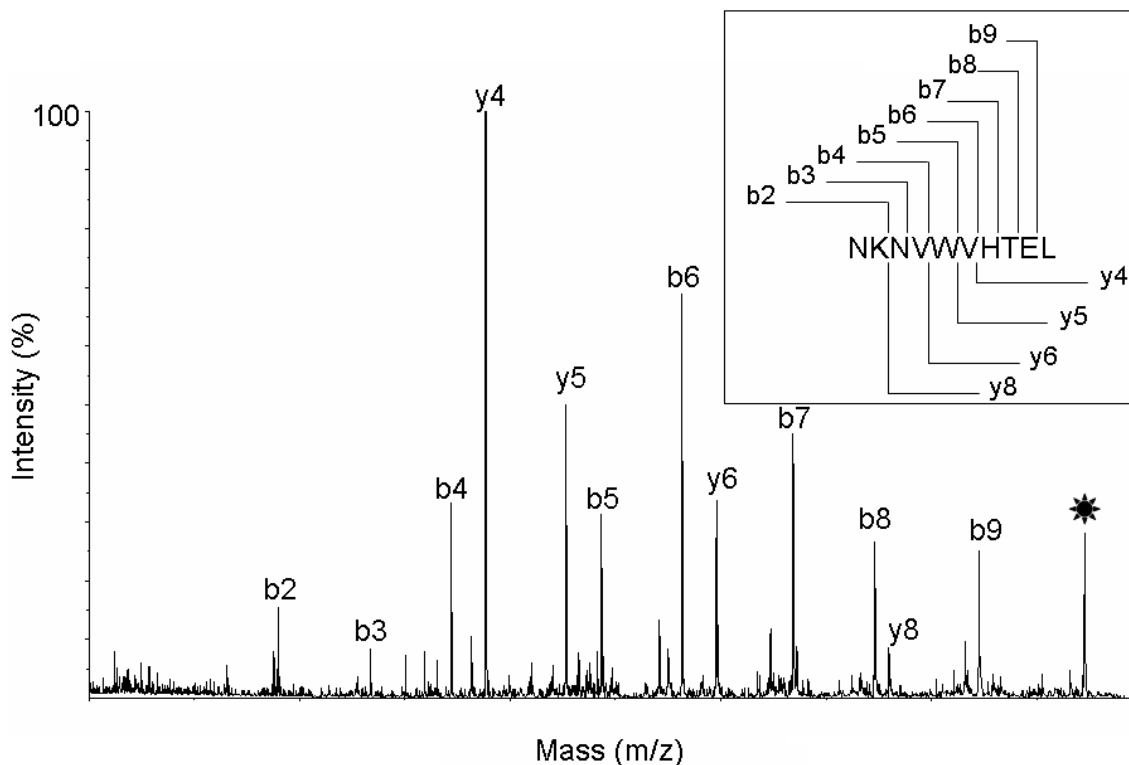
Appendix 1: ESI mass spectra resulting from the incubation of apo-BcII (11.7) μM in 15 mM ammonium bicarbonate, pH 7) with different concentrations of Co(II) ions (2.5 to 30 μM). (*) represented the salt adducts. The ions carrying the charges + 9 and + 10 are represented in the mass spectra. Experiments were carried out at sample cone voltage 200 V, pressure at interface 6.7 mbar.

APPENDIX 2:



Appendix 2: Peptide mass fingerprint (PMF) of the apoenzyme BcII digested by pepsin in non deuterated buffer (**A**) and in deuterated buffer (**B**) analyzed in 5 mg/ml CCA (acetonitrile/ethanol/TFA 20/80/0.1) using MALDI-MS.

APPENDIX 3:



Appendix 3: Example of a MS/MS mass spectrum of a peptic peptide from the apoenzyme BcII digested with pepsin. The amino acid sequence of the peptide is NKNVWVHTEL with an experimental mass of $m/z = 1239,650$. The MS/MS fragmentation of the precursor peptide labeled with (*) leads mainly to the cleavage of the amide bonds, which produce b^+ -ions when the charge is retained by the amino-terminal fragment and y^+ -ions when it is retained by the carboxyl-terminal fragment. The b^+ -ions are consecutively labeled from the original amino terminus and the y^+ -ions from the original carboxyl terminus as represented in the inset of the figure.

APPENDIX 4:

Appendix 4: Determination of the percentage of deuterons back-exchanged (% BE) for each peptic peptide of the BclI enzyme during sample preparation for HDX experiments. In column 1 and 2, the sequence of the analyzed peptides and the maximal number of observable deuterons (N) are given. In column 3 and 4, the experimental centroid mass of the undeuterated and nondeuterated peptides respectively are given. In column 5 and 6 the number of deuterons back exchanged and the percentage of deuterons back-exchanged is given respectively. % BE is calculated using the following equation:

$$BE = \left[1 - \frac{M_{deut} - M_{undeut}}{N} \right] * 100\%$$

APPENDICES

Sequence of identified peptides	Maximal number of deuterons (N)	Centroid Mass (M_{undeut})	Centroid Mass (M_{deut})	$\frac{M_{deut}}{M_{undeut}}$	BE (%)
N-term. tail (β1, β2)					
¹ SQKVEKTVIK- NETGTISISQL ²¹	20	2304.54	2317.73	13.19	34.02
β3, loop 32-39, β4, β5					
⁴⁴ LVLNTSKGLVL ⁵⁴	11	1157.52	1162.84	5.32	51.63
²² NKNVWVHTEL ³¹	10	1240.36	1245.65	5.29	47.10
³² GSFNGEAVPS- NGLVLNTSKGLVL ⁵⁴	22	2274.96	2285.40	10.44	52.54
Loop 55-66					
⁵⁵ VDSSWDDKLTKE ⁶⁶	12	1423.49	1430.72	7.23	39.75
αI, β6					
⁷¹ VEKKFQKRVTD ⁸¹	11	1378.71	1384.08	5.37	51.18
⁷⁰ MVEKKFQKRVTD ⁸¹	12	1509.84	1515.79	5.95	50.37
αII, β7					
⁸² VIITHAHADR- IGGIKTLKER- GIKAHSTAL ¹¹⁰	29	3108.37	3122.88	14.51	49.95
Connecting Loop, β8					
¹³⁰ VTNLKFGNM ¹³⁸	9	1024.09	1028.31	4.22	53.11
¹¹⁵ AKKNGYEEPL- GDLQT ¹²⁹	14	1663.82	1670.60	6.78	51.57
¹¹⁴ LAKKNGYEEPL- GDLQTVTNL ¹³³	19	2204.45	2214.68	10.23	46.16
β9					
¹³⁹ KVETFYPGKG- HTEDN ¹⁵³	14	1722.83	1728.87	6.04	56.82
¹³⁹ KVETFYPGKG- HTEDNIV ¹⁵⁵	16	1935.08	1942.85	7.77	51.44
β10					
¹⁵⁶ VWLPQYNIL ¹⁶⁴	8	1146.54	1152.75	6.21	22.37

¹⁵⁶ VWLPQYNIL ¹⁶⁴	8	1146.54	1152.75	6.21	22.37
β11, Loop 174-185					
¹⁶⁵ VGGCLVKSTS- AKDLGNVADA- YVNE ¹⁸⁸	24	2411.74	2425.76	14.02	41.58
αIV					
¹⁹⁵ NVLKRYRNIN ²⁰⁴	10	1290.49	1295.36	4.87	51.30
¹⁸⁹ WSTSIENVLK- RYRNIN ²⁰⁴	16	1994.21	2003.63	9.42	41.09
¹⁸⁹ WSTSIENVLK- RYRNINA ²⁰⁵	17	2065.53	2075.22	9.69	43
C-term. tail, β12, αV					
²²⁰ LHTLDLLK ²²⁷	8	953.13	956.70	3.57	55.39
²⁰⁵ AVVPGHGEVG- DKGLL ²¹⁹	14	1448.67	1455.00	6.33	54.78
²⁰⁵ AVVPGHGEVG- DKGLLL ²²⁰	15	1561.77	1569.09	7.32	51.16
²⁰⁵ AVVPGHGEVG- DKGLLLHTLD- LLK ²²⁷	22	2381.35	2395.01	13.65	37.93